The Role of Fat Signalling in Craniofacial Development

Zakaria, Sana

Awarding institution:
King's College London

Title: The Role of Fat Signalling in Craniofacial Development

Author: Sana Nafees Zakaria

The Role of Fat Signalling in Craniofacial Development

Sana Nafees Zakaria

Thesis submitted for the degree of Doctor of Philosophy at King's College London

2013

King's College London

Department of Craniofacial Development and Stem Cell Biology

SE1 9RT, London

Declaration

No part of the work presented in this thesis has been submitted in support of another degree or qualification at this or any other institute of education.

Data presented in Fig.5.2 A-D and Fig.7.2 B-D was given by Dr. Yaopan Mao (Rutgers University) and all the subsequent analysis was carried out by me.

The mT/mG *Dchs1* mosaic mouse line was generated by Dr. Anna Kuta (KCL). All the subsequent experimental and data analysis was carried out by me.

Acknowledgements

I would like to thank my supervisor Professor Francis-West for her support and guidance throughout the course of my degree and for the opportunity to do a PhD in her lab. I am also grateful to Dr. Ken Irvine and Dr. Mao Yaopan for their support and contribution to the project. I am thankful to Professor Guthrie and Dr. Robert Hindges for providing their expertise in the field.

My lab members Anna, Catia and Tina have been amazing in their support and were always ready for a chat to debate the mysteries of experimental failures! Their lab banter has helped lift up my spirits on countless occasions. (Tina, I really hope your monkey entertainment idea takes off! Catia, don't embark upon any baking endeavours without me!)

The last few years would not have been the same without the tearoom banter and the atrium concerts with Abbas Di Libda and the wonderful chats with Sarah Ghafoor, Nisha Patel, Thantrira First, Dahlea Bukhary and Meghna Motwani. I thank Angela Gates and Sharon Pudaruth for the endless support and friendship.

My family has been a tremendous force driving me forward in achieving all milestones in my life. I would not have been able to move forward if it had not been for my dad's strength and ambition, my mom's hugs and wonderful food and my brother and sister's love and friendship. Their support has enabled me to achieve so much more than I thought possible. I would also like to thank my in-laws for their support, patience and the food supply through the course of my degree!

Lastly, I want to thank my husband who has been my rock. His love, advice, patience and strength have got me through some tough times and without his unconditional support I would not have been able to strive for and achieve my goals.

In memory of my loving uncle…who taught us not to take life too seriously and take pleasure in small things.

Abstract

Fat/Dachsous signalling regulates planar cell polarity (PCP), which is the polarisation of tissue structures perpendicular to the apical-basal axis, and interacts with the Hippo pathway to suppress overgrowth of tissues in *Drosophila*. Recent studies in vertebrates have implicated *Fat4* and *Dchs1*, the receptor-ligand pair and the vertebrate homologues of *Drosophila* Ft and Ds, respectively, in regulating PCP in the kidney and cochlea. However, the role of Fat signalling is largely undetermined in vertebrate development.

To determine the role of Fat signalling in craniofacial development, a basic characterisation was carried out using histology, OPT scanning, skeletal preparations, immunohistochemistry and *in situ* hybridisations. This revealed that loss of *Fat4* and/or *Dchs1* results in arrested growth of salivary glands, disruption of hair polarity of the utricle, delayed differentiation of osteoblasts of the cranial bones and arrested lateral tangential migration of the Facial Branchiomotor neurons (FBNs).

In *Drosophila* and vertebrates, PCP is controlled by two pathways; the Frizzled-PCP and the Fat-PCP pathway. During development, FBNs undergo tangential caudal and lateral tangential migrations within the plane of the neuroepithelium and are a model system to study PCP. Previous studies have shown a critical role for Fz-PCP during caudal migration. The role of Fat-PCP signalling during FBN migration was analysed by using mouse mutants for *Fat4* and *Dchs1* and by expression analysis.

Loss of *Fat4/Dchs1* results in an arrest of lateral migration of the FBNs and a loss of polarity as revealed by cell shape and Golgi orientation analysis with no effect on FBN specification. Fat4 and Dchs1 are expressed as complementary gradients in the hindbrain. Generation of chimeric tissue revealed that the gradient of Dchs1 is necessary for polarised FBN migration suggesting that the role and mechanisms of Fat-PCP signalling are conserved between vertebrates and *Drosophila*. The $Islet-1^{cre}$ and $Hoxa3^{cre}$ conditional knockouts revealed that there is a requirement for Dchs1 both cell autonomously within the FBNs as well as non-cell autonomously in the neuroepithelium whereas Fat4 is largely required non-cell autonomously.

Analysis of double $Fat4^{-/-}Vangl2^{Lp/Lp}$ mutants revealed that Fz-PCP exclusively regulates caudal FBN migration whilst Fat-PCP is necessary for the lateral polarised migration of the FBNs even in the absence of Fz-PCP. The two pathways work on orthogonal axes to regulate FBN migration. This study establishes that Fat signalling is largely required during craniofacial morphogenesis, provides further evidence of Fat signalling in regulating PCP in vertebrates and the first evidence that gradients of Fat4/Dchs1 may establish PCP in vertebrates.

Table of Contents

List of Figures

List of Tables

General Abbreviations

DEPC   Diethylpyrocarbonate

PBS   Phosphate buffered saline

TAE   Tris-acetate-EDTA

TBS   Tris buffered saline

HCl   Hydrochloric acid

MgCl   Magnesium chloride

NaCl   Sodium chloride

MAB   Maleic acid buffer

SSC   Saline sodium citrate

NaOH   Sodium hydroxide

DPX   Distrene plasticiser xylene

NBT   Nitro blue tetrazolium

BCIP   5-bromo4-chloro-indolyphosphate

NTMT   Sodium tris magnesium tween/alkaline phosphatase buffer

KOH   Potassium hydroxide

EDTA   Ethylenediaminetetraacetic acid

CHAPS   3-cholamidopropyl-dimethylammonio-1-propane sulphonate

APS   Ammonium persulfate

TEMED   Tetramethylethylenediamine

DTT   Dithiothreitol

WT   Wildtype

FBN   Facial Branchiomotor Neuron

1   INTRODUCTION

1.1 Fat Signalling Family

1.1.1   Classic Cadherins and function

Classic cadherins, which were the first to be identified, are a class of transmembrane calcium dependant proteins which contain five cadherin repeats, a laminin domain and epidermal growth factor (EGF) repeats (Nagafuchi et al. 1987; Hirano et al. 2003; Pettitt 2005). Cadherins form the transmembrane domain of adherens junctions (AJs) and mediate cell-cell contact and cell adhesion (Nagafuchi et al. 1987; Gumbiner 2000; Hirano et al. 2003). They have highly conserved cytoplasmic regions with binding sites for p-120 and β-catenin, which ultimately link the cadherins to the actin cytoskeleton. The extracellular region of cadherins undergoes homophilic interactions (Hirano et al. 2003). Cadherins are key to facilitating propagation of cell-cell communication and they form a bridge between environmental cues and intracellular signalling.

1.1.2   Fat and Dachsous structure and homology

In *Drosophila*, the first record of mutations caused by the dominant *Gull* allele belonging to the *fat (ft)* gene locus was described by Mohr in 1923. Subsequently, recessive lethal and recessive viable mutations were also mapped to the *ft* locus and 18 known *ft* alleles were uncovered (Bryant et al. 1988). Currently, there are over 81 *ft* alleles listed on Flybase. The actual sequence and structure of the *ft* gene was not studied until it was first cloned in *Drosophila* and identified as part of the cadherin superfamily (Mahoney et al. 1991). Until then, cadherins were believed to be found only in vertebrates. However, upon analysis of the sequence and predicted protein structure of Ft, it was deduced that the Ft protein is part of the family of cadherins. Ft was also predicted to be cell bound rather than a diffusible protein based on the cell autonomous effects it had on the growth of tissue in *Drosophila* (Mahoney et al. 1991). The role of *ft* and phenotypes of *ft* mutants will be discussed in detail in the sections below.

The *ft* gene encodes a 560 kDa transmembrane protein which contains an extracellular domain (ECD) comprising of 34 cadherin domains, five EGF like repeats and two laminin domain repeats (Fig.1.1) (Mahoney et al. 1991). The cadherin domains of Ft show high similarity to vertebrate cadherin domains and have calcium binding sites. A striking difference however, between the classic vertebrate cadherins and Ft cadherin is the vast difference in the number of cadherin repeat domains.

Spontaneous mutation at the *dachsous (ds)* locus had been reported before by Calvin Bridges in 1917, but the *ds* gene was not identified as a cadherin at the time (Clark et al. 1995). The similarity between the *ft* and *ds* mutant phenotypes in *Drosophila* prompted Mohr in 1929 to conduct experiments in the *ft* mutants using *ds* alleles which revealed that they interact genetically (Clark et al. 1995).

When the *ft* gene was mapped and identified as a cadherin, another loci was found on the *Drosophila* genome that encoded a cadherin domain but the gene remained unidentified (Mahoney et al. 1991). This region was later identified as the *ds* gene (Clark et al. 1995). The *ds* gene encodes a 385 kDa transmembrane protein which has 27 cadherin repeats in the ECD (Fig.1.1) (Clark et al. 1995). Interestingly, the extracellular domain of Ds does not contain any EGF domain repeats or laminin domains unlike Ft (Mahoney et al. 1991; Clark et al. 1995). The cytoplasmic domain of both Ft and Ds has a conserved region similar to the β-catenin binding site present in the cytoplasmic domain of vertebrate cadherins (Clark et al. 1995).

Based on the overlapping phenotypes, RNA expression, genetic interaction and structural homology of *ft* and *ds*, it was proposed that they function in the same genetic pathway and communicate via heterophilic interactions (Bryant et al. 1988; Mahoney et al. 1991; Clark et al. 1995).

Another gene similar to the *ft* gene was uncovered in *Drosophila* during a genome wide search for cadherins. Due to sequence similarity to the *ft* gene, it was named *fat-like (ft-l)* or *ft2* (Castillejo-López et al. 2004). *ft-l* also encodes a large transmembrane protein of over 500 kDa which contains 34 cadherin repeats, six EGF repeats and one laminin domain (Fig.1.1) (Castillejo-López et al. 2004). Although some sequence similarities were observed between *ft* and *ft-l*, there are vast differences in their cadherin repeat sequences and their expression profile is also

very distinct. Whilst *ft* is mainly expressed in imaginal discs and the embryonic ectoderm, *ft-l* expression is observed in the epithelium of tubular structures (Castillejo-López et al. 2004).

In 1987, Tearle reported defects in the *Drosphila* ovary caused by mutation in the *kugelei* gene. It was later reported that mutations in *ft-l* and the *kugelei* gene result in an identical phenotype in the ovary of *Drosophila* and *kugelei* was mapped to the *ft-l* locus (Viktorinová et al. 2009).

1.1.3   Vertebrate Fat family

Four mammalian Fat orthologues have been uncovered, namely, *Fat1, Fat2, Fat3* and *Fat-j/Fat4* whilst two orthologues of *Dachsous (Dchs); Dchs1* and *Dchs2* have been identified (Fig.1.1).

1.1.3.1   *Fat1*

The first vertebrate Fat cadherin to be reported was what is now referred to as *Fat1*. *Fat1* was accidentally discovered and cloned from a T-leukaemia cell line (Dunne et al. 1995). It was later cloned in the rat and the mouse and subsequently cloned and analysed in the zebrafish (Ponassi et al. 1999; Cox et al. 2000; Down et al. 2005). The vertebrate Fat1 protein, like *Drosophila* Ft, has 34 cadherin repeats and five EGF-like repeats. Fat1 has one laminin domain in contrast to the two laminin domains found in *Drosophila* Ft (Fig.1.1) (Ponassi et al. 1999; Cox et al. 2000; Down et al. 2005). *Fat1* encodes a transmembrane protein of over 500 kDa and is highly conserved within the vertebrate species. In contrast, *Fat1* is not as highly conserved to the *Drosophila ft*.

Fat1 is expressed in a variety of developing tissues in the mouse, rat and chick such as the limb buds, ear, eye, the developing CNS and branchial arches (Ponassi et al. 1999; Cox et al. 2000; Smith et al. 2007). Fat1 plays an important role in kidney development and *Fat1*^{-/-} pups die perinatally due to defects in kidney slit junction formation (Ciani et al. 2003). Fat1 is proposed to be involved in the formation of intercellular junctions and provide spacing between the cells in the kidney (Yaoita et al. 2005). Furthermore, *Fat1*^{-/-} mice also have midline defects such as

holoprosencephaly and loss of *Fat1* disrupts cell-cell contact and cell polarity *in vitro* in wound healing assays (Ciani et al. 2003; Tanoue & Takeichi 2004; Moeller et al. 2004). *Fat1* was recently shown to interact with *Atrophin* in regulating growth and injury response of vascular smooth muscle cells (VSMC). In the zebrafish Fat1 can bind to Scribble and interact with the Hippo pathway during kidney tubule formation (Hou & Sibinga 2009; Skouloudaki et al. 2009).

1.1.3.2   *Fat2*

Human *Fat2* was discovered during a screen for large molecules in the brain by Nakayama and colleagues who later described *Fat2* expression and function in the rat (Nakayama et al. 1998; Nakayama et al. 2002). The rat *Fat2* homologue encodes a protein of approximately 480 kDa which contains 34 cadherin repeats, two EGF repeats and one laminin domain (Fig.1.1).

In rats, *Fat2* undergoes homophilic interactions resulting in cell aggregates in culture. In the postnatal brain, it is expressed in the fibers of cerebellar granule cells and is proposed to regulate the spacing between the parallel fibers which is necessary for appropriate organisation of axons (Nakayama et al. 2002). Although no direct binding partner of Fat2 intracellular domain (ICD) has been identified, it contains a conserved motif found in the Fat1 ICD which is responsible for binding to Ena/Vasp proteins and interacting with the actin cytoskeleton (Moeller et al. 2004). Fat2 also plays a role in the differentiation and radial migration of neural progenitors in the chick neural tube (Hateren et al. 2011).
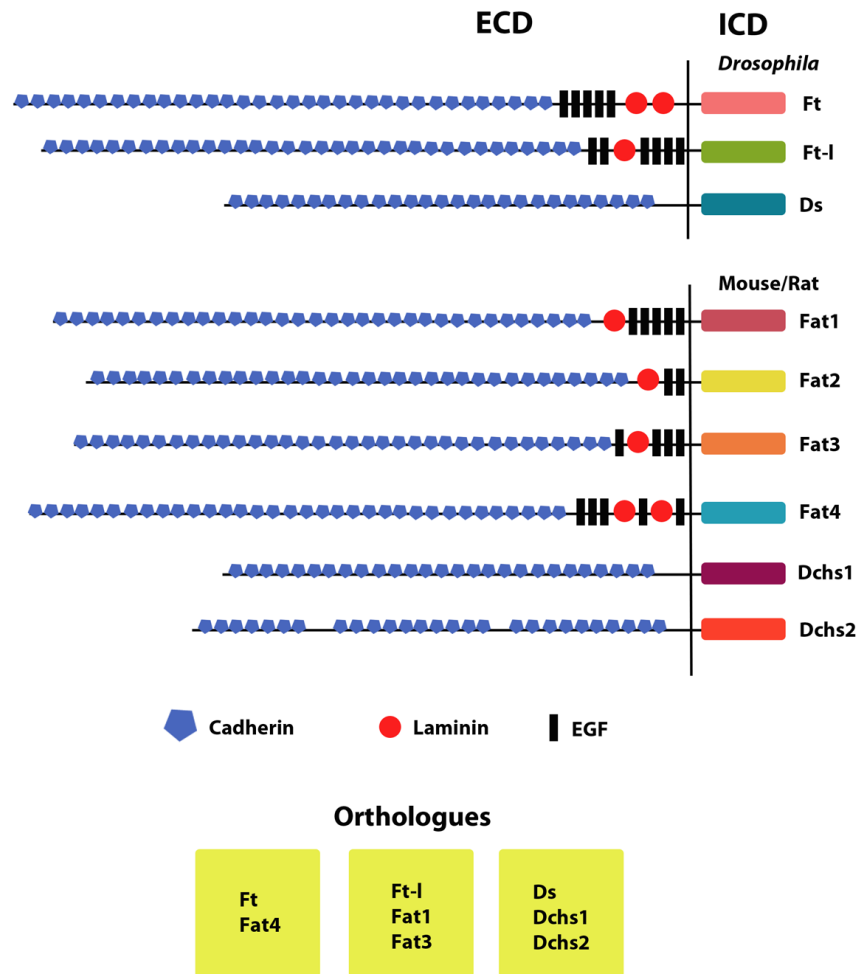
Figure 1.1. Structure and homology of the Fat signalling family. Sketch diagrams of the structure of *Drosophila ft* and *ft-l* with 34 cadherin repeats and *ds* with its 27 cadherin repeats and no EGF and Laminin domains. Just below are the sketch diagrams of the structure of mammalian *Fat1-4* with 34 cadherin repeats and *Dchs1* and *Dchs2* with 27 cadherin repeats and no EGF or Laminin domains as in *Drosophila*. The intracellular domain is represented by different coloured rectangles. Based on the sequence homology, *Ft* and *Fat4* are considered true orthologues, *ft-l* and *Fat1* and *Fat3* are considered to be more closely related orthologues and *Ds* and *Dchs1/2* are also considered orthologues. ECD= extracellular domain, ICD= intracellular domain.

1.1.3.4 *Fat3*

Human and rat *Fat3* were uncovered by computer based screening for cadherins. Rat Fat3 protein is over 500 kDa, slightly larger than the rat Fat1 and Fat2 proteins but also has 34 cadherin domains, four EGF repeats and one laminin domain (Fig.1.1) (Mitsui et al. 2002).

Fat3 expression in the developing CNS of the rat overlaps with the expression of *Fat1*(Mitsui et al. 2002). Further analysis in the mouse revealed high expression of *Fat3* in the olfactory bulb and retina (Nagae et al. 2007). Analysis of *Fat3*$^{-/-}$ mice revealed that the cells of the retina, which normally have one dendritic synapse and a unipolar morphology, have several ectopic synapses and form additional retinal layers in the eye (Deans et al. 2011). Despite these defects, the overall patterning of the retina is intact. The study also identified a potential Ena/Vasp binding site on the Fat3 ICD and proposed interaction with Ena/Vasp as a possible mechanism for maintaining the unipolar formation of dendrites (Deans et al. 2011).

Based on sequence homology, *Fat1* and *Fat3* are more similar to each other than they are to *Fat2* (Mitsui et al. 2002).

1.1.3.5 *Fat-j/Fat4*

Human *Fat-j/Fat4* was the first *Fat4* homologue identified using a screening method aiming to find cell-cell adhesion molecules with a role in embryonic morphogenesis (Höng et al. 2004). This method was also used to identify the rat and mouse orthologues (Höng et al. 2004). The mouse Fat4 protein has 34 cadherin repeats, like all other Fats in the mouse and *Drosophila ft* and encodes a large protein of over 540 kDa (Fig.1.1) (Rock et al. 2005). Fat4 has five EGF-like repeats and like *Drosophila* Ft, and unlike the other vertebrate Fats, it has two laminin domains (Rock et al. 2005). *Fat4* is expressed in the mesenchyme of various organs during development of the mouse such as the lung, kidney, cochlea and intestine. Expression was also observed in the CNS and intervertebral disks (Rock et al. 2005; Mao et al. 2011). Loss of *Fat4* results in cystic kidneys, smaller lungs, aberrant ossification of sterna and shorter cochlea with hair polarity defects (Saburi et al. 2008; Mao et al. 2011).

1.1.3.6 *Dchs1 and Dchs2*

Two orthologues of the Drosophila *ds* gene were discovered independently in the human genome; *Dchs1* and *Dchs2* (Nakajima et al. 2001; Höng et al. 2004). Similar to Ds, both Dchs1 and Dchs2 have 27 cadherin repeats and no EGF or laminin domains in their extracellular domain (Fig.1.1) (Nakajima et al. 2001; Höng et al. 2004; Rock et al. 2005). The intracellular domain of Dchs1 and Dchs2 has some sequence conservation with the β-catenin binding site sequence found in other vertebrate cadherins (Rock et al. 2005). *Dchs2* is expressed in a very restricted domain in the neural tube floor plate and the cerebrum and no clear role of *Dchs2* has been proposed as yet (Höng et al. 2004; Rock et al. 2005). *Dchs1,* however, is expressed in a variety of tissues during mouse development such as the lung, kidney, cochlea, intestine, CNS and intervertebral disks. *Dchs1* expression overlaps with *Fat4* expression in these tissues and they are expressed in the mesenchyme of the lung, kidney and intestine (Rock et al. 2005; Mao et al. 2011). Loss of *Dchs1* results in identical phenotypes to that of *Fat4* null embryos, as mentioned above and *Dchs1* is considered a true orthologue of Drosophila *ds* (Mao et al. 2011).

1.1.4 Sequence homology

Comparative analysis of the amino acid sequences of the intracellular and extracellular domains of the *Fat* and *Dchs* homologues was carried out using the psi-blast tool. Analysis in the mouse revealed that *Fat1* and *Fat3* are true orthologues of *Drosophila ft-l* whereas *Fat4* is the true orthologue of *Drosophila ft* (Rock et al. 2005). *Fat2* is similar to *Fat1* and *Fat3* however it did not appear to be analogous to the *Drosophila ft* or *ft-l* (Rock et al. 2005). Mouse *Dchs1* and *Dchs2* are 28% and 26% homologous to *ds*, respectively, whereas the sequences are highly conserved when compared to the human counterparts with over 90% sequence homology (Fig.1.1) (Rock et al. 2005). This focus of this study is on the role of *Fat4* and *Dchs1* in development which will be discussed in further detail in later sections.

1.2 Planar Cell Polarity

1.2.1 What is PCP?

Planar cell polarity (PCP) by definition is the biased orientation of cells along the planar axis of a sheet of epithelial cells, i.e. perpendicular to the apical-basal axis (Wallingford 2012). The term PCP is also synonymously used with PCP signalling pathways. For the purpose of this study, PCP will refer to the actual process that occurs during morphogenesis and any signalling activity will be referred to as core/Fz-PCP and Fat-PCP signalling.

Cell polarity itself refers to a biased orientation of a cell and this property of cells has been studied extensively in various animal models. For example, polarisation can be observed along the mother-daughter axis of the dividing yeast cell or polarity can also be seen along the axon-dendrite axis of a neuron (Black & Baas 1989; Pringle et al. 1995). However, PCP refers to the combined polarity of a group of cells in a tissue and can also be referred to as tissue polarity (Wallingford 2012).

Although, classically defined in epithelial tissues, PCP processes have also been described in mesenchymal tissues such as during gastrulation, limb elongation and cartilage condensations (Goodrich & Strutt 2011; Gao et al. 2011; Wallingford 2012). A few key examples of PCP processes will be described below, namely; convergent-extension, oriented cell division, polarised cell migration and orientation of hair on the body.

1.2.1.1 Convergent-Extension

The early morphogenetic movements that occur in embryonic development and leads to specification of ectoderm, mesoderm and endoderm is termed gastrulation. It was first described comprehensively by Holtfreter in 1943 in amphibian embryos and later demonstrated elegantly by several studies in the *Xenopus* (Fig.1.2 B) (Keller et al. 1992; Moon et al. 1993; Wallingford 2002). During gastrulation, cells undergo a collective polarised movement termed convergent-extension. During convergent-extension, the cells undergo a mediolateral convergence as they intercalate and slide over each other making the mediolateral axis narrower whilst causing a lengthening

of the animal-vegetal/antero-posterior axis of the embryo (Fig.1.2 B) (Keller et al. 1992). Convergent-extension is not limited to gastrulation and to mesenchymal tissues but is also important during neural plate formation, elongation of kidney tubules as well as elongation of the cochlea (Keller et al. 1992; Wallingford 2002; Montcouquiol et al. 2003; Karner et al. 2009).

1.2.1.2 Oriented Cell Division

Planar oriented cell divisions occur in a variety of tissues such as the developing nervous system or the elongating kidney tubules (Ciruna et al. 2006; Karner et al. 2009). Oriented cell divisions are often coupled with convergent-extension movements which ensure that the development and growth of a particular organ or the entire embryo occurs along the appropriate axis (Fig.1.2 A).

1.2.1.3 Polarised cell migration

Polarised cell migration is key to development of many structures, for example cortical layers are formed in part by tangential migration of interneurons (Tissir & Goffinet 2010). Neural crest cell migration is an important example of polarised cell migration which is dependent on a PCP pathway. Studies in *Xenopus* embryos have revealed the role of *Wnt11* and *Fz7* in regulating the polarised migration of neural crest cells (De Calisto et al. 2005). Loss of *Wnt11* results in a block in migration and reduced number of cell protrusions. Migration of the facial branchiomotor neurons (FBNs) also occurs in the planar axis under the control of a PCP pathway, which will be discussed in detail in later sections.
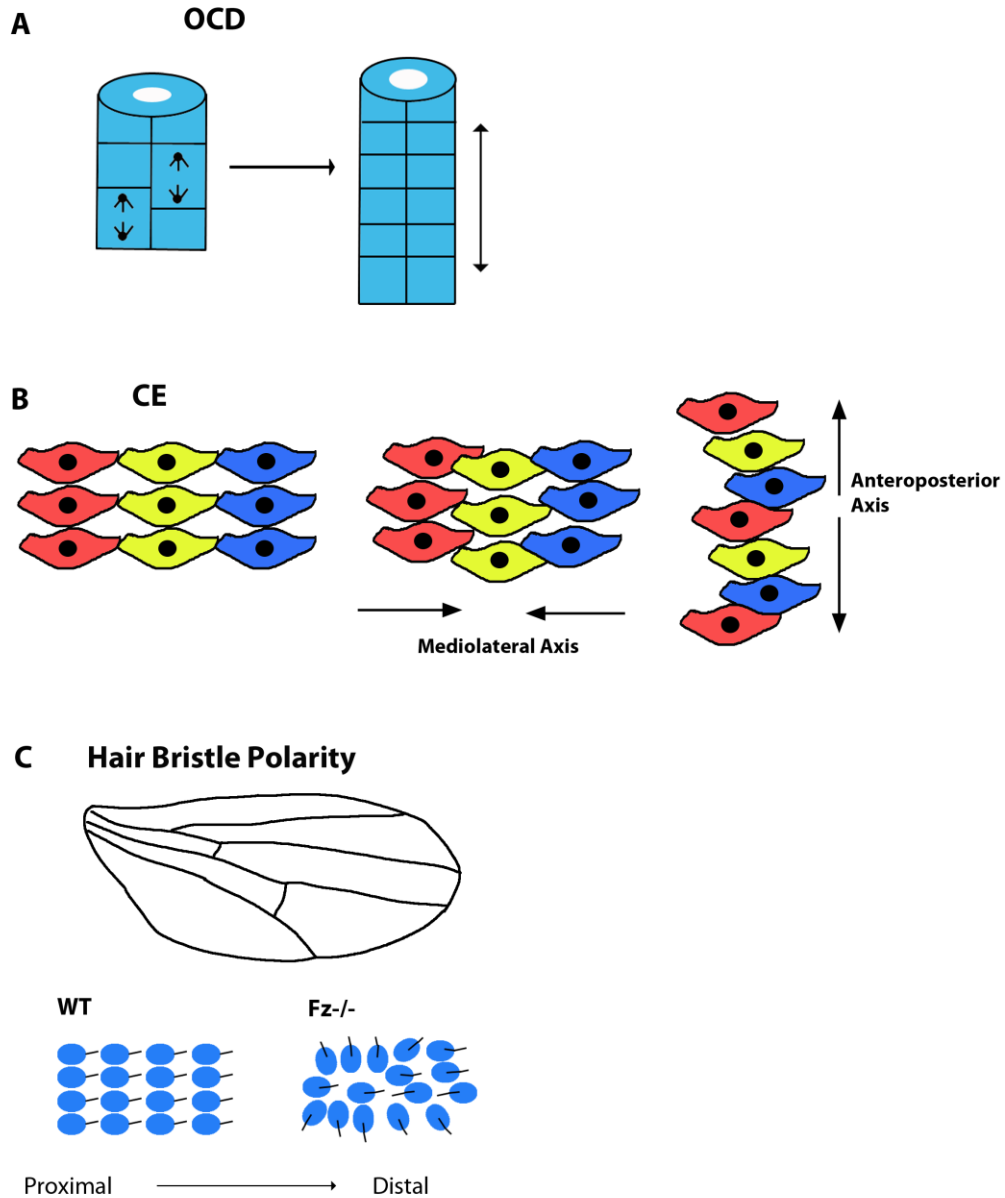
Figure 1.2. Planar Cell Polarity. Sketch diagram depicting oriented cell division which allows growth and elongation of the tissue in the appropriate axis, based on kidney tubules (A). Sketch of cells aligning next to each other and sliding over one another in the mediolateral axis subsequently results in extension of the tissue in the anterior-posterior plane (B). This process is termed convergent-extension (B). Classic example of planar cell polarity is demonstrated by the uniform orientation of the hair bristles on a *Drosophila* wing (C). Cells are represented by blue dots and the hair bristle emerges from the distal end of the cell and points distally (C). Loss of Fz-PCP results in randomisation of the bristle orientation, which emerges from the centre of the cell (C), adapted from Strutt, 2001. CE= convergent-extension, OCD= oriented cell division.

1.2.1.4   Orientation of hair bristles

A classic example of PCP comes from the orientation of hair bristles on the body of *Drosophila* where the hair extends from the distal tip of the cell and points distally (Fig.1.2 C) (Gubb & Garcia-Bellido 1982). Loss of components of the PCP pathway results in a variety of defects such as swirling patterns and extension of the bristle from the centre of the cell (Strutt 2001). PCP signalling also regulates orientation of hairs in mammals. One study reported loss of the PCP signalling component Fz6 results in disruption of orientation of the hair on the feet, head and torso of the mouse (Guo et al. 2004).

1.2.2   PCP signalling pathways; Fz-PCP and Fat-PCP

There are two well-known PCP signalling pathways amongst others that are responsible for mediating planar polarity events. The Fz-PCP pathway which is also known as the core-PCP pathway is most the extensively studied in *Drosophila* as well as vertebrates. The Fat-PCP pathway is well studied in *Drosophila*, however, its role in vertebrate development has only recently emerged.

1.2.2.1   Fz-PCP

The Frizzled (Fz) receptor family are seven-pass transmembrane proteins involved in two different pathways; the canonical Wnt pathway and the non-canonical polarity/calcium signalling pathway (Gao & Chen 2010; Wallingford 2012). These pathways are largely conserved between vertebrates and *Drosophila*. This study will discuss the non-canonical / Fz-PCP pathway.

The key Fz-PCP pathway components include the transmembrane proteins Van Gogh (Vangl1-2), Flamingo/Starrynight (Fmi/Stan/Celsr1-3), Frizzled (Fz) and the cytoplasmic proteins dishevelled (Dsh/Dvl1-3) and Prickle (Pk1-2) (Gao & Chen 2010; Wallingford 2012).

1.2.2.2 Fat-PCP

The Fat-PCP signalling pathway includes *ft* and *ds*, the Golgi kinase *four-jointed (fj),* a transcriptional co-repressor *atrophin* and an atypical myosin *dachs* (Thomas & Strutt 2012; Sharma & McNeill 2013).

In vertebrates, only *Fat4* and *Dchs1* have been linked to PCP, although recent evidence has emerged that the mouse homologue *Atrophin2l* may regulate OCD of kidney tubules in synergy with *Fat4* (Saburi et al. 2008; Mao et al. 2011; Saburi et al. 2012). The role of *Fjx1*, homologue of *Drosophila fj*, is unknown in vertebrate PCP. The role and expression of *Fjx1* will be briefly discussed later (see chapter 7).

The following sections will provide a brief overview of Fat signalling in *Drosophila* and discuss how Fz-PCP and Fat-PCP pathways establish polarity in *Drosophila* and vertebrates.

1.3 Fat signalling in *Drosophila*

The name Fat was given to the gene due to the observation made by Mohr that the thorax and abdomen of *fat (ft)* mutants in *Drosophila* was shorter and wider (Mahoney et al. 1991). A key study reported that *ft* recessive viable and lethal mutations result in excessive growth of imaginal discs and disruption of hair polarity (Bryant et al. 1988). The cells in the epithelium are less columnar and have an abnormal distribution and density of gap junctions. The cells are also less adhesive and although they are able to differentiate, the imaginal discs that form are abnormal in shape and size (Bryant et al. 1988). When mutant imaginal disc cells were transplanted into wildtype imaginal discs, a cell autonomous pattern of overgrowth was observed. The authors proposed that the array of defects showed that *ft* is involved in the control of growth as well as cell adhesion (Bryant et al. 1988) and *ft* was also classified as a tumour suppressor gene (Bryant et al. 1988; Mahoney et al. 1991).

The similar and overlapping phenotypes of loss of *ft* and *ds* prompted studies which revealed they interact with each other and function in the same pathway (Clark et al. 1995; Yang et al. 2002). Ft and Ds were proposed to undergo heterophilic interactions. Cells expressing Ft and Ds form aggregates in culture and Ft/Ds stabilise each other's protein levels at the cell membrane (Ma et al. 2003; Matakatsu & Blair 2004; Matakatsu & Blair 2006). The nature of their interaction and downstream functions was determined by deletion of their respective ICD and ECD (Clark et al. 1995; Matakatsu & Blair 2006). The studies reported that Ft and Ds behave as a receptor and ligand, respectively. It was also reported that the Ft ICD is sufficient for its function in growth and PCP without binding to Ds whereas the Ds ICD can affect growth but requires the ECD for its PCP functions (Matakatsu & Blair 2006). Ds has also been reported to promote phosphorylation of the Ft ICD which plays a role in growth control via the Hippo pathway (Feng & Irvine 2009). On the other hand, Ft also has a posttranslational effect on Ds. Ds protein is subject to proteolytic cleavage within a cell and the level of different Ds isoforms present is influenced by the absence of *ft*. However, the functional significance of this finding is undetermined (Ambegaonkar et al. 2012).

To add another layer of complexity, the role of Four-jointed (Fj), a glycoprotein, was also highlighted. *fj* mutants display minor PCP phenotypes as well as growth and patterning defects in the proximal wing (Villano & Katz 1995; Zeidler et al. 2000; Simon 2004). Although Fj was first shown to have a secreted C-terminal fragment necessary for its function, it was later demonstrated that secretion of Fj is not necessary for its function and it is more active in the Golgi tethered form (Villano & Katz 1995; Strutt et al. 2004). It was proposed that Fj modulates Ft and Ds interactions via post translational modifications (Strutt et al. 2004). This was definitively demonstrated later where Fj was shown to phosphorylate the ECD of Ft and Ds at serine and threonine residues which subsequently affects the binding affinity of Ft and Ds (Ishikawa et al. 2008; Brittle et al. 2010).

As mentioned in previous sections, a related gene *ft-l* was also discovered in *Drosophila*, and its role in imparting planar polarity in follicular cells of the ovary by interacting with actin filaments was highlighted (Viktorinová et al. 2009). The role of *ft-l* is limited to the ovary and will not be discussed further.

Ft, Ds and Fj regulate PCP in the *Drosophila* wing, eye and abdomen amongst other tissues as well as growth of the wing and appendages via the Hippo pathway. The following section will provide an overview of how PCP is established in *Drosophila*.

1.4 PCP in *Drosophila*

1.4.1 Overview and Models

PCP is observed in *Drosophila* in the wing and abdomen through the polarised orientation of hair bristles across the tissues whereas in the eye it is observed by the orientation of the ommatidia. Fz-PCP and Fat-PCP pathways appear to have distinct roles in establishing PCP in these tissues.

In the wing, loss of Fat-PCP signalling produces non autonomous effects on disruption of hair polarity. Loss of Fat-PCP results in polarity reversals and swirling patterns without affecting the asymmetry of Fz-PCP components (Ma et al. 2003). Although the asymmetry of Fz-PCP components is not affected upon loss of Fat-PCP signalling, the pattern of asymmetry is aberrant in these tissues (Strutt & Strutt 2002; Ma et al. 2003).

Loss of Fz-PCP signalling produces both cell autonomous and non-cell autonomous effects on polarity of the hair bristles (Strutt 2001; Strutt & Strutt 2002). It has been demonstrated that there are two temporally uncoupled phases of Fz activity in the wing, an early non autonomous phase and a late cell autonomous phase (Vinson & Adler 1987; Strutt & Strutt 2002). Loss of only the non-autonomous activity of Fz produces swirling pattern, however, the Fz-PCP component asymmetry is intact in the cells. In contrast, loss of cell-autonomous Fz activity produces an aberrant pattern of polarity with the hair bristle emerging from the centre of the cell rather than the distal edge and there is also a loss of asymmetry of the Fz-PCP components (Strutt 2001).

It is proposed that Fat-PCP and Fz-PCP function together at the early phase of Fz activity (Strutt & Strutt 2002). It is suggested that Fat-PCP confers the vector/direction of polarity upon the tissue which is then interpreted by the Fz-PCP pathway. It is interesting to note that there is only a requirement for Fat-PCP signalling in the proximal part of the wing where it provides directional cues to the Fz-PCP components via the asymmetric recruitment of the atypical myosin Dachs (Ambegaonkar et al. 2012; Brittle et al. 2012).

Fat-PCP and Fz-PCP signalling also regulate ommatidia polarity in the eye. Fat-PCP signalling is required throughout the eye tissue in contrast to the wing. Fat-PCP confers global directional polarity cues in the eye which are interpreted by Fz-PCP signalling, however, no molecular link has been uncovered between the two pathways (Yang et al. 2002). The effect of Fat-PCP signalling on the Fz-PCP components is not mediated by Dachs in the eye. Recently it has been proposed that a transcriptional co-repressor Atrophin might be downstream of Ft/Ds in the regulation of ommatidia polarity around the equator of the eye (Fanto et al. 2003; Sharma & McNeill 2013).

In contrast to the observations in the eye and the wing, the abdomen provides insights into the parallel modes of action of the two PCP pathways. Fat-PCP and Fz-PCP pathways act independently in the abdomen to regulate hair bristle polarity. Ft/Ds are able to pattern polarity in the abdomen in the absence of the Fz-PCP signalling whereas in the eye Fat-PCP patterning is dependent on the presence of Fz-PCP components (Casal et al. 2006). Moreover, loss of both the Fat-PCP and Fz-PCP pathways results in an exacerbation of polarity phenotypes in the abdomen demonstrating that the two pathways work in parallel and can compensate for each other (Casal et al. 2006).

Several models have been proposed to explain how the Fat-PCP and Fz-PCP systems propagate polarity through a tissue. Fz-PCP mechanism of action is centred around two main models; the gradient and the vector model (Fig.1.3). The vector model proposes that upstream cues orient the vector of polarity by initiating small polarised differences in Fz-PCP component asymmetry within cells which are then amplified by intracellular and intercellular interactions between the cells (Fig.1.3 A) (Strutt 2001; Chen et al. 2008; Blair 2012).

The gradient model proposes that a gradient of a factor X triggers differences in Fz activity between cells. Neighbouring cells are able to compare their Fz activity using Stan/Fmi and then polarise in response (Fig.1.3 B). There are key questions that remain unanswered in both the models proposed. The identity of factor X is undetermined although it has been proposed that it could be the Ft/Ds signalling gradients. However, Ft/Ds function is not universal and only affects the vector of polarity in discrete regions of tissues (Ma et al. 2003; Blair 2012). Similarly the

vector model does not account for the observation that the apparent disruption of Fz-PCP asymmetry within a cell does not necessarily disrupt the intercellular signalling between the cells (Blair 2012).

Two main models have been proposed for how Fat-PCP signalling propagates polarity; boundary-relay and the gradient model (Fig.1.4). The Boundary relay model is based on steep differences between Ds and Fj activity at a boundary of cells and relies on asymmetric recruitment of Dachs (Thomas & Strutt 2012). This model is one of the favoured models for the proximal wing based on expression patterns of Ds and Fj in the wing and is discussed in detail in the section below (Fig.1.4 C). The gradient model appears to be favoured in the eye and the abdomen of *Drosophila,* and proposes that expression gradients of Ds and Fj result in differential activation of Ft across a tissue. Subsequently, heterophilic interactions occur between Ft and Ds on adjacent cell surfaces. This in turn polarises cells that can compare the levels of Ft/Ds activity on their adjacent surfaces (Fig.1.4 B) (Yang et al. 2002; Matakatsu & Blair 2004; Thomas & Strutt 2012).

Although these models rely on intracellular and intercellular communication, it is still unclear how Fat-PCP signalling interacts with the Fz-PCP cassette at the molecular level. It is likely that the interaction is indirect as no direct molecular link between the two pathways has been uncovered and furthermore, cells in different tissues respond to the same gradient in a different manner.
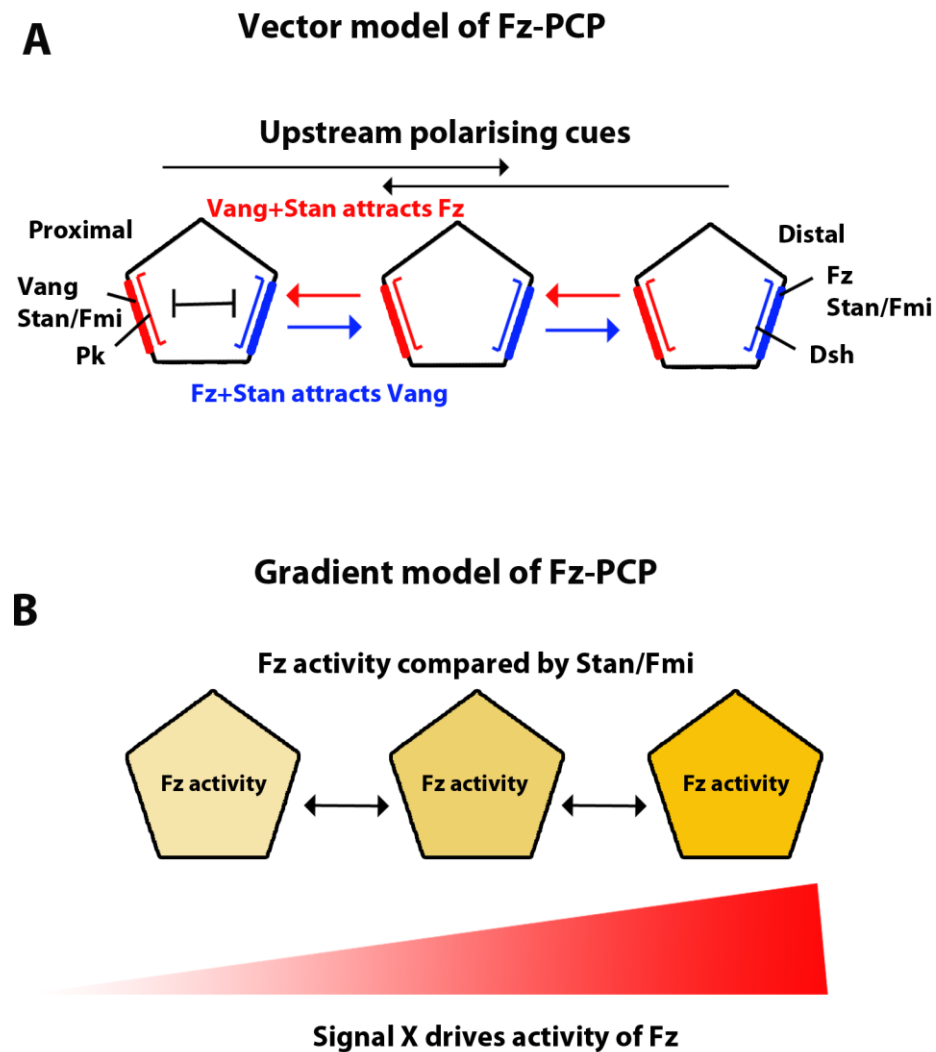
Figure 1.3. Fz-PCP models. The vector model proposes that upstream cues generate slight polarisation/asymmetry of the Fz-PCP components to proximal and distal sides of the cell (A). The core components then amplify these differences across the tissue through intercellular and intracellular attractive and antagonistic interactions (A), adapted from Blair, 2012. The gradient model proposes that a gradient of factor X triggers differences in Fz activity across cells and cells are able to compare their Fz activity using Stan/Fmi and become polarised in response (B), adapted from Blair, 2012.
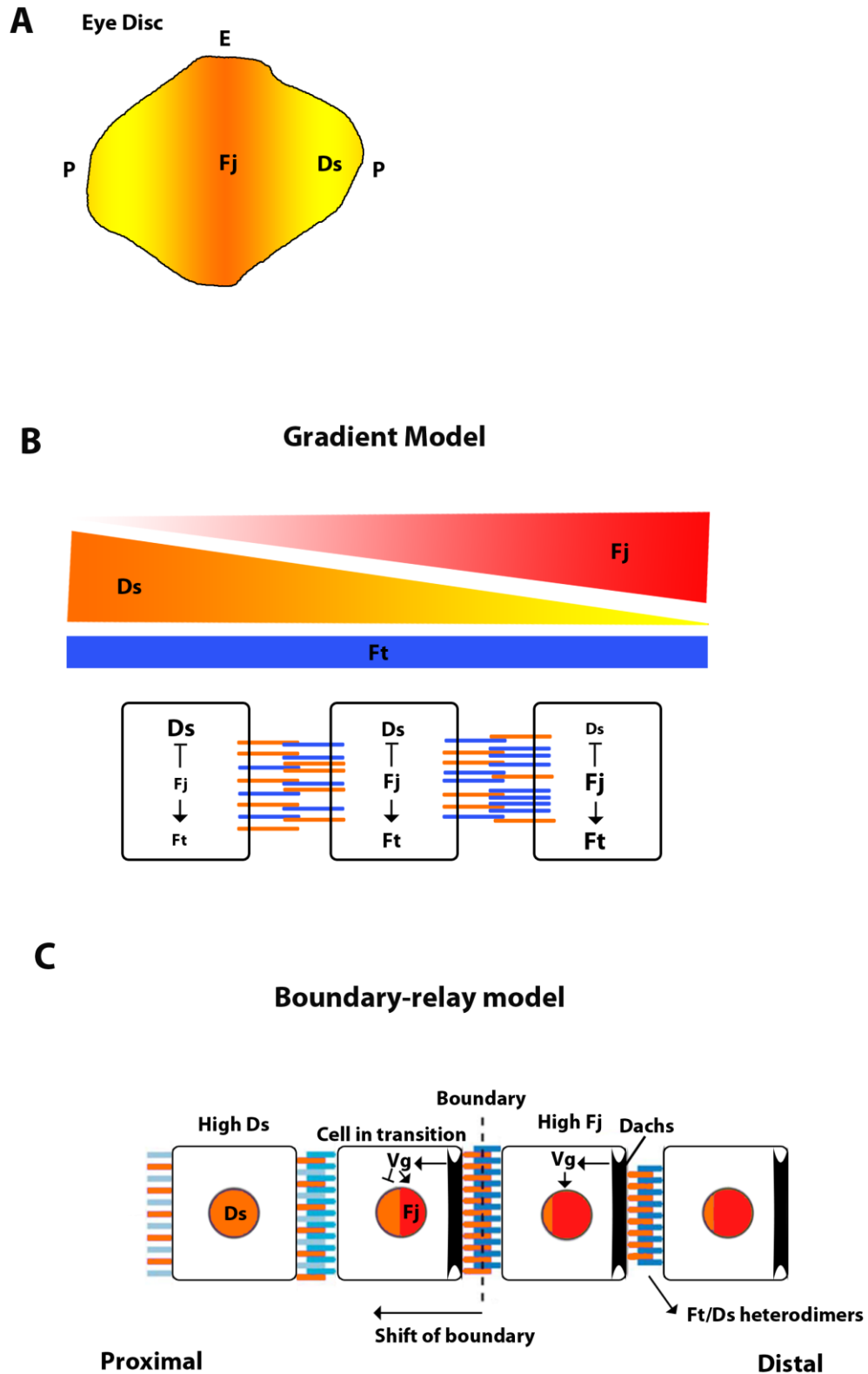
Figure 1.4. Fat-PCP models. Sketch diagram of the imaginal disc of the eye in *Drosophila* (A). Ds (yellow) is expressed at higher levels at the poles whereas Fj (orange) is expressed at higher levels at the equator (A). The gradient model proposes that Fj and Ds are expressed as opposing gradients across a tissue whilst Ft

is expressed uniformly (B). The graded expression of Fj and Ds results in variable activation of Ft across the tissue via heterophilic binding across each cell interface which imparts polarity to cells across a tissue (B), adapted from Lawrence et al., 2008. The boundary relay model proposes that the boundary of Ds and Fj expression results in polarisation of cells at the boundary of Ds/Fj expression. This in turn results in asymmetric recruitment Dachs at the cell surface triggering upregulation of Fj expression via Vg and repression of Ds. This causes the Ds-Fj expression boundary to shift by one cell and the process repeats itself for propagation across the tissue. Ft-Ds interaction weakens as the boundary shifts, however, Dachs asymmetry remains, adapted from Thomas and Strutt, 2012. E= equator, P= pole,Vg= vestigial.

1.4.2   Establishing PCP in *Drosophila*

1.4.2.1   *Drosophila* wing

In the *Drosophila* wing imaginal disc, Ds is expressed at higher levels in the proximal region whilst Fj is expressed at higher levels in the distal region hence establishing an opposing proximal-distal axis of expression. In contrast, Ft is expressed uniformly across the wing disc (Cho & Irvine 2004). The cells of the wing disc produce a trichrome or a hair bristle from its distal edge which points distally. However, before the hair bristle arises, asymmetry of the Fz-PCP components is observed within the cells of the wing (Axelrod 2001; Strutt 2001; Strutt & Strutt 2002). Fz and Dsh, accumulate asymmetrically at the distal side of the cell whilst Fmi accumulates to both sides (Axelrod 2001; Strutt 2001; Strutt & Strutt 2002).

Although both Fat and Fz-PCP signalling establish polarity in the wing, loss of their respective signalling activities produces distinct phenotypes. Mutant clones of *ft* result in a non-autonomous effect on the polarity of the hair bristles with a swirling pattern observed, mostly in the central region of the wing (Strutt & Strutt 2002). Loss of *ft* does not affect production of the hair bristle itself from the distal edge of the cell. In contrast, loss of *fz* in the wing results in a loss of polarity of the hair bristles in the proximal-distal orientation and a swirling pattern is observed with hair bristles appearing at the centre of the cell (Fig.1.2 C) (Gubb & Garcia-Bellido 1982; Strutt 2001; Strutt & Strutt 2002).

It is interesting to note that loss of *ft* only affects PCP in a limited region of the wing and therefore there is not a requirement for *ft* throughout the wing. The same is also true of *fj*, however, generation of *ds* mutant clones disrupts bristle polarity only when a large number of clones are generated, regardless of the position in the wing (Strutt & Strutt 2002).

Loss of *ft*, *ds* or *fj* does not affect the localisation of Fz-PCP components, however, loss of *ft* results in a diffuse localisation of Ds and vice versa without affecting overall protein levels of each other (Strutt & Strutt 2002; Ma et al. 2003). This suggests that Ds and Ft stabilise each other's localisation at the cell membrane. *fj* can also affect localisation of Ft and Ds but only at boundaries of *fj* mutant clones. Ds preferentially localises to the Fj positive cell when it abuts a Fj negative cell and

similarly more Ft becomes localised at the *fj* clone boundary (Strutt & Strutt 2002). Fj modulates Ft/Ds interaction by phosphorylating their extracellular cadherin domains within a cell, which results in altered adhesiveness of Ds and Ft thus affecting their heterophilic binding on adjacent cell surfaces. Fj inhibits the binding of Ds to Ft and promotes the ability of Ft to bind to Ds resulting in variable heterophilic interaction of Ft and Ds across the tissue (Ishikawa et al. 2008; Simon et al. 2010; Brittle et al. 2010).

Although loss of Fat-PCP signalling does not result in abolishment of Fz-PCP asymmetry, the pattern of asymmetry generated is aberrant across the tissue suggesting that Ft signalling might provide global orientating cues to Fz-PCP components indirectly. It has been shown that Fz signals in the wing in two separate phases consisting of an early and a late role. The loss of early Fz activity results in non-cell autonomous effects on hair bristle polarity, similar to the PCP defects observed upon loss of *ft* and *ds,* without disruption of the asymmetry of core components (Strutt & Strutt 2002; Thomas & Strutt 2012). It is proposed that Fat-PCP and Fz-PCP signalling interact at this stage. The loss of late Fz activity results in cell-autonomous disruptions of polarity and a loss of the Fz-PCP components asymmetry (Strutt & Strutt 2002).

More evidence for this temporally coupled interaction of the two pathways comes from a recent study where it is shown that the early Fz signal orientates the posterior ridges of the wing whereas the late signal organises anterior ridges (Hogan et al. 2011). The Ft/Ds system largely affect posterior wing patterning providing another link between the early Fz-PCP signalling to Fat-PCP (Hogan et al. 2011).

A key feature of Fz-PCP signalling is the asymmetry observed within the cells whereas Ft/Ds signalling appears to be dependent on gradients of Ds and Fj expression observed across the tissue. Although reversing the gradient of Ds can result in reversal of polarity in the wing, the uniform expression of Ds and Fj does not result in any major PCP phenotypes (Matakatsu & Blair 2004). The authors propose that Ds acts permissively in this system. It is likely that the Ds gradient is redundant with another polarising cue for most of the wing whereas the Fj gradient appears to have a very minor role in the wing (Matakatsu & Blair 2004).

It is clear that both Fz-PCP and Fat-PCP signalling is required for orientation of hair bristles in the wing. What is not clear is how these signalling pathways impart or propagate this polarity through the tissue. Several models have been proposed to explain their interaction and mechanism of propagation as discussed in the sections above. It is unclear whether Fz-PCP is propagated in this tissue via the gradient or the vector model since there are gaps in knowledge regarding both the models. The preferred model for Fat-PCP propagation in the wing is the boundary-relay model based on the expression of Ds and Fj and the asymmetric recruitment of Dachs within the cells (Fig.1.4 C) (Brittle et al. 2012; Ambegaonkar et al. 2012; Thomas & Strutt 2012).

The boundary-relay model proposes that the high expression of Ds in the proximal wing and high levels of Fj expression in the distal region of the wing result in a boundary at the hinge region where high levels of Ds and Fj are present in cells next to each other. The cells become polarised in response to the Ds and Ft heterodimer formation at adjacent cell surfaces which subsequently results in asymmetric recruitment of Dachs. Dachs is able to upregulate Fj transcription indirectly which causes repression of Ds and moves the expression boundary of Ds and Fj by one cell. This process is repeated and as the expression boundary moves away, Ft-Ds interaction becomes weaker but Dachs asymmetry remains to maintain polarity in the cells (Fig.1.4 C) (Ambegaonkar et al. 2012; Thomas & Strutt 2012; Brittle et al. 2012).

In line with this model, two key studies were carried out to determine the polarity propagation mechanisms used by Fat-PCP signalling. The authors reported a role for Dachs, which functions downstream of *ft,* and becomes asymmetrically localised within each cell. Dachs asymmetry is essential for correct polarisation of Fz-PCP components in the proximal wing and therefore provides a mechanism for robust PCP propagation through Fat signalling (Ambegaonkar et al. 2012; Brittle et al. 2012). In addition, slight asymmetry of Ft and Ds is observed in the cells of the wing where higher levels of Ds are present distally and high levels of Ft are observed proximally. This provides further evidence for a mechanism of Ft-Ds polarity propagation (Ambegaonkar et al. 2012; Brittle et al. 2012).

1.4.2.2 *Drosophila* **eye**

The *Drosophila* eye is divided into a ventral and a dorsal field demarcated by the presence of an equator in the middle. The photoreceptors present in the eye disc form a functional unit called the ommatidium. The ommatidia are polarised units and positioned as mirror images in the opposite fields of the eye (Yang et al. 2002). There is a high level of Ft activity at the equator which is a result of an opposing gradient of Ds and Fj (Yang et al. 2002). The Ds gradient is a consequence of *Wingless (Wg)* expression at the poles which results in high levels of Ds expression at the poles of the eye disc whereas an opposing gradient of Fj, which is high at the equator, fine tunes the Ds gradient (Fig.1.4 A) (Yang et al. 2002; Simon 2004).

Studies in the eye have revealed that cell fate specification and ommatidia polarity are closely linked. The Ds and Fj gradients result in a graded activation of Ft resulting in high amount of Ft activity in the cells at the equator compared to the cells closer to the poles (Yang et al. 2002; Simon 2004). As a consequence of high Ft activity, a higher level of Fz activity is detected in the cells at the equator as well (Yang et al. 2002). The higher level of Ft/Fz activity confers an R3 photoreceptor fate upon the cells at the equator and an R4 fate in the adjacent polar cell. Once this fate is established the ommatidia rotate to generate mirror image polarity in the dorsal and ventral fields (Yang et al. 2002; Simon 2004; Sopko & McNeill 2009).

Loss of *ft* produces non-cell autonomous disruption of ommatidial polarity. Loss of *ft* results in reversal of ommatidia polarity and the fate of R3 and R4 photoreceptors is switched (Yang et al. 2002). Loss of *fz* results in aberrant pattern of ommatidial polarity but a defect in photoreceptor specification is also observed, which is not observed upon loss of Fat-PCP signalling. Therefore, analogous to the wing, Fz-PCP can still function in the absence of Ft signalling albeit with an aberrant pattern of asymmetry of Fz-PCP core proteins (Yang et al. 2002; Simon 2004; Sopko & McNeill 2009).

Ft signalling is required throughout the eye in contrast to the wing and the positional information provided to Fz-PCP in the eye appears to be regulated independently of *Dachs,* unlike the wing (Brittle et al. 2012). Fz has an early non autonomous role in regulating ommatidia polarity, similar to the early activity of Fz observed in the wing (Strutt & Strutt 2002). Fz-PCP is required in order for Fat-PCP signalling to affect

polarity in the eye as Ft is unable to pattern in the absence of Fz (Yang et al. 2002). This suggests that regardless of whether there is a direct interaction between Ft and Fz signalling, polarity in the eye is propagated by Fat signalling through the core PCP components.

Further evidence for Ft/Ds affecting ommatidia polarity comes from altering the gradients of Ds and Fj. Uniform expression of Ds has no effect on polarity, however, uniform expression of both Fj and Ds results in PCP defects in the eye (Matakatsu & Blair 2004; Simon 2004). An ectopic gradient of Ft is also able to largely override intrinsic gradients and cause reversal of ommatidia polarity (Simon 2004). This is in contrast to the wing where uniform expression of both Ds and Fj does not result in PCP defects suggesting the gradients in the wing are sufficient for PCP but not essential (Matakatsu & Blair 2004).

Despite the clear role of Ft/Ds signalling in orchestrating ommatidia polarity across the eye, there is evidence that ommatidia can also polarise in the absence of Ft and Ds. This suggests that there are other cues responsible for organising ommatidia polarity which are unidentified (Brittle et al. 2012). This point is emphasised by suppressing the Hippo pathway target, Yki, in *ft/ds* mutants, which rescues PCP phenotypes in the eye. This suggests that growth control and PCP are tightly interlinked or that Hippo pathway itself might have some input into the PCP pathway (Brittle et al. 2012).

A gradient model of Ft-Ds has been proposed for regulating polarity in the eye. According to the model, gradients of Ds and Fj expression result in a graded activity of the otherwise uniformly expressed Ft. Low levels of Fj expression results in more Ds binding to less Ft whereas higher levels of Fj promotes more Ft binding to Ds on adjacent cell surfaces. The differential heterophilic interaction of Ft and Ds at adjacent cell surfaces polarises the cells in response, which can be propagated across the tissue (Fig.1.4 B).

Although it has been shown in the proximal wing that Ft, Ds and Dachs asymmetry provides a robust mechanism of long range propagation of polarity, this is not the case in the eye. *dachs* is not required for polarity patterning in the eye therefore Ft-Ds gradients must be able to carry out long range propagation either directly or by

relying on another downstream target (Yang et al. 2002; Brittle et al. 2012; Ambegaonkar et al. 2012; Thomas & Strutt 2012).

atrophin has been proposed as a possible candidate. Atrophin can bind to the cytoplasmic domain of Ft and establish PCP in the eye (Fanto et al. 2003). Loss of either *atrophin* or *ft* produces a similar pattern of ommatidia reversals in the eye and the presence of Atrophin confers an R3 fate in cells (Fanto et al. 2003). However, loss of *atrophin* produces polarity defects at the equator with no effect in polar regions of the eye (Sharma & McNeill 2013). The question therefore remains, what is downstream of Ft-Ds signalling in the eye for long range polarity propagation?

1.4.2.3 *Drosophila* abdomen

The abdomen contains a series of segments and each segment is divided into an anterior and a posterior compartment. Ds and Fj are expressed as complementary gradients but the direction of their respective gradients is reversed in the anterior and posterior compartments (Casal et al. 2002; Thomas & Strutt 2012). All the hair bristles point in the posterior direction which means that the cells point up a gradient in one compartment and point down that gradient in the other compartment (Casal et al. 2002). Loss of *fj* only disrupts polarity in the anterior most part of the anterior compartment where the Fj expression is the highest. Loss of *ft* or *fj* have the same polarity reversal phenotypes whereas loss of *ds* mimics *fj* gain of function phenotype (Casal et al. 2002).

In a similar fashion to the eye, expression of morphogens such as Wg and Hedgehog (Hh) are responsible for the Fj and Ds gradients. It is proposed that these genes propagate polarity based on the gradient model suggested in the eye where Ds and Fj activate Ft in a graded fashion and cells are able to polarise by detecting levels of activated Ft and compare the activity of Ft in the neighbouring cells (Casal et al. 2002; Thomas & Strutt 2012).

In the abdomen, Fat-PCP and Fz-PCP operate independently of each other. Unlike the eye, it was observed that loss of *Ft* could repolarise hair bristles in *fz* negative tissue meaning that Fat-PCP does not require Fz-PCP in this tissue (Casal et al. 2006). However, loss of Fat-PCP makes cells more sensitive to Fz-PCP signalling

and loss of both systems results in an exacerbation of the phenotype (Casal et al. 2006). This shows that the two pathways function in parallel and can compensate for each other to an extent in this tissue.

It is proposed that both Fat-PCP and Fz-PCP regulate polarity in this tissue via the gradient model. The Fz-PCP gradient model depends on a gradient of X which defines the vector of polarity by polarising Fz activity. Cells become polarised due to varying levels of Fz activity which can be compared between neighbours by Fmi/Stan homodimers. X could be a diffusible or a non-diffusible factor which can relay information from one cell to another (Fig.1.3 B) (Casal et al. 2006). Although several questions remain unanswered such as the identity of X, it is clear that Fat-PCP and Fz-PCP signalling must incorporate intercellular and intracellular feedback mechanisms to be able to polarise and then repolarise in response to changes in the neighbouring cells.

1.5 Role of Fat in Hippo signalling in *Drosophila*

Elucidating the role of Fat in regulating PCP events in development has been at the forefront of research over the last two decades, however, there are defects observed in *ft* mutants that do not fit into the niche of PCP. These include the aberrant shape of imaginal discs, change in shape and patterning of the wing and several overgrowth phenotypes (Bryant et al. 1988; Sopko & McNeill 2009).

In the wing of *ft* mutants, ectopic expression of Wg is observed in the proximal wing, which is believed to contribute to the overgrowth of the proximal wing (Cho & Irvine 2004). This overgrowth can be partially rescued by overexpression of Dachs, which is a downstream effector of Fat signalling (Cho & Irvine 2004; Mao et al. 2006). Ft activity is required in the proximal wing to represses the expression of Wg through Dachs. This suggests that Ft can act through Dachs not only to affect PCP in the proximal wing but also to regulate growth (Cho & Irvine 2004; Mao et al. 2006; Brittle et al. 2012; Ambegaonkar et al. 2012).

This study amongst others called for the idea that another branch of Fat signalling exists which is distinct from Fat-PCP and regulates growth and patterning. Several studies implicated *ft* in the Hippo signalling pathway which regulates growth and cell death. The Hippo pathway family consists of the kinase Hippo (Hpo), adaptor protein Salvador (Sav), Warts (Wts) kinase and transcriptional co-activator Yorkie (Yki) (Fig.1.5) (Silva et al. 2006; McNeill & Woodgett 2010).

Upstream of this cascade are the cytoskeletal protein Merlin (Mer) and Expanded (Ex) that localise to apical junctions and function redundantly (Fig.1.5) (Silva et al. 2006; McNeill & Woodgett 2010). Hpo phosphorylates and activates Wts, which then phosphorylates and inactivates Yki. Loss of Hippo signalling results in upregulation of both Cyclin E, which causes excessive cell proliferation, and Diap1, which inhibits cell death (Silva et al. 2006; McNeill & Woodgett 2010).

Loss of *ft* also results in increased expression of Cyclin E and Diap1, as observed upon loss of Hippo signalling. Based on a few studies, it was proposed that Ft functions upstream of Ex to regulate the Hippo pathway (Silva et al. 2006). However, it was later proposed that Ft acts in parallel to Ex in the Hippo pathway since loss of both exacerbates the overgrowth phenotype. Furthermore, loss of *ft*

results in overgrowth of tissues despite overexpression of Ex therefore it seems unlikely that *ft* signals through *ex* in the Hippo pathway rather they contribute to the pathway via overlapping yet separate mechanisms (Feng & Irvine 2007).

Loss of *ds* and *fj* also affects growth. Overexpression of Ds results in upregulation of Hippo targets in the imaginal discs of the wing and eye (Willecke et al. 2008). However, this effect was observed at boundaries of Ds overexpression clones where discontinuities in levels of Ds are present. Ds is unable to upregulate Hippo targets without the presence of Ft ECD or Dachs in the wing disc thereby demonstrating that Ds upregulates Hippo targets via Dachs at Ds expression boundaries. Ds is required cell-autonomously to respond to a boundary signal and upregulate the Hippo pathway targets, challenging the view that Ds is a traditional ligand (Willecke et al. 2008; Reddy & Irvine 2008).

Another study also reported that the discontinuities between levels of Fj and Ds promotes proliferation at the cell boundaries in the wing disc, whereas uniform expression inhibits cell proliferation consistent with the boundary model (Rogulja et al. 2008). However, a recent study has presented conflicting findings that Ds ICD engages in a parallel branch of signalling to regulate growth of the wing disc via the Hippo pathway and that this effect is not dependant on Dachs (Degoutin et al. 2013). The role of Ds in regulating growth via the Hippo pathway is more complex than previously believed and Ds is not a traditional ligand to Ft in this context.

A new role for Fat-Hippo signalling in maintaining neural homeostasis of photoreceptor neurons in *Drosophila* was also uncovered. The study revealed that mutations of *ft* or Hippo components result in a block in autophagy and subsequent accumulation of autophagosomes full of debris in the cells (Calamita & Fanto 2011). Ft and Hippo have a neuroprotective role in this context and prevent neurodegeneration. This study reveals a novel role of Fat-Hippo interaction which is not related to growth control.
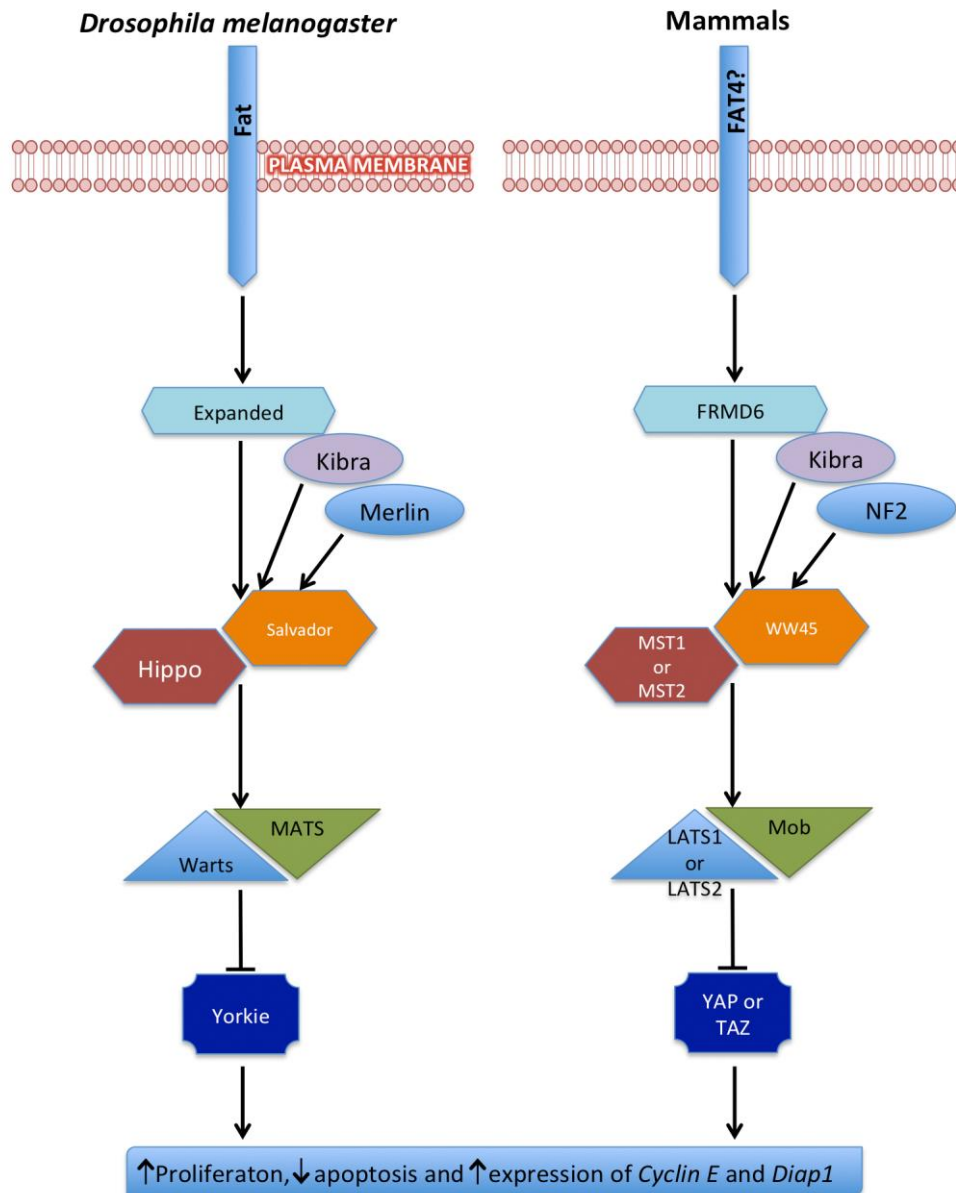
Figure 1.5. Fat and Hippo Signalling. Sketch of the Hippo signalling pathway in *Drosophila* and mammals (A). *Ft/Fat4* functions upstream or in parallel to *Expanded*, *Merlin* and *Kibra* which results in activation of *Hippo/Mst1&2* and subsequent phosphorylation of *Warts/Lats1&2* (A). *Warts/Lats1&2* in turn phosphorylate and inhibit activity of *Yki/Yap/Taz* (A), adapted from McNeill and Woodgett, 2010.

1.5.1 Separating PCP and Hippo signalling

Some studies have attempted to understand how Fat signalling orchestrates PCP and growth and if there is cross-talk between these two branches of Fat signalling. *ft*, *ds* and *fj* control both polarity in the wing as well as polarisation of the microtubules via Dachs for oriented cell division (Yang et al. 2002; Ma et al. 2003; Harumoto et al. 2010). Oriented cell division is essential for control of organ growth and shape and requires polarisation of microtubules thus it was proposed that *ft*, *ds* and *fj* could be regulating both growth and polarity via the same gradient across the tissue (Fig.1.4 B) (Day & Lawrence 2000; Casal et al. 2002; Strutt 2005).

It is proposed that there is a linear gradient across a tissue in which cells have a constant maximum and a minimum at the edges of a tissue and the intermediate cells divide and adopt the values in between. Once the gradient reduces to a certain threshold level it acts as a cue for cells to stop proliferating (Lawrence et al. 2008). This would control the growth in a linear dimension or axis. This means that Fat-PCP would depend on the direction (vector) of the gradient whereas growth via Fat-Hippo would depend on the slope of the same gradient (Fig.1.4 B). The models proposed are by no means complete or free of caveats, for example, mutant clones of *ft* have non-cell autonomous effects on PCP but not on growth via the Hippo pathway, making a linear model of growth and PCP problematic (Lawrence et al. 2008).

A recent study looked at the function of Ft and Ds ECD and ICD to separate their PCP and Hippo activities. Overexpression of Ft ICD was able to rescue the PCP and Hippo phenotypes in *ft* mutant tissue (Matakatsu & Blair 2012). Distinct regions of Ft ICD were identified in this study that are responsible either for PCP or Hippo activity, however, there are regions of the ICD that have an effect on both Hippo and PCP activities (Matakatsu & Blair 2012). The study revealed that the Ft ECD was also able to participate in growth and PCP activities coupled with binding to Ds. Ds ECD and ICD can affect growth via the Hippo pathway in the absence of Ft ICD illustrating that Ds doesn't simply act as a ligand for Ft but could also function as a receptor (Matakatsu & Blair 2012). Another study revealed that certain regions of Ft ICD are phosphorylated to participate specifically in the Hippo pathway whereas a

unique C-terminal motif is responsible for Fat-PCP mediated activities (Pan et al. 2013).

Several studies have demonstrated that the asymmetric localisation of Dachs, which is dependent on Fat signalling, seems to participate in both PCP and growth control at least in the wing (Cho & Irvine 2004; Brittle et al. 2012; Ambegaonkar et al. 2012; Pan et al. 2013). Although structural studies are now providing proof of distinct domains in Ft and Ds being responsible for PCP and Hippo activities, it is clear that these pathways overlap and OCD is an example of how these processes are interlinked. Dachs appears to be a point of convergence for these pathways and further insight into what occurs downstream or in parallel to Dachs will be instrumental in delineating the activities of Fat-PCP and Fat-Hippo even further.

1.6 PCP in vertebrates

1.6.1   Fz-PCP

Several key Fz-PCP components in *Drosophila* are well conserved in vertebrates. Most Fz-PCP components in vertebrates consist of more than one orthologue of the same gene such as *Vangl1-2 (Van Gogh)*, *Celsr1-3 (Flamingo/Starrynight)*, several Fz receptors, *Dvl1-3 (Dishevelled)* and *Pk1-2 (Prickle)*. The Fz-PCP family also includes some Wnt ligands such as *Wnt5a, Wnt9b and Wnt11* that appear to play a role in PCP in vertebrates unlike in *Drosophila* (Wallingford 2012; Tissir & Goffinet 2010).

Fz-PCP signalling plays a role in several PCP processes in developing vertebrates such as convergent-extension during gastrulation and neurulation, OCDs, organisation of the stereocilia of the cochlea as well as neural crest cell (NCC) migration (Deardorff et al. 1998; Jessen et al. 2002; De Calisto et al. 2005; Montcouquiol et al. 2006; Wallingford 2012).

One of the first events that occur in the developing embryo is the morphogenetic movements that drive gastrulation and several components of the Fz-PCP pathway are involved in regulating this process across different vertebrate species. For example in *Xenopus* embryos, *Wnt5a* is expressed at high levels in the ectoderm and at low levels in the mesoderm. Overexpression of Wnt5a in dorsal blastomeres specifically interferes with cell intercalation causing a shortening of the antero-posterior axis and a wider medio-lateral axis of the embryos with no effect on patterning or differentiation of the mesoderm (Fig.1.2 B) (Moon et al. 1993).

Similarly, *Fz8* also plays a role in gastrulation of *Xenopus* embryos. It is expressed in the cells of the Spemann organiser and interference with its normal function by using a dominant negative isoform causes gastrulation defects resulting in a wider body axis (Deardorff et al. 1998).

Kypnek, a proteoglycan that is part of the non-canonical Wnt pathway in zebrafish, polarises cells along the medio-lateral axis during convergent-extension via modulation of *Wnt11* (Topczewski et al. 2001). Loss of *kypnek* results in a failure of convergent-extension (Topczewski et al. 2001).

Studies carried out in mice reported the importance of *Dvl1-2* and *Vangl2* during convergent-extension of the neural plate (Wang et al. 2006). Loss of *Dvl1* and *Dvl2* causes a failure of neural plate elongation because of defective convergent-extension. *Vangl2* genetically interacts with *Dvl2* during neural plate elongation (Wang et al. 2006). Mutations in human *Vangl2* have also been linked to neural tube defects such as anencephaly and spina bifida due to defects in neural tube closure (Lei et al. 2010). The mouse cochlea also undergoes convergent-extension and this process is defective in Fz-PCP mutants causing a shortening of the cochlea (Wang et al. 2006; Rida & Chen 2009). These studies reflect the central role of the Fz-PCP pathway in convergent-extension.

The mouse cochlea has recently emerged as a classic example of PCP as the stereocilia on the hair cells of the cochlea are polarised (Montcouquiol et al. 2003; Montcouquiol et al. 2006). Loss of any of the genes such as *Vangl2*, *Dvl1-2* or *Scribble-1* (vertebrate specific PCP effector) causes loss of polarity in the hair cells of the cochlea. The asymmetry of Fz-PCP components in the mouse cochlea is reminiscent of tissues in *Drosophila*. Celsr1 is required for the asymmetric recruitment of Vangl2 at the proximal edge of the hair cells where it co-localises with Fz3 in the mouse cochlea (Fig.1.6) (Montcouquiol et al. 2003; Montcouquiol et al. 2006).
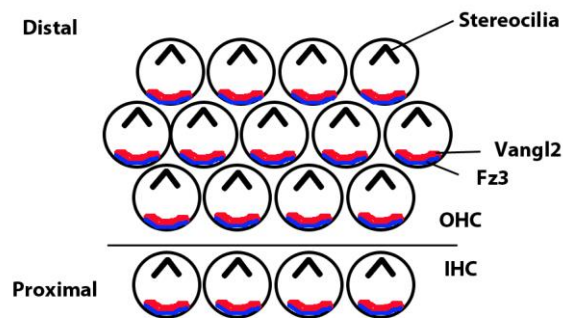
Figure 1.6. Asymmetric localisation of Fz-PCP components in the cochlea. Sketch diagram of an E18.5 mouse cochlea revealing three rows of outer hair cells and one row of inner hair cells. Vangl2 and Fz3 are asymmetrically co-localised at the proximal edge of each cell. The stereocilia/hair are represented by the polarised black V at the distal edge of the cell. Adapted from Montcouquiol et al., 2006. IHC= inner hair cells, OHC= outer hair cells.

Polarised migration of neurons is also regulated by Fz-PCP signalling as in the case of Facial Branchiomotor Neurons (FBNs). Loss of *Celsr1-3*, *Vangl2* and *Scribble* in mice results in an arrest of FBN tangential migration (Vivancos et al. 2009; Qu et al. 2010). Similarly in the zebrafish perturbing the function of Fz3 and Celsr2 results in defective and aberrant FBN migration (Wada et al. 2006). The role of PCP signalling in regulating neuronal migration will be discussed in detail later on (see section 1.8).

One recent study highlighted the importance of *Vangl2* and *Wnt5a* for polarised chondrocyte orientation and limb outgrowth in the mouse. Loss of *Vangl2* and its asymmetry results in wider, thicker and shorter limbs and has been compared to the Brachydactyly type B human disorder, which causes a shortening of the digits (Wang et al. 2011). More importantly, reducing the level of Wnt5a in the *Vangl2* mutant background causes a worsening of the defect and has been linked to the Robinow syndrome in humans (Wang et al. 2011). Wnt5a also orchestrates oriented cell division and polarised proximal-distal elongation of the limb (Gros et al. 2011).

Although no models of polarity propagation have been proposed in vertebrates, recently some studies have provided a molecular/cellular basis of Fz-PCP component asymmetry. One exciting example comes from a study on hair follicles on the mouse skin. The authors reported that Celsr1, Vangl2 and Fz6 asymmetrically co-localise along the anterior-posterior axis of the hair follicles. Loss of these components results in aberrant hair polarity. Furthermore, Celsr1 is required for the asymmetric localisation of Vangl2 and Fz6. Chimeric analysis indicated that Vangl2 plays a non-autonomous role in organising hair polarity (Devenport & Fuchs 2008).

Another study provides an example of Fz-PCP asymmetry in the mouse tissue by illustrating the role of Sec24b, a component of the endoplasmic reticulum (ER) to Golgi transport machinery. Loss of *Sec24b* causes an identical phenotype to that of the *Vangl2*$^{Lp/Lp}$ mice ; a completely open neural tube and polarity defects of the cochlea (Merte et al. 2010). *Vangl2* genetically interacts with *Sec24b* and is preferentially sorted into COPII vesicles. Failure of sorting causes Vangl2 to become trapped in the ER which subsequently results in PCP defects (Merte et al. 2010). It is proposed that the activity of Sec24b is essential for the asymmetry of Vangl2 observed at the plasma membrane. Further studies are required to determine the

mechanism behind Fz-PCP component asymmetry and its functional importance in vertebrates.

1.6.2 Fat-PCP

Although the role of Fat signalling in PCP is relatively undefined in vertebrates, a few key studies have implicated *Fat4* and *Dchs1* in regulating PCP processes. A study carried out in *Fat4*^{-/-} mice reported that loss of *Fat4* results in cystic kidneys due to extremely dilated kidney tubules. The authors reported a randomisation of the mitotic angle of the dividing cells of the tubules inferring that the kidney cysts are a result of a loss of OCD in the tubules (Saburi et al. 2008). The authors also reported a significant upregulation of *Fjx1* expression in the kidney tubules and surrounding tissue upon loss of *Fat4*. Simultaneous loss of *Fat4* and *Fjx1* led to severe cystic defects resulting occasionally in enlarged kidneys (Saburi et al. 2008).

The study implicated *Fat4* in regulating OCD in kidney tubules and that *Fat4* interacts genetically with *Vangl2* in cyst formation by producing an additive phenotype. In further support of a model of Fat-PCP in vertebrates, loss of *Fat4* also results in defective cochlea elongation with subtle defects in cochlea hair polarity (Saburi et al. 2008; Mao et al. 2011).

A key study characterised the *Dchs1*^{-/-} mouse and demonstrated that loss of *Fat4* and *Dchs1* produces identical phenotypes; shorter cochlea, shorter and wider sternum, cystic kidneys, shorter intestine, smaller lungs and atrial septation defects (Mao et al. 2011). Furthermore, loss of both genes does not cause an exacerbation of the phenotypes indicating that they are part of the same signalling pathway. Drawing parallels from *Drosophila*, it could be postulated that *Fat4* and *Dchs1* behave as a receptor ligand pair.

A study carried out in the cerebral cortex of mice also highlighted the relationship of Fat4 and Dchs1 by transfecting the full length constructs into L cells, which lack cadherins. Upon transfection with both constructs, cells formed aggregates in culture and heterotypic interactions took place at cell-cell boundaries of these cells. Furthermore, this study also reported mutual regulation of Fat4 and Dchs1 protein levels (Ishiuchi et al. 2009).

A similar finding was reported by Mao et al that loss of *Dchs1* results in upregulation of Fat4 in the lung and kidney and loss of *Fat4* results in upregulation of Dchs1. This mutual modulation of protein levels occurs post-transcriptionally (Mao et al. 2011).

A more recent study has shed some light upon genetic interactions and synergy between the *Fat* genes in cochlea elongation and polarity as well as formation of kidney tubules. Although no PCP defects have been directly linked to loss of *Fat1-3*, the simultaneous loss of *Fat4* and *Fat1* causes exacerbation of the kidney and cochlea phenotypes. Similarly, loss of *Atrophin2* and *Fat4* also exacerbates the kidney phenotype. Loss of *Fat3* and *Fat4,* however, results in a partial rescue of the kidney defect (Saburi et al. 2012). This study shows that Fat4 interacts with other Fats in a tissue context dependant manner and the function of *Atrophin* seems to be somewhat conserved in regulating PCP.

Evidence of conservation of the PCP activities of *Fat4* and *Drosophila Ft* comes from a study where human Fat4 ICD could rescue PCP defects in wings and abdomen of *Ft* mutants but not the overgrowth phenotypes associated with Hippo signalling (Pan et al. 2013). Although it is evident from these studies that *Fat4* and *Dchs1* are involved in regulating some aspects of PCP in vertebrates, it is unclear how they function and no models have been proposed in vertebrates.

1.7 Role of Fat in Hippo signalling in vertebrates

Loss of *Fat4* and *Dchs1* results in perinatal death of the pups within 48 hours (Saburi et al. 2008; Mao et al. 2011). Although no embryonic overgrowth phenotypes have been reported thus far, it is difficult to study possible overgrowth and cancer phenotypes in adult mice in the context of Hippo signalling.

A study carried out in the neural tube of the chick proposed a link between Fat and the Hippo pathway in regulating proliferation of a subset of neurons. RNAi knockdown of Fat4 results in a modest increase in specific neuronal progenitor pools from the intermediate neural tube, which subsequently results in an increase in differentiated Lim1/Lim2 positive neurons (Van Hateren et al. 2011). RNAi knockdown of Yap along with Fat4 results in a rescue of this phenotype whereas knockdown of Fat4 alone results in decreased levels of phosphorylated Yap (inactive Yap). However, no changes in phosphorylation levels of upstream Hippo components were detected, therefore, it is not clear whether this association reflects the role of *Fat4* in Hippo signalling or an alternative Yap dependent pathway (Van Hateren et al. 2011).

A recent study has implicated Fat4 and Dchs1 in regulating differentiation of a subgroup of cortical interneurons that contribute to the cerebral cortex. It was observed that loss of *Fat4* or *Dchs1* results in an arrest in the radial migration of these neurons due to lack of differentiation and an increase in proliferation. This phenotype was rescued by shRNA mediated knockdown of Yap, implicating the Fat-Hippo pathway in regulating neural differentiation and subsequent radial migration in the cortex. A similar disorganisation of the cerebral cortex is also observed in patients with Van Maldergem Syndrome, which is linked to *Fat4* and *Dchs1* mutations in humans (Cappello et al. 2013).

As is the case in *Drosophila*, PCP and Hippo pathways also appear to intersect in vertebrates. Recently, a study highlighted the role of Hippo signalling in kidney cyst formation. In the renal cysts in $Pkd1^{-/-}$ mice, high levels of nuclear Yap expression was observed which accompanied increased levels of *Fjx1*. This was also true of the human kidneys from patients with polycystic kidney disease. The authors proposed that the upregulation of *Fjx1* in the renal cysts is Hippo signalling dependant (Happé

et al. 2011). This observation suggests that both PCP and Hippo pathways could be acting in parallel to regulate kidney tubule elongation and development.

Further evidence of this is conclusively provided in a recent study by Das and colleagues. The study revealed that Fat4 expression in the stromal cells of the kidney is responsible for the activity of Yap/Taz in a subset of nephron progenitor cells in the kidney (Das et al. 2013). Fat4 promotes expression of differentiation targets and inhibits expression of progenitor renewal targets. It is proposed that Fat4 activity results in inhibition of Yap activity thus resulting in differentiation of progenitors whereas loss of Fat4 results in nuclear Yap/Taz activity which promotes progenitor renewal (Das et al. 2013).

This study provides evidence that Fat4 not only regulates kidney tubule formation by OCD but also maintains the renewal/differentiation of nephron progenitors by controlling Yap/Taz activity.

1.8 Neural Development

1.8.1   Hindbrain development and segmentation

Neurogenesis closely follows gastrulation and is a well-coordinated event which involves complex cell-cell interactions such as convergent-extension and oriented cell divisions. The focus in this section will be on the specification of the hindbrain which occurs just after neural induction.

The embryonic rhombencephalon or the hindbrain is transiently segmented and forms the cerebellum, pons and medulla in the adult brain (Guthrie & Lumsden 1992; Chandrasekhar 2004). The segmented swellings of the hindbrain are called neuromeres or rhombomeres (r) and the hindbrain consists of 7-8 rhombomeres depending on species (Keynes & Lumsden 1989). The identity of the rhombomeres is determined by the Hox genes, which are expressed in overlapping domains along the rostro-caudal axis of the hindbrain (Fig.1.7 A) (Keynes & Lumsden 1989; Gilland & Baker 1993). Retinoic acid is synthesised in the underlying mesoderm of the caudal hindbrain and retinoic acid degrading enzymes are present in the mesoderm underlying the midbrain-hindbrain boundary (Marshall et al. 1992; Niederreither et al. 2000). This results in a rostro-caudal concentration gradient of retinoic acid along the hindbrain which determines the expression of the Hox genes (Keynes & Lumsden 1989; Gilland & Baker 1993).

Each rhombomere contains a distinct population of neurons and the Hox gene expression specifies the identity of these neurons (Fig.1.7 A) (Gilland & Baker 1993). A key example is illustrated in studies where facial branchiomotor neurons (FBNs), which are specified by Hoxb1 expression in r4, are unable to migrate caudally in *Hoxb1*$^{-/-}$ mice and switch to the fate of the trigeminal neurons of r2 (Studer et al. 1996). Conversely, overexpression of Hoxb1 in r2/r3 results in trigeminal neurons, which arise in r2/r3, to switch to the FBN fate (Bell et al. 1999). Altering the retinoic acid concentration gradient by applying ectopic retinoic acid results in misexpression of the Hox genes which also alters neuronal identity (Marshall et al. 1992).

The segmental pattern of the hindbrain and the neuronal populations within rhombomeres are largely conserved across vertebrates such as mouse, chick and zebrafish (Fig.1.7 A) (Gilland & Baker 1993).

Ventral to the rhombomeres are the branchial arches 1-4 and 6. The rhombomeres give rise to neural crest cell populations that migrate into the branchial arches to form the craniofacial skeleton and connective tissue, e.g. neural crest cells from rhombomere 2 migrate into branchial arch 1, rhombomere 4 neural crest cells migrate into branchial arch 2 and rhombomere 6 and 7 contribute to branchial arch 3. Neural crest cells do not exit from rhombomeres 3 and 5 (Lumsden et al. 1991; Köntges & Lumsden 1996). The facial muscles that arise in the branchial arches are the targets of the branchiomotor axons exiting the rhombomeres (Keynes & Lumsden 1989; Guthrie & Lumsden 1992) . There is a correlation between the neural crest migration and cranial nerve axon exit into the branchial arches. For example, both the neural crest cells and the axons from r2 migrate into branchial arch 1 (Graham et al. 1991; Köntges & Lumsden 1996).

1.8.2   Branchiomotor Neurons

There are 12 cranial nerves in the PNS and the hindbrain contains cranial nerve IV-XII. Each cranial nerve consists of subtypes of motor neurons; Somatic motor (SM), Visceral motor (VM) or Branchiomotor (BM) neurons (Fig.1.7 A) (Gilland & Baker 1993; Gilland & Baker 2005; Jacob et al. 2001). The SM neurons innervate the muscles of the eye and tongue, VM neurons innervate the parasympathetic ganglion of the tear glands, sweat glands and smooth muscles whilst the BM neurons innervate the musculature of the face (Jacob et al. 2001; Chandrasekhar 2004).

All BM neuron axons exit the brainstem dorsally via specific cranial nerves to innervate their respective target tissues. BM neurons comprise of the trigeminal neurons, facial neurons, glossopharyngeal, vagus and cranial accessory neurons (Fig.1.7 A) (Keynes & Lumsden 1989; Gilland & Baker 1993; Chandrasekhar 2004). The trigeminal motor axons exit via the fifth cranial nerve (nV) from rhombomere 2 and innervate muscles of mastication. The facial motor axons exit via the seventh cranial nerve (nVII) from rhombomere 4 and innervate muscles of facial expression

in mammals, the stapedius and the posterior belly of digastric. The glossopharyngeal motor axons exit via the ninth cranial nerve (nIX) from rhombomere 6, the vagus motor axons exit via the tenth cranial nerve (nX) from rhombomere 7 and the cranial accessory motor axons exit via the eleventh cranial nerve (nXI) and these cranial nerves innervate muscles of the larynx and pharynx (Keynes & Lumsden 1989; Jacob et al. 2001; Gilland & Baker 1993; Guthrie 2007).

All motor neurons including the BM neurons express the homeobox gene *Islet-1* as soon as they are born in the ventricular layer of the brain (Ericson et al. 1992). For differentiation of BM progenitor neurons to occur, *Phox2a* and *Phox2b* expression is essential, however, *Phox2a* expression is downregulated in late differentiation (Pattyn et al. 2000; Jacob et al. 2001). *Tbx20* is another important transcription factor required for the differentiation and migration of BM neurons (Song et al. 2006).

A common feature of BM neurons, at least in the mouse, is that all the neuronal cell bodies which are born in the ventricular zone at the midline of the neural tube, eventually migrate laterally away from the midline and settle in a dorso-lateral position within the neural tube (Garel et al. 2000; Gilland & Baker 2005; Meléndez-Herrera & Varela-Echavarría 2006).
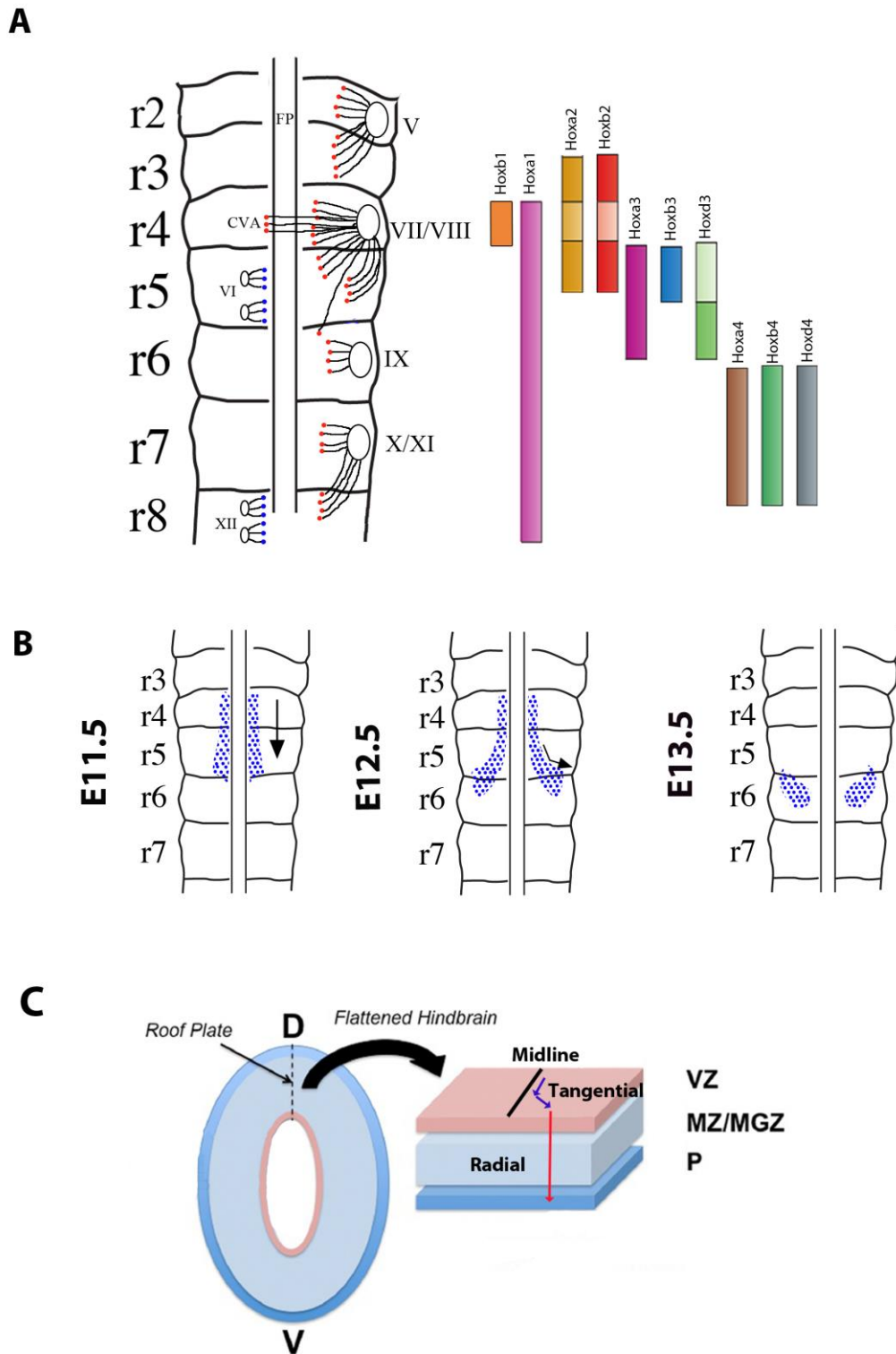
Figure 1.7. Specification of the rhombomeres and migration of the FBNs. Sketch of the flattened mouse hindbrain in an open book conformation revealing position of the branchiomotor and visceromotor neurons depicted in red and somatic motor neurons depicted in blue (A). The position where the axons exit the hindbrain is indicated by a sphere (A) and the nerves are numbered as roman numerals. Each

rhombomere corresponds to expression of a specific set of *Hox* genes (A). *Hox* genes are represented by different colour rectangles next to the rhombomeres in which they are expressed (A), adapted from Guthrie, 2007. Sketch of FBN migration from E11.5-E13.5 (B). FBNs, depicted by blue dots, migrate caudally at the midline on the ventricular surface and reach r6 by E11.5 (B). By E12.5, FBNs initiate a lateral turn and migrate laterally on the ventricular surface in r5/r6 and by E13.5 they can be seen on the pial surface condensing lateral to the midline (B). Sketch of the neural tube illustrating the layers through which FBNs migrate; ventricular, mantle, marginal and pial (C). FBNs are born on the ventricular surface and undergo caudal and lateral tangential migration shown by blue arrows, after which they migrate radially to settle in the pial surface, shown by the red arrow (C). D= dorsal, FP= floor plate, MGZ= marginal zone, MZ= mantle zone plate, P= pial, r= rhombomere, V= ventral, VZ= ventricular zone.

1.8.3 Overview of Neuronal Migration

There are two axes in which migration of the neuronal cell body can occur in the CNS; radial and tangential. Radial migration occurs after the progenitor neurons have divided in the ventricular zone and then migrate through the mantle and marginal zone to finally settle in the outermost layer; the pia (Fig.1.7 C). Radial migration occurs along the apical-basal axis of the neural tube and is aided by the radial glia neurons, which span all the layers of the neural tube and act as a scaffold (Gao & Hatten 1994).

A key example of radial migration and its importance is illustrated by the formation of the cerebellar cortex. The neurons migrate from the ventricular zone aided by radial glia and form the layers of the cerebellar cortex (Altman & Bayer 1985). Aberrant radial migration occurs in the $Reelin^{-/-}$ and $Cdk5^{-/-}$ mice (Ohshima et al. 2002; Rossel et al. 2005). These mice fail to develop the normal layers of the cerebral and cerebellar cortex. The cortical interneurons project dendrites in all directions and fail to undergo directed radial migration. The radial migration of FBNs is also affected in these mice. Reelin appears to be involved in organising the radial glia scaffold and in attaching the radial glia end feet processes to the pial surface (Rossel et al. 2005; Franco & Müller 2011).

Although radial migration is largely responsible for cortical layer formation, subpopulation of neurons also undergo tangential migration which is not dependent on the radial glia. Tangential migration occurs perpendicular to the apical-basal axis or in the planar axis of the neural tube (Fig.1.7 C). In the forebrain, interneurons migrate tangentially from the ganglionic eminences into the layers of the cortex. Another important example of tangential migration is illustrated by the migration of interneurons from the ventricular zone of the cortex into the olfactory bulb (Hatten 2002; Faux et al. 2012).

Several defects in tangential migration have been documented due to alteration of cell adhesion, perturbation of attractive or repulsive forces generated by secreted proteins or loss of PCP signalling. For instance, the repulsive activity of Unc6 and Netrin-1 is required for formation of the cortical layers of the cerebellum (Yee et al. 1999; Faux et al. 2012). Conversely, precerebellar neurons form the inferior olivary nucleus in response to the attractive cues from Netrin-1 (Wingate & Hatten 1999).

Wnt5a, a component of Fz-PCP signalling pathway, is another example of an extrinsic cue which is able to guide FBNs away from the midline towards a region of ectopic Wnt5a expression (Vivancos et al. 2009).

A common feature of neuronal migration in the planar axis is the extension of a leading process from the dendrite in response to the environmental or intrinsic cues. After the protrusion is established in a particular direction, the Golgi complex and centrosome translocate into the leading edge and contractile forces generated at the rear of the cell body allow it to move forward towards the Golgi and the centrosome (Bellion et al. 2005; Faux et al. 2012; Valiente & Marín 2010).

Different pathways are involved in regulation of tangential and radial migration in the CNS. Defective neuronal migration has severe consequences. Aberrant radial migration has been linked to human neurological disorders such as lissencephaly, Alzheimers disease and polymicrogyria whilst defective tangential migration has been linked to Schizophrenia and depression (Valiente & Marín 2010).

1.8.4   Facial Branchiomotor Neurons (FBNs)

In the mouse, the FBNs are born at E10 in the ventricular layer at the midline of r4 and are specified by the expression of Hoxb1 (Fig.1.7 A-B) (Garel et al. 2000). The FBNs initiate a rostral-caudal tangential migration at E10.5 and migrate from r4 to r6 along the midline. By E11.5, the FBNs form a migratory stream spanning r4 and r5 (Fig.1.7 B) (Garel et al. 2000; Studer 2001). As FBNs reach the boundary of r5/r6 they initiate the mediolateral tangential migration and move away from the midline (Fig.1.7 B-C) (Song 2007 + unpublished observations). FBNs are different from other neurons because they migrate tangentially in two parallel planar axes; rostro-caudal and medio-lateral. After the FBNs migrate laterally they also undergo a radial migration; they move from the ventricular layer of r6 and start to condense at the pial surface (Fig.1.7 B-C). Between E13.5-E14.5, the FBNs condense to form nuclei on the pial surface in r6, lateral to the midline (Garel et al. 2000).

In contrast, the FBNs in the zebrafish hindbrain migrate radially first before migrating caudally and mediolaterally (Wada et al. 2006). In the chick, the FBNs do

not migrate caudally but rather arise in r4- r5 and migrate mediolaterally and radially within r4-r5 (Jacob & Guthrie 2000; Studer 2001).

A multitude of factors regulate the tangential and radial migrations of FBNs. Rhombomeres themselves contain important environmental cues that aid migration. This is illustrated by mouse-chick transplantation assays where the r5 and r6 of E8.5 mouse is transplanted into the embryonic st10 chick hindbrain. FBNs in the chick do not undergo caudal migration, however, upon transplantation of the mouse r5/r6 the FBNs in the chick are able to respond to the cues from these rhombomeres and migrate caudally. This highlights the importance of environmental cues for initiation/maintenance of migration (Studer 2001).

FBNs express an array of cell surface molecules as they migrate such as *Tag-1*, *Ret*, *Neogenin* and *Cadherin-8*. *Tag-1* is expressed in the FBNs in r4 and r5 whilst *Ret* is only expressed as the FBNs enter r5 and r6. *Neogenin* and *Cadherin-8* are expressed as the FBNs start radial migration in r6 (Garel et al. 2000). *Nkx6.1* and *Ebf1* are two of several genes that regulate caudal tangential migration of FBNs and control the expression of cell surface markers mentioned above. Loss of either *Nkx6.1* or *Ebf1* results in an arrest of caudal migration and causes premature lateral and radial migration of FBNs (Garel et al. 2000; Müller et al. 2003).

As mentioned earlier, FBN radial migration is also disrupted in the *Reelin$^{-/-}$* and *Cdk5$^{-/-}$* mice (Ohshima et al. 2002; Rossel et al. 2005).

Migration of the FBN axons differs from that of the cell bodies in not only the trajectory but the set of cues they respond to. Although the two processes are largely independent of each other, some overlap has been proposed. For instance, Neuropilin-1 interacts with SEMA-3A to guide facial motor axons whilst it interacts with VEGF-164 to regulate the FBN cell body migration (Jacob et al. 2001; Schwarz et al. 2004; Meléndez-Herrera & Varela-Echavarría 2006).

A recent study in the zebrafish revealed an interdependence of the FBN axon and cell body migration. The authors reported that ablation of the axon of the leading FBN results in a block in caudal migration of the FBN cell bodies from r4-r5 (Wanner & Prince 2013). However, the late migration of FBNs from r5- r6 is not dependent on the axon of the leading neuron (Wanner & Prince 2013). This study

suggests that the migration of cell bodies and axons might be more dependent on each other than previously believed.

Components of the Fz-PCP pathway have been implicated in regulating the caudal tangential migration of FBNs in both mice and zebrafish. Their role in regulating FBN migration is outlined in the section below.

1.8.5   Role of PCP pathway in Neuronal Migration

Tangential migration occurs all over the CNS but the role of the PCP pathway has not been extensively determined in the various regions of the CNS. Recently, however, the role of *Dvl2* and *Vangl2* was established in regulating neuron migration into the olfactory bulb of postnatal mice. Loss of Dvl2 or Vangl2 function results in abnormal neuron morphology and hinders tangential migration of neurons into the olfactory bulb (Hirota et al. 2012).

The role of PCP signalling has been most extensively studied in the regulation of FBN migration. This section will focus on the tangential migration of the FBNs in the hindbrain and the involvement of the PCP pathway in regulating this process.

The majority of studies carried out on FBN migration have been in the zebrafish with a few key studies recently emerging from the mouse model. In the zebrafish, several Fz-PCP components have been implicated in regulating caudal migration of the FBNs; *Fz3a, Celsr2, trilobite/Vangl2, Scribble* and *Prickle1b.*

The *trilobite* mutation, mapped to the *Vangl* locus, results in defective convergent-extension movements during gastrulation and defective caudal migration of FBNs (Jessen et al. 2002). The authors reported both an autonomous and non-autonomous role of *trilobite* on FBN migration and found that the cells were unable to stabilise the polarised protrusions required for directed migration (Jessen et al. 2002). Similarly, another study reported that the cell surface marker *Tag-1*, *Vangl2* and extracellular matrix molecule *laminin* genetically interact with each other to regulate caudal migration of FBNs in the zebrafish. Loss of any of these genes results in a loss of polarised protrusions of the neurons (Sittaramane et al. 2009).

Prickle1b also plays a similar role in regulating caudal migration of FBNs by stabilising the polarised cell protrusions. Although loss of *Prickle1b* results in loss of polarised cell protrusions and defective cell elongation along the migratory axis, the centrosome positioning in the FBNs is not affected in these mutants (Mapp et al. 2010). *Prickle1b* has a cell autonomous role in the FBNs, which is to interpret the cues from the neuroepithelium. However, it was recently demonstrated that *Prickle1b* undergoes a lipid modification for its nuclear activity in the FBNs which might be independent of its role in regulating FBN migration via PCP signalling (Mapp et al. 2011).

In contrast to the role of Fz-PCP components mentioned above, *Celsr2* and *Fz3a* regulate FBN migration by a different mechanism. Celsr2 and Fz3a are essential for maintaining the FBNs near the pial surface during migration in the zebrafish and also for preventing integration of neurons into the neuroepithelial layers. Loss of these genes results in aberrant radial migration and an arrested caudal migration of the FBNs (Wada et al. 2006).

Lastly, a new gene that regulates FBN caudal migration was identified by a genetic screen in zebrafish. *Nhsl1b* is required for the caudal migration of the FBNs. Loss of the human homologue of *Nhsl1b* is responsible for Nance-Horan syndrome which causes mental illness, dental problems and cataracts (Walsh et al. 2011). Nhsl1b binds to the Fz-PCP component Scribble and is expressed in the polarised protrusions of the FBNs. Nhsl1b has a cell autonomous role in executing polarised cell movements of the FBNs and is proposed as a novel PCP effector (Walsh et al. 2011).

Key studies in the mouse have also highlighted the importance of Fz-PCP components in regulating caudal migration of FBNs. For example, $Fz3^{-/-}$ and $Vangl2^{Lp/Lp}$ mutant mice display defects in the caudal migration of the FBNs (Vivancos et al. 2009). *Wnt5a* is expressed as a rostro-caudal gradient in the hindbrain and is also implicated in guiding caudal FBN migration. Although ectopic expression of *Wnt5a* is sufficient to attract the FBNs towards it, loss of *Wnt5a* does not affect FBN migration suggesting a redundant function (Vivancos et al. 2009).

The role of *Celsr1-3* in the regulation of FBN migration is different in the mouse compared to the zebrafish. *Celsr2* and *Celsr3* interact with *Fz3* to regulate the caudal

migration of FBNs (Qu et al. 2010). Loss of *Celsr1,* however, does not affect caudal migration of FBNs but results in a stream of FBNs migrating rostrally into r3 (Qu et al. 2010). A recent study demonstrated that although several components of the Fz-PCP pathway play a role in FBN tangential migration, these effects might be independent of *Dvl* activity since loss of *Dvl1/2* has no effect on caudal FBN migration (Glasco et al. 2012). Interestingly, the rostral migration of the FBNs observed in *Celsr1$^{-/-}$* mutants requires the function of Dvl (Glasco et al. 2012).

Lastly, *Tbx20*, a transcription factor, necessary for tangential migration of the trigeminal neurons as well as FBNs has been proposed to be upstream of the Fz-PCP pathway in regulating caudal migration of FBNs. Loss of *Tbx20* alters the expression of *Fz7*, *Wnt11*, *Vangl1/2* and *Prickle1* and arrests caudal migration of the FBNs (Song et al. 2006).

Although several studies have reported caudal migration defects in FBNs, no defect has been reported in the mediolateral tangential migration of the FBNs.

1.8.6   Role of Hippo pathway in Neuronal Migration

The Hippo pathway has not been directly linked to the regulation of neuronal migration. A recent study highlighted the involvement of Fat4 and Dchs1 in regulating differentiation of a subset of interneurons in the cerebral cortex. Loss of *Fat4* and *Dchs1* results in an increase in proliferation of the progenitor neurons and a decrease in their differentiation which indirectly results in a block in radial migration. This defect was improved upon knockdown of Yap activity implicating a role of Fat-Hippo/Yap signalling in cortical development (Cappello et al. 2013).

1.9   Aims

In *Drosophila*, Fat signalling plays important roles in regulating PCP via the Fat-PCP branch of signalling and growth via the Hippo transcriptional pathway. Fat signalling has recently been the focus of a few vertebrate studies which have implicated this pathway in regulation of PCP in the kidney and cochlea as well as interaction with the Hippo pathway in neuronal differentiation. However, it is largely undetermined whether Fat signalling is involved in any other PCP related events in vertebrates and currently no models have been proposed for Fat-PCP signalling in vertebrates.

Using genetic mouse models, this study aims to;

- Determine the requirement of Fat4/Dchs1 signalling during the development of organs in the craniofacial region including the salivary glands, utricle, cranial bones and the Facial Branchiomotor Neurons (FBNs)
- Elucidate the role of Fat signalling in FBN migration and characterise the mechanism of action by using genetic tools and cellular analyses
- Determine the relationship between the Fz-PCP and Fat-PCP pathways during tangential migration of the FBNs

2   MATERIAL AND METHODS

2.1 General Solutions

All stock solutions were autoclaved and all RNAse free solutions, except SSC, were treated with 0.1% DEPC (Sigma-Aldrich D5758) overnight prior to autoclaving. All recipes listed are for solutions made up to a volume of 1 litre.

1xPBS	100ml of 10X stock (Santa Cruz Biotech SC24946) with 900ml distilled water
1xPBS-T	1xPBS with 0.1% Tween-20 (Sigma-Aldrich P2287)
1xPBS-Tri	1xPBS with 1% Triton-X 100 (Sigma-Aldrich X-100)
TAE	242g Trizma base (Sigma-Aldrich T1503), 57.1ml Glacial acetic acid (Sigma-Aldrich 320099), 100ml 0.5 M EDTA (Invitrogen 15575-020)
5xTBS	24.2g Trizma base, 292.4g NaCl (Sigma-Aldrich S3014), adjust pH to 7.0
1 M Tris-HCl	121.1g Trizma base, add HCl (Sigma-Aldrich H1758) to adjust pH
5M NaCl	292.2g NaCl in distilled water
1M MgCl$_2$	203.3g MgCl$_2$ (Sigma-Aldrich M8266)
5xMAB	58g Maleic acid (Sigma-Aldrich M0375), 43.8g NaCl, add NaOH (Sigma-Aldrich S5881) pellets to adjust pH to 7.5
20xSSC	175.3g NaCl, 88.2g sodium citrate (Sigma-Aldrich W302600), adjust pH to 4.5 with HCl
4% PFA	40g paraformaldehyde (Sigma-Aldrich P6148) dissolved in 1000ml of PBS at 65^{0}C, pH 8.0

2.2 Animals

2.2.1 Handling and Breeding

All mouse lines were maintained on a mixed C57BL/6 and 129/Sv background. CD1 embryos were used for electroporation experiments. Conditional lines were based on the Cre-LoxP system driven with specific promoters. All tamoxifen (Sigma-Aldrich T5648) injections were given at E10.5. For timed matings, the day of the plug was counted as embryonic day 0.5 (E0.5).

Table 2.1. Mouse lines used in experiments

Mouse lines	References
$Fat4^{-/-}$	Exon 3 deleted (Saburi et al. 2008)
$Dchs1^{-/-}$	Exon 2 deleted (Mao et al. 2011)
$Fat4^{-/-}$ $Dchs1^{-/-}$	Generated in Francis-West's lab
$Fjx1^{-/-}$	(Probst et al. 2007)
$Dchs1^{fl/fl}$	Generated in Kenneth D. Irvine's lab
$Fat4^{fl/fl}$	Generated in Helen McNeill' lab
Gt(ROSA)26Sor^{tm1Sor}	(Soriano 1999)
Islet1 $^{tm1 (cre) Sev}$	(Yang et al. 2006)
Hoxa3 $^{tm1(cre)Moon}$	(Macatee et al. 2003)
Gt(ROSA)26Sor$^{tm4(ACTB-tdTomato-EGFP)Luo}$	(Muzumdar et al. 2007)
Gt(ROSA)26Sor$^{tm1(cre/ERT2)Tyj}$/J	(Ventura et al. 2007)

2.2.2 Embryo Collection and Processing

Mice were culled using a schedule 1 method of cervical dislocation. Embryos were collected and dissected in sterile PBS and kept on ice. Fresh tissue was used for genotyping. Embryos were transferred to 4% PFA and kept at 4^0C for 6-18 hours for use in histology, immunohistochemistry or *in situ* hybridisation. Alternatively, embryos were fixed in 95% ethanol for use in skeletal preparations.

2.3 Histology

2.3.1 Tissue Processing

Embryos fixed in 4% PFA for 18 hours were washed in sterile PBS, twice for 15 minutes at room temperature. Samples were transferred through a series of ethanol (VWR 101077Y) dilutions for 45 minutes each in 50% ethanol/PBS, 70% ethanol/water, 80%, 85%, 90%, 95% and100%. Samples were dehydrated twice in 100% ethanol and then transferred to histoclear (AGTC Bioproducts HS-200) twice for 30 minutes. Samples were processed into wax and kept at 65^0C for at least an hour with 2-3 wax changes. Samples were orientated with needles until the wax solidified. Once cool, samples were mounted onto a wooden block and sectioned on a microtome at a thickness of 10 microns (μm). Sections were mounted on glass slides (Solmedia MSS 10810) for immunohistochemistry and histology or Superfrost plus slides (Thermo Scientific 4951PLUS) for *in situ* hybridisations. Sections were mounted in DEPC water and slides were left on a 45^0C heating rack overnight.

2.3.2 Haematoxylin and Eosin staining

Tissue slides were dewaxed in histoclear twice for 10 minutes and then rehydrated through a series of ethanol dilutions at 100%, 90%, 70%, 50% and then distilled water for 2 minutes each. Slides were stained in Ehrlich's Haematoxylin (Solmedia HST003) for 10 minutes and washed under running water for 10 minutes. After another wash in distilled water, slides were treated with 0.5% acid alcohol for 15 seconds (1% HCl and 0.5% Acetic acid -VWR 20104.323) and stained with 1% Eosin (Solmedia HST101) for 3 minutes before being washed in distilled water again. Slides were dehydrated through a series of ethanol dilutions at 90%, 95% and 100% x 2 for 2 minutes each. Slides were left to air dry in the fume hood for 20 minutes and mounted with coverslips using DPX (Solmedia REA201) mountant. Slides were baked in a 45^0C oven overnight before being photographed.

2.3.3   Sirius red and Alcian blue trichrome staining

The same protocol as described above was used to carry out the staining on tissue slides. The Haematoxylin and Eosin solutions were replaced with Haematoxylin, Sirius red and 1% Alcian blue. Acid alcohol was replaced by phosphomolybdic acid.

2.3.4   Alkaline Phosphatase staining

Slides were dewaxed in histoclear for 5 minutes. Sections were rehydrated through an ethanol series in 100%, 95% and 70% for a minute each. Sections were washed in 1xTBS with 0.1% Triton X-100 for 10 minutes. A 100µl of staining solution, containing a 50X dilution of NBT-BCIP (Roche 11681451001) in NTMT (2.5ml of 2M Tris-HCl pH 9, 2.5ml of 1M $MgCl^2$ and 1ml of 5M NaCl in 50ml of water) was added to each slide. The solution was left on for 15 minutes in the dark and then slides were washed in TBST for 10 minutes. This was followed by a wash in distilled water for 10 minutes. Slides were counter stained in 1% Alcian blue (Sigma-Aldrich A3157) solution with 0.5% acetic acid for 10 minutes and excess stain was removed by 2-3 washes in distilled water. Slides were mounted and coverslipped in Aquatex mounting medium (Merck Millipore 108562).

2.4   Immunohistochemistry

2.4.1   Whole-mount

Hindbrains were washed four times in PBS-Tri for an hour each, after being fixed in 4% PFA overnight. Samples were incubated in blocking buffer made up of 10% horse serum (Invitrogen 26050-088) in PBS-Tri for one hour at room temperature. Primary antibodies were diluted in blocking buffer at the following concentrations:

Mouse anti-Islet (DSHB 39.4D5) 1:150

Rabbit anti-Golgi (Abcam 24586) 1:500

Goat anti-GFP (Abcam 5450) 1:500

Chick anti-β-galatosidase (Abcam 9361) 1:200

Mouse anti-Myosin VI (from Mathew Kelley) 1:500

Samples were incubated with primary antibodies on a shaker at 4^0C for 5 days followed by five washes in PBS-Tri for an hour each. Secondary antibodies were added in the blocking buffer at the following concentrations:

Donkey anti-Mouse 594 (Invitrogen A21203) 1:200

Donkey anti-Rabbit 488 (Invitrogen A21206) 1:200

Donkey anti-Goat 647 (Invitrogen A21447) 1:200

Goat anti-Rabbit 635 (Invitrogen A31576) 1:200

Phalloidin 647 (Invitrogen A22287) 1:100

Samples were kept at 4^0C on a shaker for 3-4 days and then washed five times in PBS-Tri for an hour each. Samples were mounted on slides in Vectashield anti-fadent mountant (Vector labs H-1000) under 22 x22 mm glass coverslips (Menzel-Glaser BB022022A1) with dots of vaseline in the four corners on top of which the coverslip was placed.

For wholemount immunostaining of utricles, samples were washed in PBST (0.1% Triton) for 1 hour and then blocked in 10% goat serum in PBST (0.1% Triton) instead before proceeding with overnight primary antibody incubation. The utricles were subsequently washed and mounted as described above.

2.4.2   Neurofilament staining

This staining was carried out to visualise axonal migration in embryos. E11.5 embryos were fixed in 4% PFA overnight at 4^0C. Samples were washed in PBS overnight and then bleached in Dent's bleach (90% Dent's fix-80% methanol-VWR 20847.307 and 20% DMSO Sigma-Aldrich 472301 and 10% hydrogen peroxide Sigma-Aldrich H1009) overnight at 4^0C. Embryos were washed five times in methanol the next day for an hour each and incubated in Dent's fix overnight. Samples were washed three times in PBS for an hour each and placed in a primary antibody staining solution (75% PBS, 20% DMSO and 5% heat inactivated goat

serum) with mouse monoclonal Anti-Neurofilament antibody (a gift from Dr. Ivo Liebram) at 1:500 dilution for 3 days at 4^0C. Embryos were washed in PBS five times for an hour each and secondary antibody solution (Goat Anti-Mouse 568 at 1:200 in the primary antibody block) was added and kept on for 2 days.

Embryos were washed five times in PBS for an hour each and then transferred into 50% PBS 50% methanol solution for an hour. This was followed by three washes in methanol for an hour each and then embryos were transferred into 50% methanol and 50% BABB (Benzylalcohol Sigma-Aldrich 305197 and Benzylbenzoate Sigma-Aldrich B6630 1:1 mix fresh) solution for an hour. Finally, embryos were cleared in BABB for 1 hour and photographed using a Zeiss dissection microscope followed by scanning on the Leica Confocal microscope.

2.5 Skeletal Preparations

Embryos were fixed in 95% ethanol for 2 days and the skin, stomach, gut, and lungs were removed by dissection. Embryos were stained in 1% Alcian Blue for a week at room temperature on a shaker. Samples were transferred into 1% KOH (Sigma-Aldrich P1767 1g in 100ml water) for 2 weeks until all remaining skin and organs were digested. Samples were stained with Alizarin Red (Sigma-Aldrich 122777) for 4 hours followed by several washes in distilled water. Samples were left in distilled water overnight and then transferred into a 20% KOH/Glycerol solution for a week to remove excess stain. This was followed by an ethanol/glycerol dilution series and samples were processed through the dilutions for 2-3 days and finally into 80%glycerol/20% ethanol.

2.6 Optical Projection Tomography (OPT)

P0 salivary glands were fixed in 4% PFA overnight at 4^0C and then rinsed in PBS three times for 5 minutes. They were stained for 20 minutes in 1% Alcian blue and then washed thoroughly in PBS all day until the excess dye had washed off and only the sublingual gland remained blue. Salivary glands were embedded in 1% low melting point agarose (LMPA) and washed in 100% methanol with four changes

over two days. Salivary glands were then cleared in BABB (2 part Benzyl Benzoate to 1 part Benzyl Alcohol) for 16 hours. The specimens were then super glued to magnetic rods which were immersed in BABB in the OPT scanning chamber and scanned under UV and white light channels.

2.7 *In situ* Hybridisation

2.7.1 Whole-mount

Embryos were washed in PBS after PFA fixation and transferred into 100% methanol and stored at -20^0C. For *in situ* hybridisation, embryos were rehydrated into 75%, 50% and 25% methanol in PBS for 5 minutes each. Samples were then washed three times in DEPC PBS for 5 minutes. Samples were bleached in 20% hydrogen peroxide for 30 minutes and then washed three times in PBS for 5 minutes. Proteinase K 10mg/ml (Sigma-Aldrich P2308) was used to permeabilise samples (E11.5 hindbrain: 5 minutes, E12.5: 6 minutes and E13.5: 7 minutes, E14.5: 9 minutes). Samples were washed three times in PBS for 5 minutes and then refixed in 4% PFA for 20 minutes.

Washing in PBS was repeated three times and then hybridisation buffer (50% formamide VWR 24311.320, 5mM EDTA pH8 Sigma-Aldrich 93283, 0.5% CHAPS Sigma-Aldrich C9426, 100µg/ml Heparin Sigma-Aldrich H3393, Total Yeast RNA 50µg/ml Roche 10109223001, 5X SSC pH4.5 and 0.5g of blocking reagent Roche 11096176001, topped up to 50 ml with DEPC water) was warmed at 65^0C and added to the samples. Samples in hybridisation buffer were incubated at 65^0C for 2-4 hours. Fluorescein or Dig-labelled antisense probes (see section 2.8.5) were added to the hybridisation buffer at a concentration of 1ug/ml and the samples were incubated overnight at 65^0C.

Washing buffers I (50% formamide, 2X SSC and 0.1% Tween-20) and II (solution I and MABT 1:1) were made up in DEPC water and warmed up at 65^0C. Samples were washed in buffer I twice for an hour each. Samples were then washed in buffer II for 15 minutes at 65^0C. Samples were washed in MABT at room temperature twice for 30 minutes each and blocked in blocking buffer (10% blocking reagent and

20% goat serum in MABT) for one hour at room temperature. Antibody (Anti-Dig AP Roche 11093274910, Anti-Fluorescein AP Roche 11426338910 1:2000) made up in MABT block was added and samples were incubated overnight at 4^0C. Samples were washed six times in MABT the next day, every hour, and left washing in MABT overnight. Samples were washed twice in NTMT for 15 minutes each the next day. The developing reaction was then carried out in the dark in NTMT with BCIP and NBT for Dig labelled probes and BCIP only for fluorescein labelled probes at 0.3µl/ml + 2mM levamisole at room temperature and monitored until the colour developed to a desirable level. Samples were then fixed in 4% PFA at 4^0C overnight and then transferred into PBS before being flat mounted and photographed or processed further for sectioning. For double whole-mount *in situs*, alkaline phosphatase was activity was quenched by heat inactivation in MAB at 65^0C for an hour and then the samples were blocked again and incubated overnight with anti-Dig or anti-fluorescein antibody. Subsequent washing and staining steps were carried out as detailed above.

2.7.2 Sections

Slides were dewaxed in xylene for 30 minutes, twice, followed by rehydration through an ethanol series in 100%, 95%, 90%, 70%, and 30% for 10 minutes each. Slides were washed in PBS for 10 minutes and then fixed in 4% PFA for 20 minutes before being washed in PBS with glycine (Sigma-Aldrich G8898) for 5 minutes. This was followed by two washes in PBS and digestion in Proteinase K for 10 minutes at 37^0C. Slides were washed again in PBS for 5 minutes and refixed in 4% PFA for 5 minutes. After another 5 minute PBS wash, slides were transferred into 0.1 M triethanolamine (TEA Sigma-Aldrich 90278) with HCl and Acetic Anhydride (Sigma-Aldrich 242845) and shaken vigorously for 10 minutes. Slides were washed in PBS and then DEPC water for 5 minutes each.

Slides were transferred into a humidifying chamber and incubated with hybridisation buffer at 65^0C for 2-4 hours and then incubated with antisense RNA and sealed with parafilm. Slides were incubated at 65^0C overnight. The next day, slides were washed in solution I (50% formamide, 5X SSC and 1% SDS) twice for 30 minutes at 65^0C. This was followed by a one hour long wash in TNT (10mM Tris HCL pH7.5, 0.5M

NaCl, 0.1% Tween-20) at 37^0C with ribonuclease (Sigma-Aldrich R6513). Slides were then washed in solution II (50% formamide, 5X SSC and 0.2% SDS) twice for 30 minutes at 65^0C. Two 30 minute washes in MAB at room temperature were followed by blocking of slides in blocking buffer (2% blocking reagent with 20% goat serum in MABT) for one hour at room temperature. Blocking buffer was replaced by anti-DIG labelled antibody in block and slides were incubated overnight at 4^0C. Slides were washed in MABT the next day 4-5 times for 30 minutes each. Slides were then washed twice in NTMT for 15 minutes each. NTMT with NBT and BCIP (0.3 µl /ml) was then added to the slides and slides were kept in the dark and monitored until sufficient level of staining had developed. Slides were washed in 5XTBST and then washed in distilled water before being mounted and coverslipped in aquatex mountant.

2.8 Molecular Biology

2.8.1 Transformation of competent *E.Coli*

50-500ng of plasmid DNA to be transformed was aliquoted and kept on ice. DH5-alpha cells (Invitrogen 18265017) were thawed on ice and 30µl was used per reaction. Plasmid was added to the competent cells and kept on ice for 10 minutes before being heat shocked at 42^0C for 45 seconds. Sample was placed back on ice for 20 minutes and then 300µl of LB Broth (Sigma-Aldrich L2542) was added and the sample was left shaking at 37^0C for 40 minutes for recovery. 100µl of the sample was then spread out onto agar plates (Sigma-Aldrich L2897) made up with the relevant antibiotic for selection (e.g. Kanamycin or Ampicillin at a stock concentration of 50mg/ml). Plates were incubated at 37^0C overnight.

2.8.2 Mini Preparation of Plasmid DNA

Colonies of bacteria were individually picked using a pipette tip. The tip was then placed in a 15ml sterile falcon tube with 5ml of LB broth containing the relevant antibiotic. The falcon tubes were left shaking at 37^0C overnight at 225rpm. 2ml of the overnight culture was centrifuged at 13000 rpm for 2 minutes. All the subsequent

steps were carried out using the buffers from Qiagen mini prep kit (Qiagen 27106). The resulting pellet of bacterial cells was resuspended in 250µl of RNAse free Buffer P1. This was followed by the addition of 250µl of Buffer P2 for cell lysis. Tubes were inverted 4-6 times and then 350µl of Buffer N3 was added to neutralize the lysis reaction and tubes were inverted again to mix everything. A cloudy precipitate formed and the samples were centrifuged for 10 minutes at 13000 rpm. The supernatant was transferred to mini spin columns. Columns were centrifuged for 1 minute and then washed with 750µl of Buffer PE. Columns were centrifuged again for 1 minute and the supernatant was discarded. 50µl of nuclease free water was added to the spin column which was then centrifuged for 1 minute to collect the DNA in an eppendorf.

2.8.3   Gel Electrophoresis of DNA and RNA

To make a 1% agarose gel, 1g of agarose (Sigma-Aldrich A5304) was dissolved in 100ml of 1X TAE buffer (50X stock from 242g Trizma base, 57.1ml acetic acid, 100ml 0.5 M EDTA, top up to 1000 ml with distilled water) by heating the solution in the microwave until the agarose dissolved. The agarose solution was then allowed to cool for 2 minutes before 2.5µl of ethidium bromide (Sigma-Aldrich E1510) was added. The gel was poured into a gel tray with combs in place and allowed to cool and set. Once set, the gel was transferred into a gel tank and the combs were removed. DNA/RNA samples were diluted with water and a 6X loading dye (Fermentas R0611).The gel was run at 120 volts for 20-40 minutes and then visualised under UV light to detect DNA or RNA bands.

2.8.4   Restriction Enzyme Digestion of Plasmid DNA

To setup a 50µl digestion reaction, 44µl of the relevant DNA plasmid (1-2µg) was used. Depending upon which enzyme (all from Promega) was used, a corresponding buffer was added at 10% of the volume to the DNA sample. 2µl of the relevant enzyme was added to the reaction and the eppendorf was placed at 37^0C overnight. An aliquot of DNA was run on a gel the next day to check for linearization. The reaction was cleaned by adding 50µl of phenolchloroform (Sigma-Aldrich P3803)

and vortexed to mix it thoroughly. The samples were centrifuged for 2 minutes and the aqueous phase of the sample was pipetted up carefully and transferred into a new eppendorf.

To precipitate the DNA, absolute ethanol was added to the DNA (1:1 ratio) and 3M sodium acetate (Sigma-Aldrich S2889) pH5.2 was added at 10% of the volume of DNA. The sample was stored at -20^0C for 1 hour before being centrifuged for 15 minutes at 13000 rpm to pellet the DNA and the supernatant was carefully decanted. An additional ethanol wash was performed with double the original volume of ethanol. Samples were centrifuged again for 15 minutes and the supernatant was decanted into waste. The pellet was left to air dry for 10 minutes before being dissolved in 50µl of nuclease free water.

2.8.5   Transcription of Linearized Plasmid DNA

Transcription reactions were setup at 37^0C for 2-3 hours at a total volume of 20µl. The following are the list of reagent and quantities used per reaction;

5X transcription buffer (Promega P1181): 4µl

DTT (Promega P1171): 2µl

Dig (Roche 11277073910) or Fluorescein (Roche 11685619910) NTPs: 2µl

DEPC water: 6µl

DNA: 4µl (100-500ng)

T3 (Roche 11031163001), T7 (Roche 10881767001), or SP6 (Roche 11487671001) polymerase: 1.5µl

RNAse inhibitor (Roche 03335399001): 0.5µl

An aliquot of the reaction was run on a gel to confirm the presence of RNA and then samples were incubated for 10 minutes with 1µl of RNAse free DNAse (Qiagen 79254) at 37^0C. Samples were precipitated and washed with ethanol and sodium acetate as described above (see section 2.8.4). The riboprobe was resuspended in 50µl of nuclease free water and stored at -20^0C.

Table 2.2. Plasmids used for *in situ* hybridisation

DNA plasmid	Antisense Probe	Reference
Rat Islet-1	HindIII and T7	Made by Thomas Jessell, sold by Addgene cat. # 16268
Tbx20	HindIII and T7	(Kraus et al. 2001)
Ret	SalI and T3	(Pachnis et al. 1993)
Cadherin-8	BglII and T7	(Korematsu & Redies 1997)
Hoxb1	XbaI and T7	(Wilkinson et al. 1989)
EphA4	XhoI and T7	(Gilardi-Hebenstreit et al. 1992)
Neogenin	NotI and Sp6	(Keeling et al. 1997)
Sema3A	EcoRI and T7	(Meléndez-Herrera & Varela-Echavarría 2006)
Fat4	EcoRI and T3	Made in Kenneth D. Irvine lab
Dchs1	EcoRI and T7	Made in Kenneth D. Irvine lab
Fjx1	EcoRI and T3	Made in Kenneth D. Irvine lab

2.8.6 PCR Genotyping

Ear clips from post-natal mice or tail clips from embryos were collected in individual eppendorfs and digested at 56^0C overnight in 100µl of Direct Lysis PCR buffer (Viagen 402-E) and 5µl of Proteinase K (10mg/ml stock concentration). The following day samples were incubated at 80^0C for 45 minutes and the PCR reaction was set up to a total volume of 20µl per sample using the following reagents from the GoTaq Hot start polymerase kit (Promega M5001):

5X Flexi green buffer: 4µl

Nuclease free water: 12.5µl

MgCl: 1.2µl

Primers: 0.5µl of reverse and 0.5µl of forward

Nucleotide mix (Promega C1141): 0.15µl

Go Taq enzyme: 0.15µl

DNA: 1µl

The reaction was setup with an annealing temperature of 59^0C for 33 cycles.

Table 2.3. Primer sequences used in PCRs for genotyping

Gene	Primer Sequence	Product size
Fat4 WT Forward	GAGGATAAATATCACCATCAG	1-1.3 kb WT
Fat4 WT Reverse	GGCAGTGATTGGTGCCAGTAGTCATTT	
Fat4 Neo Forward	GCGGTGTAAGCTCAATCGATCGACCTT	1.4 kb Neo
Fat4 Neo Reverse	CGCAGCGCATCGCCTTCTAT	
Fat4 Flox Forward	GAGTGCAACAAGATATGGTGGC	0.45 kb flox 0.3 kb WT
Fat4 Flox Reverse	TACAGGGAACAAAGGTGCTGAG	
Dchs1 WT Forward	CCCCCAGACATTCTCAGCCCTTCTTCTA	0.67 kb WT
Dchs1 WT Reverse	CACAGGGCCAGCAGCTCATCCATTT	
Dchs1 Mutant Forward	CCCCCAGACATTCTCAGCCCTTCTTCTA	0.6 kb Mut
Dchs1 Mutant Reverse	GCTGGGCTTACAGTGCTGAGCAATGAT	
Dchs1 left lox-p sites	Dchs1 WT primers	0.77 kb Loxp 0.67 kb WT
Cre Forward	CCTGGAAAATGCTTCTGTCCG	0.39 kb Cre
Cre Reverse	CAGGGTGTTATAAGCAATCCC	No band -cre negative
R26R WT Forward	AAGTCGCTCTGAGTTGTTAT	0.55 - 0.6 kb WT
R26R WT Reverse	GGAGCGGGAGAAATGGATATG	
R26R Positive Forward	AAGTCGCTCTGAGTTGTTAT	0.3 kb R26R
R26R Positive Reverse	GCGAAGAGTTTGTCCTCAACC	
Tomato WT and Mut Forward	CTCTGCTGCCTCCTGGCTTCT	0.33 kb WT 0.25kb Tomato
Tomato WT Reverse	CGAGGCGGATCACAAGCAATA	
Tomato Mut Reverse	TCA ATG GGCGGGGGTCGTT	

2.8.7   RNA extraction from hindbrain

RNA extraction was carried out by using TRIzol reagent (Invitrogen 15596-018). Hindbrains were isolated by dissection in PBS and each hindbrain was placed in an eppendorf with 200µl of TRIzol. Cells were lysed by pipetting up and down until no clumps of tissue were visible. 40µl of Chloroform (Sigma-Aldrich 288306) was added to the homogenised lysate in an eppendorf. The eppendorf was inverted and mixed and then centrifuged at 12000 rpm for 10 minutes at 4^0C to get phase separation of the lysate.

The upper aqueous phase contains the RNA which was pipetted up carefully into a new eppendorf. 100µl of isopropanol was added to the samples followed by centrifugation at 12000 rpm for 10 minutes at 4^0C. The supernatant was carefully decanted from the eppendorf and the RNA pellet was washed with 200µl of 75% ethanol by mixing with a vortex and then centrifugation at 7500 rpm for 5 minutes at 4^0C. The supernatant was decanted and the pellet was air dried for 10 minutes. Nuclease free water was used to dissolve the pellet at volume of 10-30µl.

2.8.8   cDNA synthesis

RNA that was isolated from TRIzol extraction method was quantified using a Nanodrop machine. The subsequent steps were carried out using a Precision Nanoscript Reverse Transcription Kit (Primer Design RT-nanoscript). The annealing reaction was setup in PCR tubes using 200ng of RNA template, 1µl of random nanomer primers and the total volume was made up to 10µl using nuclease free water. The reaction was heated at 65^0C for 5 minutes and then kept on ice. For the extension step, 2µl of the 10X nanoscript buffer, 1µl of dNTPs, 2µl of DTT, 4µl of nuclease free water and 1µl of nanoscript enzyme was added to each PCR tube. The final 20µl reaction was then heated to 55^0C for 20 minutes. Heat inactivation of the reaction was then carried out at 75^0C for 15 minutes. 0.2µl of DNAse free RNAse was added to each reaction which was then incubated at 37^0C for 15 minutes. The cDNA was stored at -20^0C.

2.8.9   Quantitative Polymerase Chain Reaction (QPCR)

QPCR was carried out by using the Precision real-time PCR MasterMix with SYBR green (Primer Design). The reaction was setup on an ice block in triplicate for each primer pair per sample. In Rotor-Gene style tubes (Starlab I1402-0400), 10µl of Precision MasterMix, 0.5µl of Forward and Reverse Primers (10µmol), 2µl of cDNA template, 7.5µl of nuclease free water was added. Samples were loaded into Qiagen Rotor-Gene Q machine and QPCR program was setup using a 2-step melt curve. All analysis was carried out by using the Delta-delta CT method.

Table 2.4. QPCR Primers

Dchs1 Forward	GGCCTGCCTCCTTTAGTCTC
Dchs1 Reverse	TGTCAGCATCTGTGGCTGTT
GAPDH Forward	AGGTCGGTGTGAACGGATTTG
GAPDH Reverse	TGTAGACCATGTAGTTGAGGTCA

2.9 Ex Vivo Electroporation

E11.5 CD1 embryos were collected and dissected in PBS. Embryos were transferred into Leibovitz15 media (Invitrogen 11415-049) and the 4th ventricle was filled with a DNA construct (co-electroporated with a GFP construct at 1µg/µl 1:1) mixed with 0.2µl of Fast green dye and 0.1µl of glycerol (Sigma-Aldrich F7258). CUY650P3 electrodes (Sonidel) were used with a CUY21 electroporator (Sonidel). The embryos were electroporated at 20 volts for a 50ms pulse repeated 5 times with a gap of 950ms between each pulse. The electrodes were place on either side of the 4th ventricle for lateral targeting and were placed at a slanted angle for medial targeting.

Table 2.5. DNA constructs used for electroporation

Fat4 Expression construct	pCA-IRES-Neo backbone (Ishiuchi et al. 2009)
Dchs1 expression construct	pCA-IRES-Neo backbone (Ishiuchi et al. 2009)
GFP PCAX construct	pCAX vector backbone driven by chick β-actin promoter with a CMV enhancer (Swartz et al. 2001)

2.10 Hindbrain Explant Cultures

The following reagents were used to setup cultures;

24 well plate Costar Fischer filters (3422)

Neurobasal medium (Invitrogen 10888-022)

L15 medium

Laminin (Invitrogen 23017-015) 1:330

GDNF (R&D Systems 512-GF-010) 1:1000

Glutamax (Invitrogen 35050079) 1:100

Antimycotic antibacterial (Invitrogen 15240-096) 1:100

B27 supplement (Invitrogen 17504044) 1:50

Filters were incubated with 200 µl of laminin solution at 37^0C for an hour. Dissection of E11.5 hindbrains was done in L15 media and all mesenchyme was removed. Wells were blotted on tissue and then 340µl of media was added per well. Hindbrains were orientated pial side up and cultured for 48 hours at 37^0C. GFP expression was visualised using a Leica stage microscope and hindbrains were fixed in 4% PFA for 5 hours before proceeding with wholemount immunolabelling (see section 2.4.1).

2.11 Gelatine Embedding and Vibratome Sectioning

After wholemount *in situ* hybridisation, samples were embedded in 20% gelatine (Sigma G9382, made up in PBS and dissolved at 65^0C). Samples were incubated in gelatine in plastic moulds at 65^0C for 20-30 minutes and then cooled on ice whilst orientating. Once the samples had set, the blocks of gelatine were trimmed and fixed in 4% PFA with 10% glutaraldehyde (Sigma-Aldrich G5882). Blocks were stored in this solution at 4^0C overnight or longer and then sectioned using a vibratome (Leica VT1000S) at 40 µm thickness.

2.12 Microscopy/Photography

All imaging was done using a Zeiss Stemi SV11 dissection microscope in brightfield and darkfield, Zeiss Axiocam Mrc5 stage microscope, Leica inverted microscope and a Leica Confocal TCS SPE microscope.

2.13 Image Analysis and Statistical Tests

The Rayleigh test was performed to analyse the distribution of the Golgi complex angles. Rayleigh test determines whether a data set has a uniform distribution (not polarised) or a biased distribution (polarised). A value of $p<0.05$ indicates significant polarisation (Mardia & Jupp 2000). The Mardia-Watson-Wheeler test was carried out to determine if the Golgi complex angle distribution was significantly different between mutants and wildtypes. A value of $p<0.05$ indicates a significant difference (Mardia & Jupp 2000). Cell shape analysis was carried out by Cell profiler software using the elliptical measure tool. Quantification of RNA and protein expression across tissues was done by using ImageJ software using the line plot tool. Golgi orientation was determined by calculating angles using Photoshop CS3 using a virtual protractor and angles were plotted onto rose plots.

2.14 N numbers for experiments

All experiments carried out in this study have been repeated with three different mutant embryos of either $Fat4^{-/-}$ and/or $Dchs1^{-/-}$ (N≥3) and the corresponding wildtypes from the same litter for comparison. QPCR analysis was carried out with N=3 and set up as technical triplicates. Details of wildtype and mutant embryo analysis are provided in a table in the appendix.

3 CHARACTERISATION OF CRANIOFACIAL DEFECTS IN *FAT4*^{-/-} AND *DCHS1*^{-/-} MUTANTS

3.1 Introduction

Fat signalling plays an important role during development of several organs of the trunk. Apart from the cochlea, the role of *Fat4* and *Dchs1* has not been analysed in the craniofacial region. A basic characterisation was carried out to determine the roles of Fat signalling in craniofacial development. This included analysis of branching organs, the utricle of the inner ear, skeletal differentiation of bones and the migration of facial branchiomotor neurons (FBNs) in the hindbrain. Following the preliminary analysis, the regulation of FBN migration was chosen as the main focus of the study and will be introduced and discussed later on in subsequent chapters.

Loss of *Fat4* or *Dchs1* results in dilated kidney tubules and formation of cysts. Fat signalling is required for kidney branching and tubule elongation and regulates oriented cell divisions (Saburi et al. 2008; Mao et al. 2011). Similarly, the lung, which is also a branching organ, is significantly smaller in *Fat4*^{-/-} and *Dchs1*^{-/-} mutant mice compared to the wildtype littermates (Mao et al. 2011). These studies illustrate the importance of Fat signalling in development of branching organs. To determine if Fat signalling plays a role in development of other branching organs, the submandibular and sublingual salivary glands were analysed in the *Fat4*^{-/-} and *Dchs1*^{-/-} mutant mice.

Loss of Fat signalling also results in convergent-extension defects of the cochlea and minor disruption of hair cell polarity in the cochlea (Saburi et al. 2008; Mao et al. 2011). Similar defects are observed in Fz-PCP mutant mice with more severe polarity disruption in the cochlea (Montcouquiol et al. 2003). There is also a requirement for *Vangl2* in regulating polarity of hair cells of the utricle in the inner ear (Warchol & Montcouquiol 2010). To further investigate the role of Fat signalling in the development of the inner ear, analysis of the hair cell polarity of the utricle was carried out in *Fat4*^{-/-} mutants.

Another consequence of loss of Fat signalling is the aberrant ossification pattern observed in the sterna and the split vertebral disks in the *Fat4*^{-/-} and *Dchs1*^{-/-} mutant

mice (Mao et al. 2011). Given the effect of loss of Fat signalling on bone forming tissues in the trunk, a characterisation of the craniofacial bones was carried out in the *Fat4*$^{-/-}$ and *Dchs1*$^{-/-}$ mice.

3.2 Results

3.2.1 Loss of *Fat4* and *Dchs1* results in decreased ossification of facial bones

To investigate if *Fat4* and *Dchs1* are involved in bone formation in the craniofacial region, skeletal preparations were carried out on *Fat4*$^{-/-}$ and *Dchs1*$^{-/-}$ P0 pups. The heads were stained with Alizarin red to visualise bone and Alcian blue for cartilage (Fig.3.1 A-F, Fig.3.2 A-C). Analysis of the *Fat4*$^{-/-}$ and *Dchs1*$^{-/-}$ P0 heads revealed a defect in the palatine bone, which together with the premaxilla, forms the roof of the mouth (Fig.3.1 A, C, E). In the *Fat4*$^{-/-}$ and *Dchs1*$^{-/-}$ mice, the palatine bone is smaller and does not extend towards the midline and fuse as in wildtype mice (dashed in black, Fig.3.1 A', C', E'). The defect in the growth and fusion of the palatine bones can be classified as a submucosal cleft palate which is completely penetrant in the *Fat4*$^{-/-}$ and *Dchs1*$^{-/-}$ mice. Another striking defect was observed in the frontal, parietal and interparietal bones of the skull vault (Fig.3.2 A-C). Loss of *Fat4* and *Dchs1* causes a reduction in the size of the frontal, parietal and interparietal bones of the skull vault resulting in enlarged fontanelles (dashed in black, Fig.3.2 A-C).

In addition, the mandible is also shorter in the *Fat4*$^{-/-}$ and *Dchs1*$^{-/-}$ mice, however, the patterning and overall morphology are normal (Fig.3.1 B, D, F). Loss of *Fat4* and *Dchs1* results in identical phenotypes indicating that they function in the same pathway. Furthermore, simultaneous loss of *Fat4* and *Dchs1* recapitulate the phenotype of the single mutants (Fig.3.1 G-H). Loss of *Fjx1*, however, has no effect on bone ossification and the cranium and mandible of *Fjx1*$^{-/-}$ mutants are comparable to that of the wildtype animals (Fig.3.1 A-B, I-J).

To evaluate when the defect in the bones arises, skeletal preparations were carried out at two different time points (Fig.3.3). The palatine bone starts to form by E15.5 (Fig.3.3 A, A'). The palatine bone of the *Dchs1*$^{-/-}$ embryos appears smaller and dysmorphic at this stage (Fig.3.3 A, A', C, C'). The mandible also appears slightly shorter but not dysmorphic (Fig.3.3 B, D). The development of the basoccipital and the pterygoid bones is comparable in the wildtype and *Dchs1*$^{-/-}$ embryos (Fig.3.3 A, C). By E16.5, the palatine bone in *Dchs1*$^{-/-}$ embryos appears smaller but similar in shape to the palatine bone in wildtype embryos (Fig.3.3 E, E', G, G'). The mandible of the *Dchs1*$^{-/-}$ embryos is also smaller in comparison to the wildtype mandible.
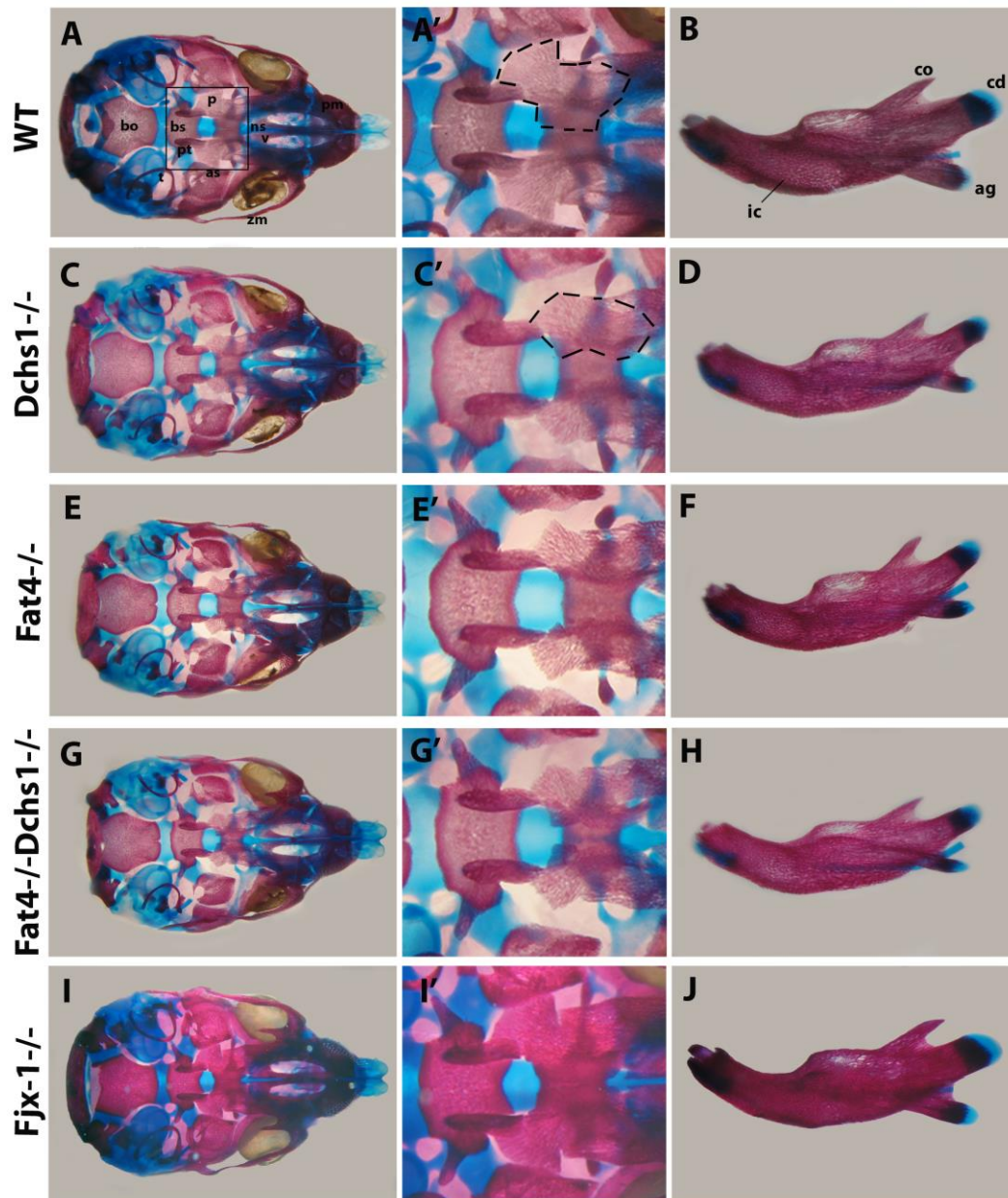
Figure 3.1. Loss of *Fat4* and *Dchs1* results in a submucosal cleft palate. Skeletal preparations of wildtype (A-B), *Dchs1*^{-/-} (C-D), *Fat4*^{-/-} (E-F), *Fat4*^{-/-}*Dchs1*^{-/-} (G-H) and *Fjx1*^{-/-} (I-J) P0 pups. The heads were viewed from the base of the cranium (A, C, E, G, I) which revealed an ossification defect of the palatine bone in the *Dchs1*^{-/-} and *Fat4*^{-/-} mice (C, E) and an identical phenotype in the double *Fat4*^{-/-}*Dchs1*^{-/-} mice (G). The *Fjx1*^{-/-} mice appeared completely normal (I-J). High magnification images of the palatine bone outlined in black (A', C', E', G', I') revealed smaller bones with no fusion in the midline in the *Dchs1*^{-/-}, *Fat4*^{-/-} and *Fat4*^{-/-}*Dchs1*^{-/-} mice (A', C', E', G').

The mandible of the *Dchs1*^{-/-}, *Fat4*^{-/-} and the double mutants also appeared smaller, however with normal processes (B, D, F, H). *Fjx1*^{-/-} mice had normal mandibles (J). ag= angular, as= alisphenoid, bo= basoccipital, bs= basisphenoid, cd= condylar, co= coronoid, ic= incisor, ns= nasal septum, p= palatine, pm= premaxilla, pt= pterygoid, t= tympanic, v= vomer, zm= zygomatic arch.
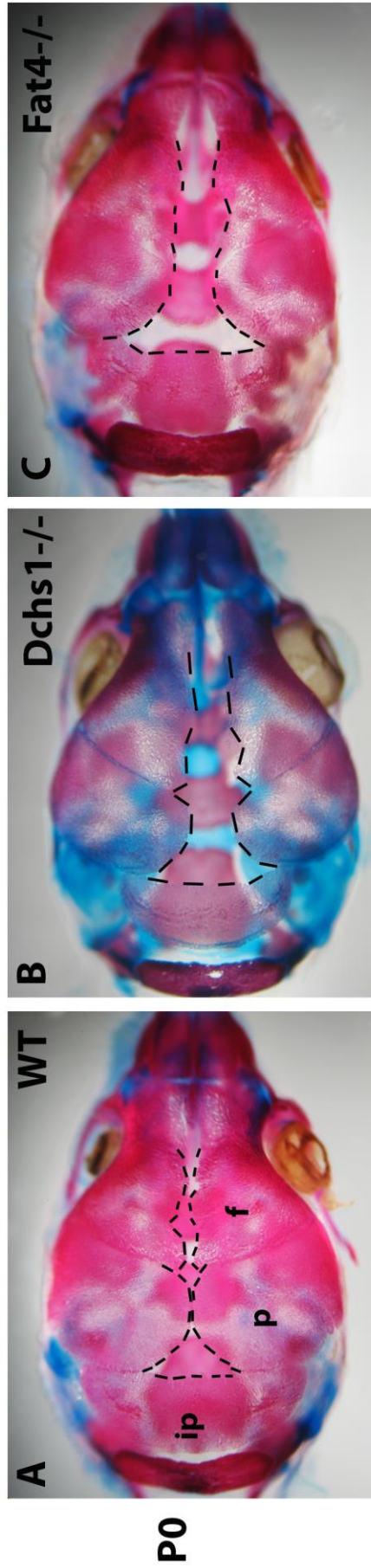
Figure 3.2. Loss of *Fat4* and *Dchs1* affects bones of the cranial vault. Skeletal preparations of P0 heads of wildtype (A), *Dchs1*^{-/-} (B) and *Fat4*^{-/-} (C) mice viewed from the top of the skull vault. The frontal, parietal and interparietal bones of the skull vault appear smaller in the *Dchs1*^{-/-} (B) and *Fat4*^{-/-} (C) mice compared to the wildtype (A). The sutures between these bones, outlined in black, appear very wide in the *Dchs1*^{-/-} (B) and *Fat4*^{-/-} (C) mutants. f= frontal, ip= interparietal, p= parietal.
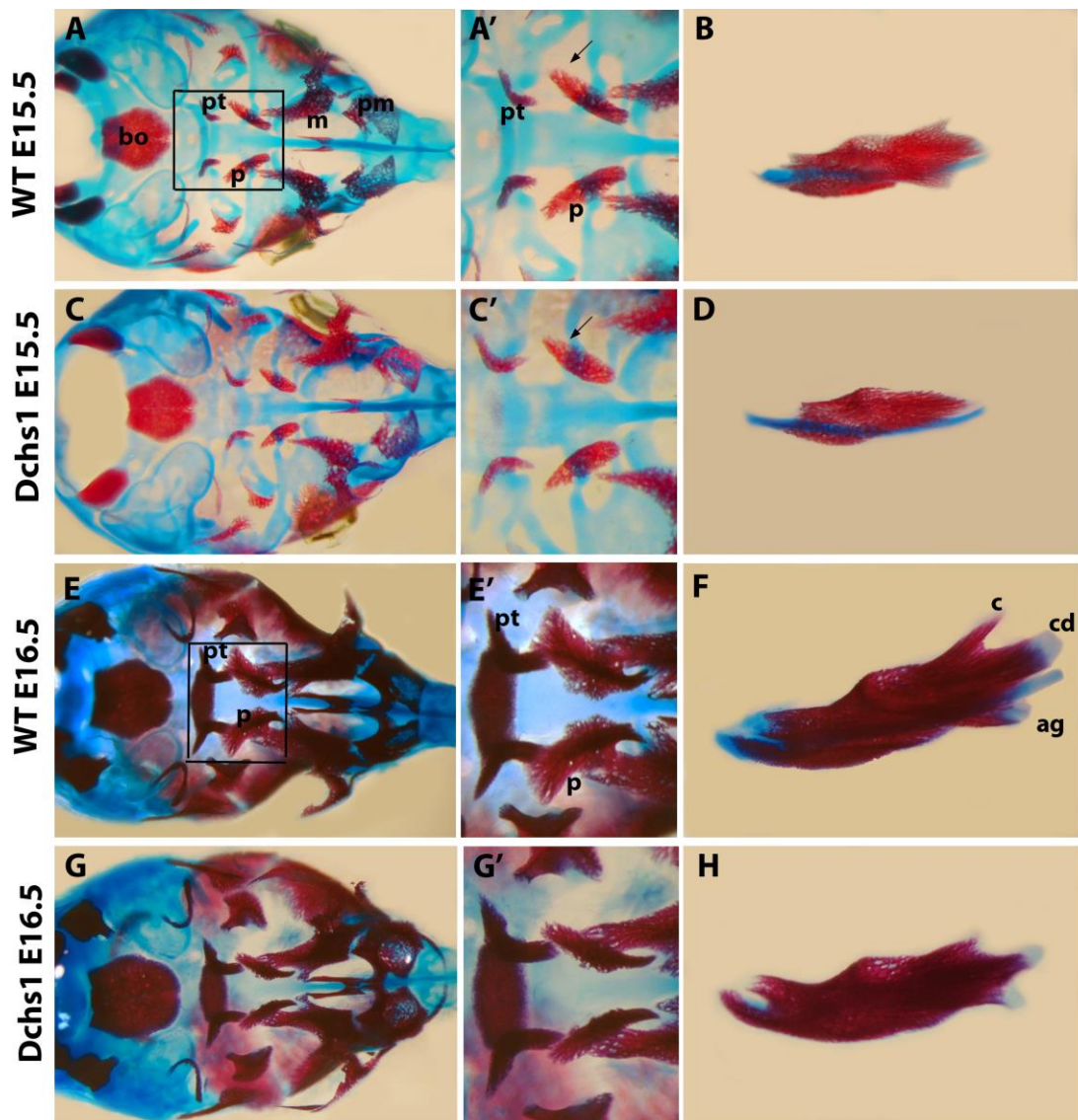
Figure 3.3. Skeletal preparation time course reveals an early ossification defect. Skeletal preparations of E15.5 (A-D) and E16.5 (E-H) wildtype (A, B, E, F), and *Dchs1*^{-/-} (C, D, G, H) heads and mandibles. The heads were viewed from the cranial base (A, C, E, and G). The palatine bone starts mineralising at E15.5 and appears smaller in the *Dchs1*^{-/-} embryos (black arrow, C, C'). Similarly, the mandible also appears smaller in overall size at E15.5 (D). By E16.5, the ossification defect can be clearly seen in the palatine bone of the *Dchs1*^{-/-} embryos (G, G') whilst the mandible, although smaller, starts developing normal processes (H). ag= angular, bo= basoccipital, c= coronoid, cd= condylar, m= maxilla, p= palatine, pm= premaxilla, pt= pterygoid.

The coronoid, condylar and angular processes of the mandible start to appear in the mutant embryos by this stage, whereas the mandibular processes were visible at E15.5 in the wildtype embryos (Fig.3.3 B, F, H). The skull vaults were difficult to examine at these stages as they are thin and prone to collapse due to processing of the skulls into glycerol.

Given that the palatine bone appears smaller at E15.5 as ossification begins, the matrix deposition and morphology of the bone was examined by histology. Transverse sections of E15.5 heads were stained for H&E (Fig.3.4 A-C). Analysis of the sections did not reveal any differences in the condensation or the matrix deposition of the palatine bone between $Fat4^{-/-}$, $Dchs1^{-/-}$ and wildtype embryos (Fig.3.4 A-C).

To determine the expression of $Fat4$ and $Dchs1$ in the developing bones $in\ situ$ hybridisation was carried out to transverse sections of E15.5 embryos (Fig.3.4). $Fat4$ expression was observed in the outer layer/periosteum of the palatine bone and the mandible and in the surrounding mesenchyme (dashed in yellow, Fig.3.4 D and G). $Fat4$ expression could also be seen in the bones of the skull cap (black arrows, Fig.3.4 J). $Dchs1$ expression was observed in the periosteum of the palatine bone and the mandible (Fig.3.4 E and H). Hints of $Dchs1$ expression were observed in the skull vault (black arrows, Fig.3.4 K). Sense probes were used as a negative control which revealed negligible staining (Fig.3.4 F, I and L).

High level of alkaline phosphatase activity is observed during differentiation of the osteoblasts which are the bone forming cells. To investigate whether any differences in the activity of osteoblasts could be detected between the wildtype and mutant bones, an alkaline phosphatase (ALP) assay was carried out on transverse sections of E15.5 embryos (Fig.3.5). ALP staining was observed in the periosteum of the palatine bone, the mandible as well as the calvaria in the wildtype tissue (black arrows, Fig.3.5 A-A''). The ALP staining was visibly reduced in the periosteum of the palatine and the calvaria bones of the $Fat4^{-/-}$ and $Dchs1^{-/-}$ embryos (Fig.3.5 B, B'', C, C''). However, the ALP staining in the mandible was comparable to that of the wildtype embryos (Fig.3.5 A', B', C').
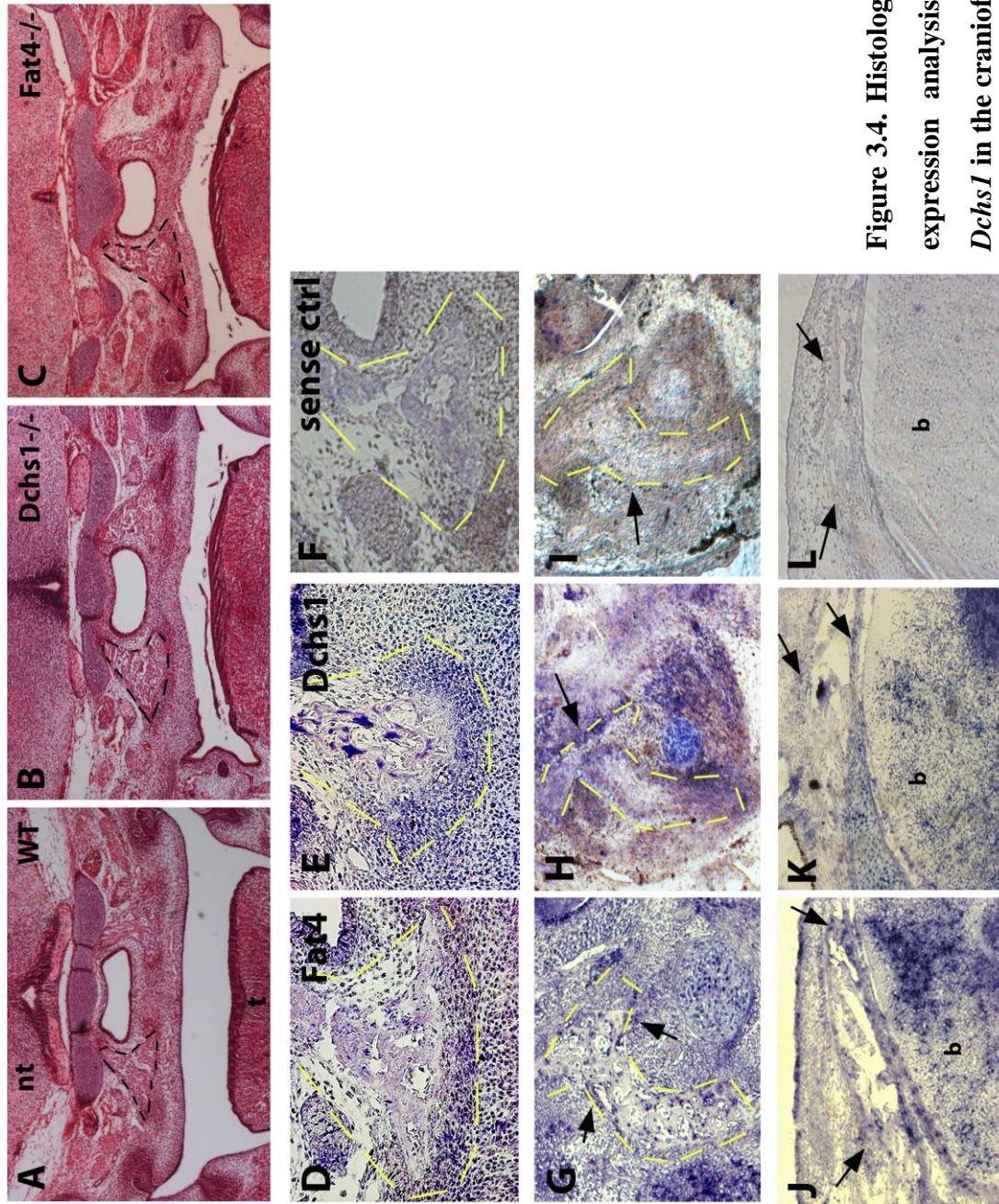
Figure 3.4. Histology analysis and expression analysis of *Fat4* and *Dchs1* in the craniofacial bones.

Figure 3.4. Histology analysis and expression analysis of *Fat4* and *Dchs1* in the craniofacial bones. Haematoxylin and Eosin staining of the frontal sections of E15.5 wildtype (A), *Dchs1*$^{-/-}$ (B) and *Fat4*$^{-/-}$ (C) mutant embryos. The condensation of the palatine bone is outlined (A-C). The mesenchymal condensation of the developing palatine bone appears normal in the mutant embryos (A-C). *In situ* hybridisation was carried out on transverse sections of E15.5 wildtype embryos with antisense probes against *Fat4* (D, G, J), *Dchs1* (E, H, K) and a *Fat4* sense probe (F, I, L). *Fat4* expression is observed in the periosteum of the palatine bone and the surrounding mesenchyme (D) as well as in the mandible (G) and the calvaria bones (J). *Dchs1* expression is also seen in the periosteum of the palatine bone (E), and in the mandible (H) and calvaria (K). Sense control revealed no staining in the bones (F, I, L) confirming the expression of *Fat4* and *Dchs1*. Palatine and mandible bones are outlined by yellow dashes (D-I) and mandible is arrowed in black (G-I). b= brain, nt= neural tube.
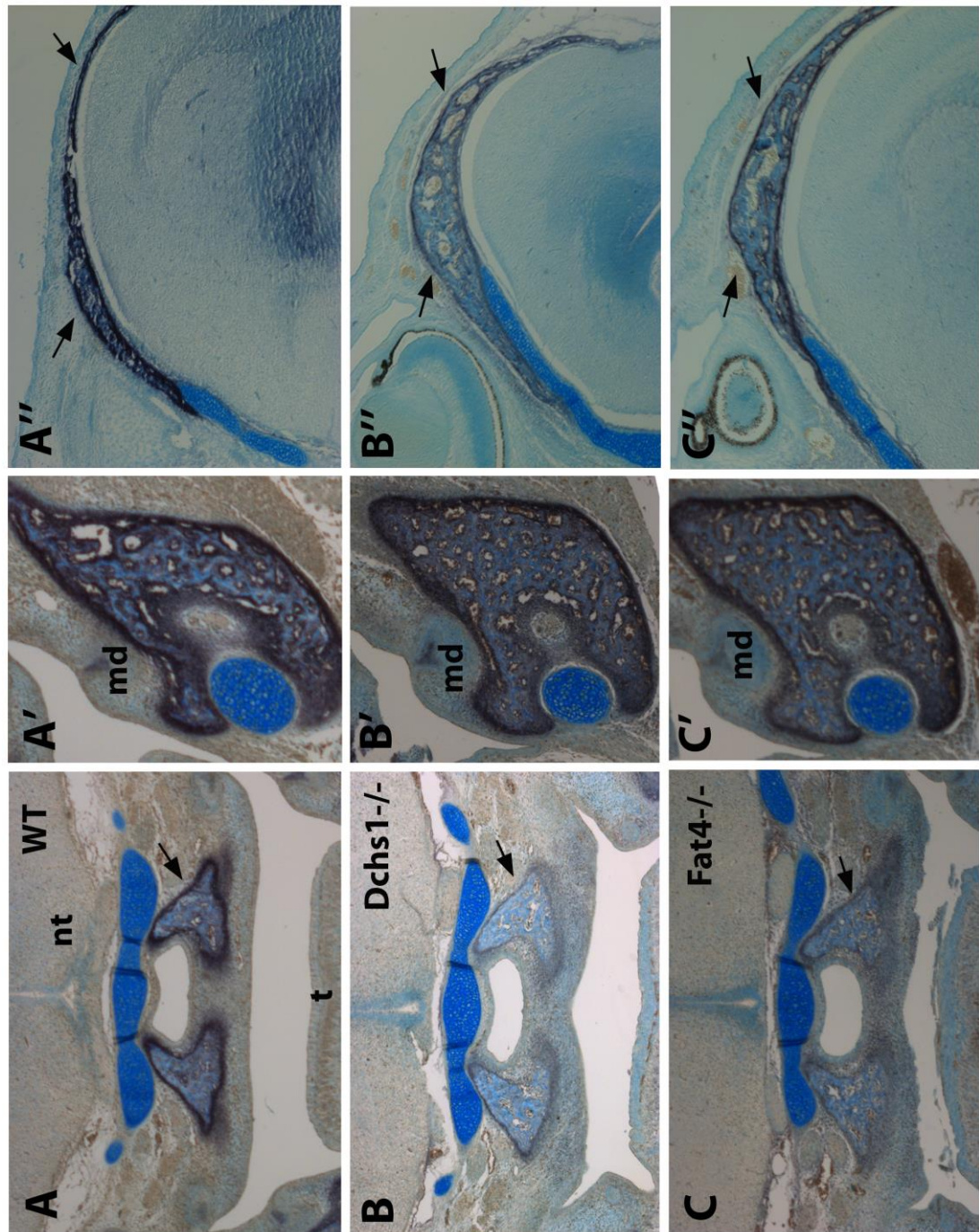
Figure 3.5. ALP staining *in vivo* reveals a differentiation defect upon loss of *Fat4* and *Dchs1*

Figure 3.5. ALP staining *in vivo* reveals a differentiation defect upon loss of *Fat4* and *Dchs1*. ALP staining was carried out on transverse sections of E15.5 wildtype (A), *Dchs1*$^{-/-}$ (B) and *Fat4*$^{-/-}$ (C) embryos. Differentiation in the palatine bone as well as the calvaria of the *Dchs1*$^{-/-}$ and *Fat4*$^{-/-}$ mutants (B, B'', C, C'') was drastically reduced marked by lower levels of ALP staining compared to the wildtype bones (A, A''). On the contrary, ALP staining of the mandible did not appear reduced in the *Dchs1*$^{-/-}$ and *Fat4*$^{-/-}$ mutants (B', C') compared to the wildtype mandible (A'). Palatine bone and calvaria arrowed in black (A-C). md= mandible, nt= neural tube, t= tongue.

3.2.2 Salivary glands are smaller in *Fat4*^{-/-} and *Dchs1*^{-/-} mutants

Branching defects occur in the kidneys of *Fat4*^{-/-} and *Dchs1*^{-/-} mutants and the lungs are also hypoplastic which is assumed to be due to a branching defect (Mao et al., 2011). Salivary glands are also branching organs, therefore, the sublingual and submandibular salivary glands were analysed in the *Fat4*^{-/-} and *Dchs1*^{-/-} mutants. Observation of the salivary glands *in situ* revealed that they were dysmorphic (observations, data not shown) in the mutants.

Histological analysis was carried out on the P0 glands which were stained with trichrome stain. The analysis revealed that the cells of the salivary glands are able to differentiate as determined by the blue staining of the matrix of sublingual glands which contain polysaccharides and the dark blue staining of the submandibular glands which secrete amylase (Fig.3.6 A-D). To determine the size and shape of the salivary glands, an OPT study was carried out in which the P0 sublingual gland was visualised by alcian blue staining and the submandibular gland by auto fluorescence (Fig.3.6 A'-D'). This confirmed that the salivary glands in *Fat4*^{-/-} and *Dchs1*^{-/-} mice are dysmorphic as they are wider and shorter (Fig.3.6 A'-D'). Analysis of the collective volume of both the salivary glands revealed that the mutant glands are approximately30% smaller than the glands of wildtype littermates (Fig.3.6 E). This difference is statistically significant based on the student t-test with values of $p< 0.02$ for *Fat4*^{-/-}, *Dchs1*^{-/-} and the *Fat4*^{-/-}*Dchs1*^{-/-} double mutants. The phenotype of the salivary glands of the *Fat4*^{-/-}*Dchs1*^{-/-} double mutants did not appear exacerbated, indicating that they are functioning in the same pathway to regulate salivary gland development (Fig.3.6 D, D', E).
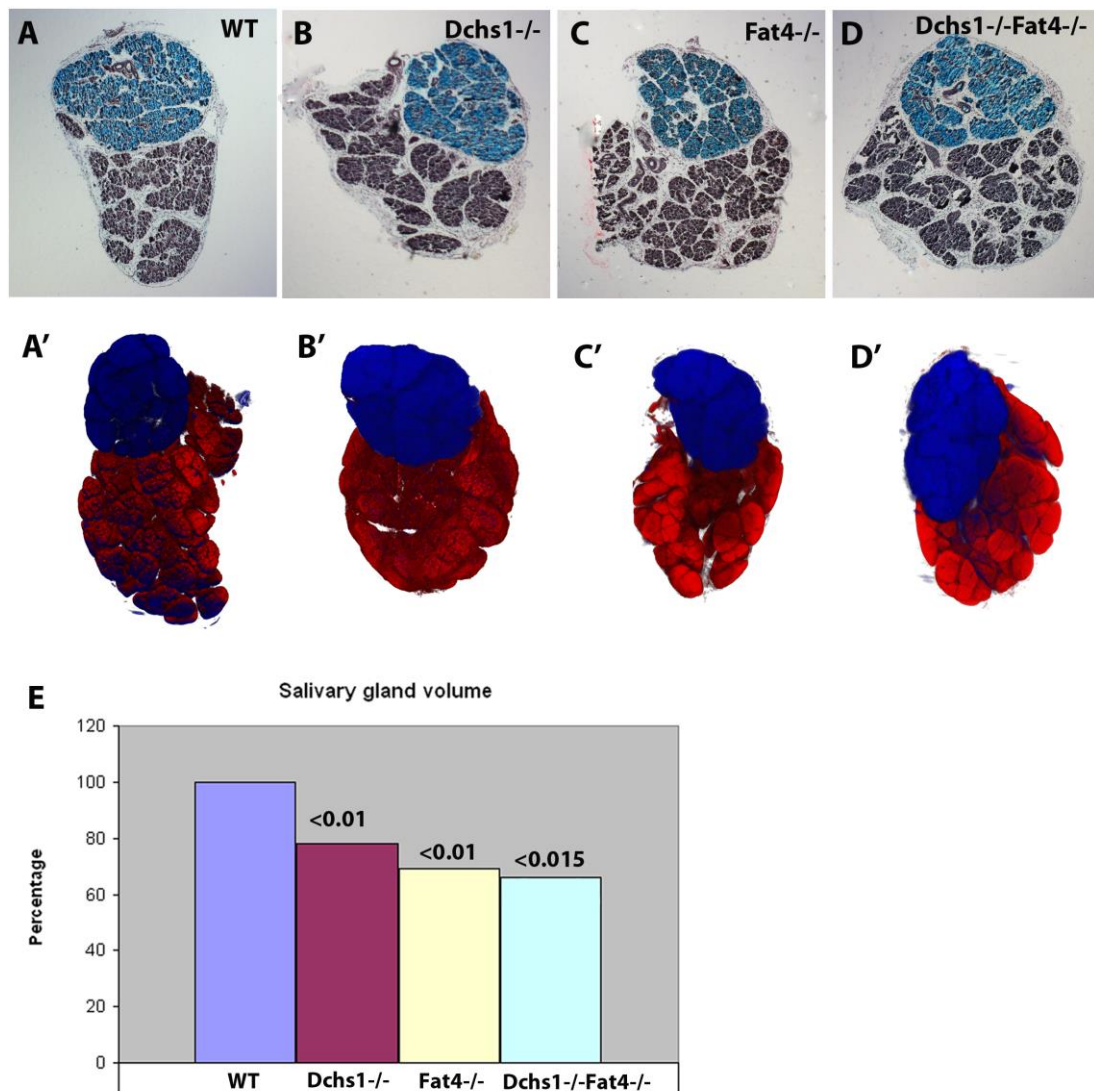
Figure 3.6. Loss of *Fat4* and *Dchs1* results in smaller salivary glands. Trichrome staining was performed on sections of P0 sublingual and submandibular salivary glands of the wildtype (A), *Dchs1$^{-/-}$* (B), *Fat4$^{-/-}$* (C) and *Dchs*1$^{-/-}$*Fat4$^{-/-}$* double mutant (D) embryos. 3-D reconstructions using OPT scanning (A'-D') revealed the difference in volume and shape of the mutant glands. The Student t-test was performed to evaluate the significance of the volume difference (E) which shows that salivary glands in the mutant mice are significantly smaller ($p<0.05$). Furthermore, the double mutants do not have a worsened phenotype (D, D', E) Sublingual gland is stained blue and submandibular gland is stained red (A'-D').

3.2.3 Loss of *Fat4* and *Dchs1* affects polarity in utricle of the inner ear

The Fz-PCP pathway controls convergent extension of the cochlea and also lays down polarity cues in the epithelium of the vestibular system such as in the utricle (Montcouquiol et al. 2003; Warchol & Montcouquiol 2010). Recent analysis has shown that *Fat4* and *Dchs1* are involved in cochlea development; the cochlea is shorter in *Dchs1* and *Fat4* mutants (Mao et al. 2011). However, other components of the inner ear have not been studied in these mutants. Although the disruption of the cochlea hair polarity observed in *Fat4* or *Dchs1* mutants is not significant, it is possible that Fat-PCP controls hair cell polarity in the utricle.

To analyse hair polarity in the utricle, wholemount immunostaining with an anti-myosin VI antibody and phalloidin was performed (in Matthew Kelley's lab with his supervision, *Fat4*$^{-/-}$ N=1). This revealed a defect in the orientation of the hair cells in the utricle of *Fat4*$^{-/-}$ mutants (Fig.3.7 A-B). A swirling pattern of hair cell orientation was observed in the utricles of *Fat4* mutants (Fig.3.7 A-B). A line was drawn across the utricle and the polarity of the hair cells along the line was analysed and plotted as a scatter plot (Fig.3.7 C). This analysis confirmed the observation that there is a disruption of polarity in the utricle of the *Fat4*$^{-/-}$ mutant embryo and needs to be repeated and statistically analysed for polarity reversals and disruption.
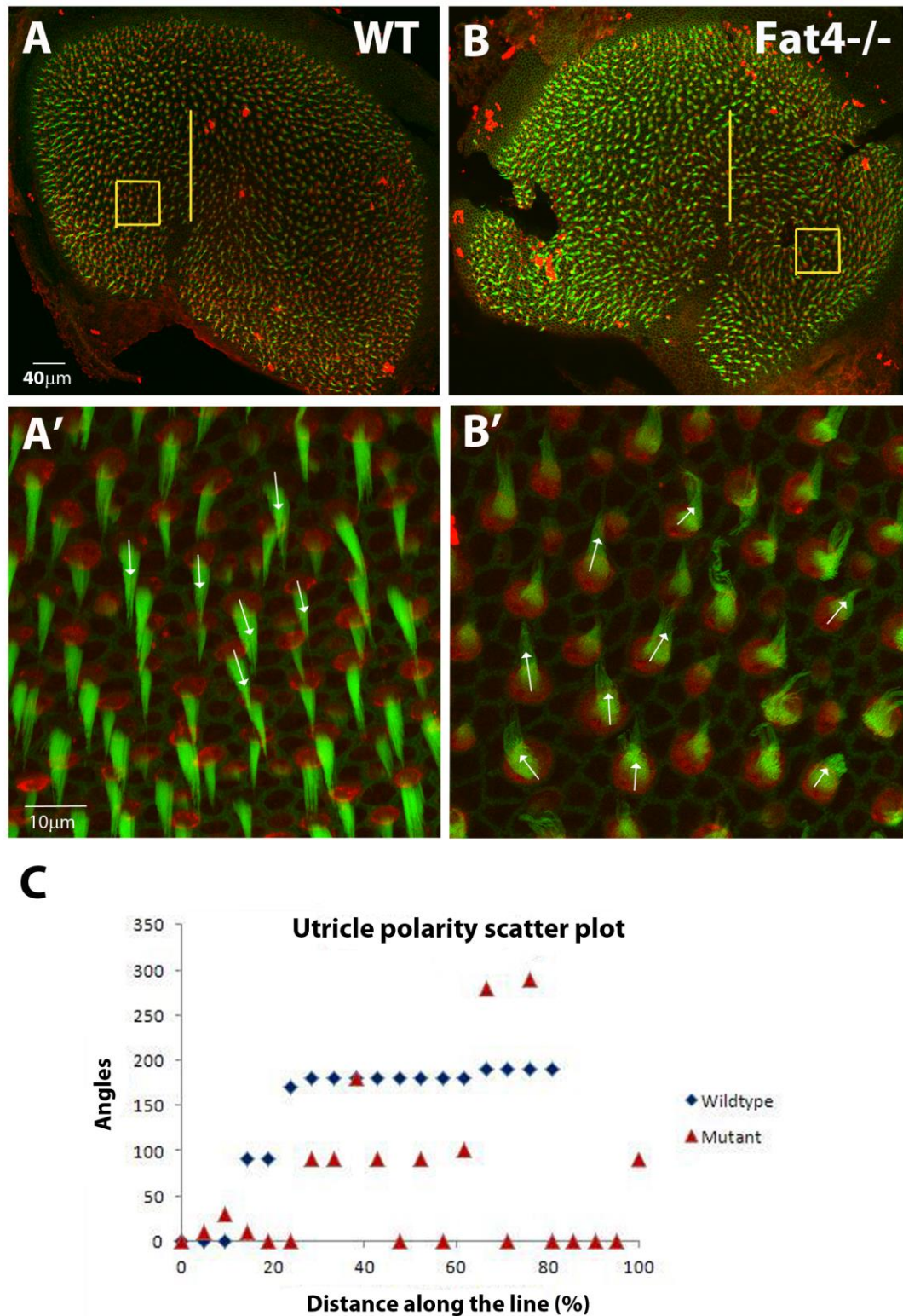
Figure 3.7. Polarity of the hair cells in the utricle is disrupted upon loss of *Fat4.*
Orientation of the hair cells in the utricle of wild-type (A, A') and *Fat4^{-/-}* P0 mice (B,
B''). The boxed region in (A) and (B) is shown at higher magnification in (A') and
(B') respectively. The hair cells are visualised by immunolabelling using antibodies

against phalloidin and myosinVI. In the wildtype utricle, the hair cells appear polarised whereas the polarity is disrupted in the *Fat4*$^{-/-}$ mutant (A-B). A line was drawn across the utricle in the wildtype and *Fat4*$^{-/-}$ mutant embryo (A-B) along which the polarity of cells was measured and plotted onto a scatter plot (C). This revealed differences in the hair cell orientation between the wildtype and *Fat4*$^{-/-}$ mutant embryo (C).

3.3 Discussion

A basic characterisation of the developing craniofacial region has revealed the involvement of Fat signalling in salivary gland development, differentiation of osteoblasts as well as regulating polarity of hair cells in the utricle.

Loss of *Fat4* or *Dchs1* results in a submucosal cleft palate and large fontanelles of the skull vault. Based on the analysis, it does not appear that the defects are a result of a developmental delay as the other bones of the facial region appear similar in shape and size compared to the wildtype bones. The ALP assay reveals a visible reduction in osteoblast activity upon loss of *Fat4* or *Dchs1* which subsequently affects bone formation. *Fat4* and *Dchs1* are expressed in the osteoblasts of these bones which suggests that the function of *Fat4* and *Dchs1* is intrinsically required within the osteoblasts.

Several studies have outlined the involvement of Yap/Taz, the downstream targets of the Hippo pathway, in bone formation. It was observed that both Taz and Yap can interact with Runx2 and act as a switch for differentiation of mesenchymal stem cells into adipocytes or osteoblasts (Zaidi et al. 2004; Hong et al. 2005; Dupont et al. 2011). It has also been illustrated in a few different tissues that increased activity of Yap can block differentiation and promote proliferation (Van Hateren et al. 2011; Cappello et al. 2013). This makes the Hippo/Yap pathway an ideal candidate to explore in order to elucidate the mechanism behind the bone defects observed in the *Fat4*^{-/-} and *Dchs1*^{-/-} mice.

The decrease in the ALP activity of osteoblasts observed upon loss of *Fat4* and *Dchs1* may be due to an increase in number of progenitors which may block differentiation or osteoblast commitment could be blocked in these cells. Yap/Taz could be interacting with Runx2 and modifying osteoblast commitment or the cells could be undergoing excessive proliferation rather than differentiation due to upregulation of Yap/Taz activity. These possibilities need to be explored further for a potential connection with the Hippo pathway.

No direct role of PCP has been implicated in bone formation, however, the Fz-PCP pathway plays a key role in cartilage formation of several tissues. One such example is of cartilage formation in the limb where loss of Wnt5a or Vangl2 activity results

shorter and wider limbs (Gao et al. 2011). Based on the preliminary analysis it is unlikely that Fat signalling plays a role in bone formation via PCP, however, further analysis is required to completely eliminate involvement of the PCP pathway.

The inner ear consists of the vestibular domain which senses movement and gravity. In the vestibular system, sensory hair cells are located on the utricle and saccule, which lie at the base of the semicircular canals (Rida & Chen 2009). Although loss of Fat signalling does not result in significant disruption of polarity of hair cells in the cochlea, the polarity of the hair cells in the utricle is more visibly affected in the *Fat4*$^{-/-}$ mutants (Mao et al. 2011). A swirling pattern of hair cells can be observed in the utricle upon loss of *Fat4*. Detailed analysis of polarity in the utricle in *Fat4*$^{-/-}$ and *Dchs1*$^{-/-}$ mice may help identify how Fat-PCP regulates polarity in the utricle and whether it intersects with the Fz-PCP pathway.

It is evident from the studies carried out previously that Fat-PCP plays a role in kidney branching morphogenesis (Saburi et al. 2008; Mao et al. 2011). In addition, the lung is also smaller in the *Fat4*$^{-/-}$ and *Dchs1*$^{-/-}$ mutants (Mao et al. 2011). The analysis of salivary glands revealed that Fat signalling is also important for development of the sublingual and salivary glands. Loss of *Fat4* or *Dchs1* does not affect the differentiation of the salivary glands. It not known how or if Fat signalling regulates branching of the salivary glands and it remains to be determined if the role of *Fat4* and *Dchs1* is conserved across different branching organs.

The analysis of the craniofacial region has revealed that loss of *Fat4* and *Dchs1* results in identical phenotypes suggesting that they are part of the same pathway and reinforces their proposed receptor-ligand relationship (Ishiuchi et al. 2009; Mao et al. 2011).

The basic characterisation analysis of the craniofacial region has revealed that Fat signalling plays a varied role in this region. This characterisation also included the analysis of the facial branchiomotor neuron migration in the hindbrain, however, this phenotype will be introduced and discussed later in detail over several chapters and is the main focus of this thesis.

4 Characterisation of FBN Migration and Specification of the Hindbrain in $Fat4^{-/-}$ and $Dchs1^{-/-}$ Mutants

4.1 Introduction

In mice, FBNs migrate caudally from rhombomere 4 (r4), where they are born, to r6 between E10.5-E12.5. At E12.5, within r5 and r6, the FBNs also undergo a lateral migration during which they move away from the midline. FBNs eventually form a condensed nucleus and settle lateral to the midline of the hindbrain by E14.5 (see Fig.1.7 B). The caudal and mediolateral migration of the FBNs occur perpendicular to the apical basal axis of the neuroepithelium and are classified as tangential migration. FBNs also undergo radial migration between E12.5-E14.5 from the ventricular surface, where they are born, to the outermost layer, the pial surface (see Fig. 1.7 C).

Tangential migration of the FBNs is a classic example of PCP. Several known components of the Fz-PCP pathway such as *Vangl2*, *Scribble* and *Celsr1-3* have been shown to regulate the caudal migration of the FBNs (Qu et al. 2010; Wada et al. 2006; Vivancos et al. 2009). In mice, loss of these PCP genes results in a caudal migration defect, ranging from a complete arrest of FBNs in r4 in the *Vangl2* $^{Lp/Lp}$ mutants to a partial arrest in r4-r5 in $Celsr2^{-/-}$ and $Celsr3^{-/-}$ mutant mice (Vivancos et al. 2009; Qu et al. 2010). This highlights the crucial role of the Fz-PCP pathway in regulating the caudal tangential migration of the FBNs.

In *Drosophila,* the Fat signalling pathway is an important modulator of PCP (Yang et al. 2002; Thomas & Strutt 2012). The FBNs present an attractive model for studying PCP because of their unique migration trajectory and since components of the Fz-PCP pathway affect their migration. Therefore, the role of *Fat4* and *Dchs1* was investigated to assess if Fat signalling is required for FBN migration.

4.2 Results

4.2.1 Loss of *Fat4* and *Dchs1* results in a FBN migration defect

To characterise FBN migration in *Fat4*$^{-/-}$ and *Dchs1*$^{-/-}$ mutants, wholemount *in situ* hybridisation was carried out using *Islet-1* as a marker for the FBNs. The hindbrains were subsequently flatmounted in an 'open book' conformation and viewed from the ventricular surface for stages E11.5-E12.5 and the pial surface for stages E13.5-E14.5 (Fig.4.1)

At E11.5, migration of the FBNs in the *Fat4*$^{-/-}$ and *Dchs1*$^{-/-}$ mutant hindbrains appears comparable to that of the wildtype FBNs (Fig.4.1 A-C). The neurons are at the midline and the neural stream has moved caudally from r4 to the boundary of r5/r6 (Fig.4.1 A-C). The E11.5 wholemounts were also sectioned. This revealed that the FBNs were at the ventricular surface of r4/r5 in both wildtype and mutant hindbrains indicating that initiation of the caudal migration is unaffected in *Fat4*$^{-/-}$ and *Dchs1*$^{-/-}$ mutants (Fig.4.2 A-C).

By E12.5, the FBNs in the wildtype hindbrain undergo a mediolateral migration, moving away from the midline in r5 and r6 (arrowed Fig.4.1 D). However, the FBNs in the *Fat4*$^{-/-}$ and *Dchs1*$^{-/-}$ mutants are unable to move away from the midline or move further caudally. The FBNs appear arrested and span r4, r5 and the rostral edge of r6 close to the midline (Fig.4.1 E, F). This was confirmed in sections of the wholemounted hindbrains. At the rostral edge of r6, the FBNs in the wildtype hindbrain turn and move away from the midline and simultaneously move into the pial surface (Fig.4.2 D). In contrast, the FBNs in *Fat4*$^{-/-}$ and *Dchs1*$^{-/-}$ mutants are at the midline in both r5 and r6 and do not move laterally, however, hints of radial migration are observed (arrowed, Fig.4.2 E, F).

By E13.5, there is a delay in the caudal migration of FBNs in *Fat4*$^{-/-}$ and *Dchs1*$^{-/-}$ mutant hindbrains (Fig.4.1 G-I). This is illustrated by the position of the trigeminal neurons (arrowed, Fig.4.1 G-I) which are positioned in r2 and were used as an internal control to assess the extent of FBN caudal migration. FBNs in the *Fat4*$^{-/-}$ and *Dchs1*$^{-/-}$ mutants can be seen in r4 and r5 very close to the midline whereas in the wildtype hindbrain, the FBNs have migrated into r6 and condensed as nuclei, lateral to the midline (Fig.4.1 G-I). The delay in migration of the FBNs in *Fat4*$^{-/-}$ and

Dchs1^{-/-} mutants can be seen in the wholemount sections at E13.5, where a subset of neurons is present in r5 at the ventricular surface (Fig.4.2 H). In contrast, no neurons were observed in r5 of the wildtype hindbrain (Fig.4.2 G). In r6 of the wildtype hindbrain, FBNs were observed as condensed nuclei at the pial surface (Fig.4.2 I). Despite the mediolateral arrest of FBNs in the *Fat4*^{-/-} and *Dchs1*^{-/-} mutants, the neurons take an abnormal trajectory and migrate radially whilst remaining close to the midline (Fig.4.2 J). However, at E13.5, the FBNs had not reached the pial surface of the hindbrain (Fig.4.2 J).

By E14.5, the FBNs form condensed nuclei on both sides of the hindbrain lateral to the midline in r6 in the wildtype hindbrain (Fig.4.1 J). The FBNs in the *Fat4*^{-/-} and *Dchs1*^{-/-} mutant hindbrains are unable to condense into a tight nucleus and instead appear as a cluster of neurons spanning r5-r6, very close to the midline (Fig.4.1 K, L).
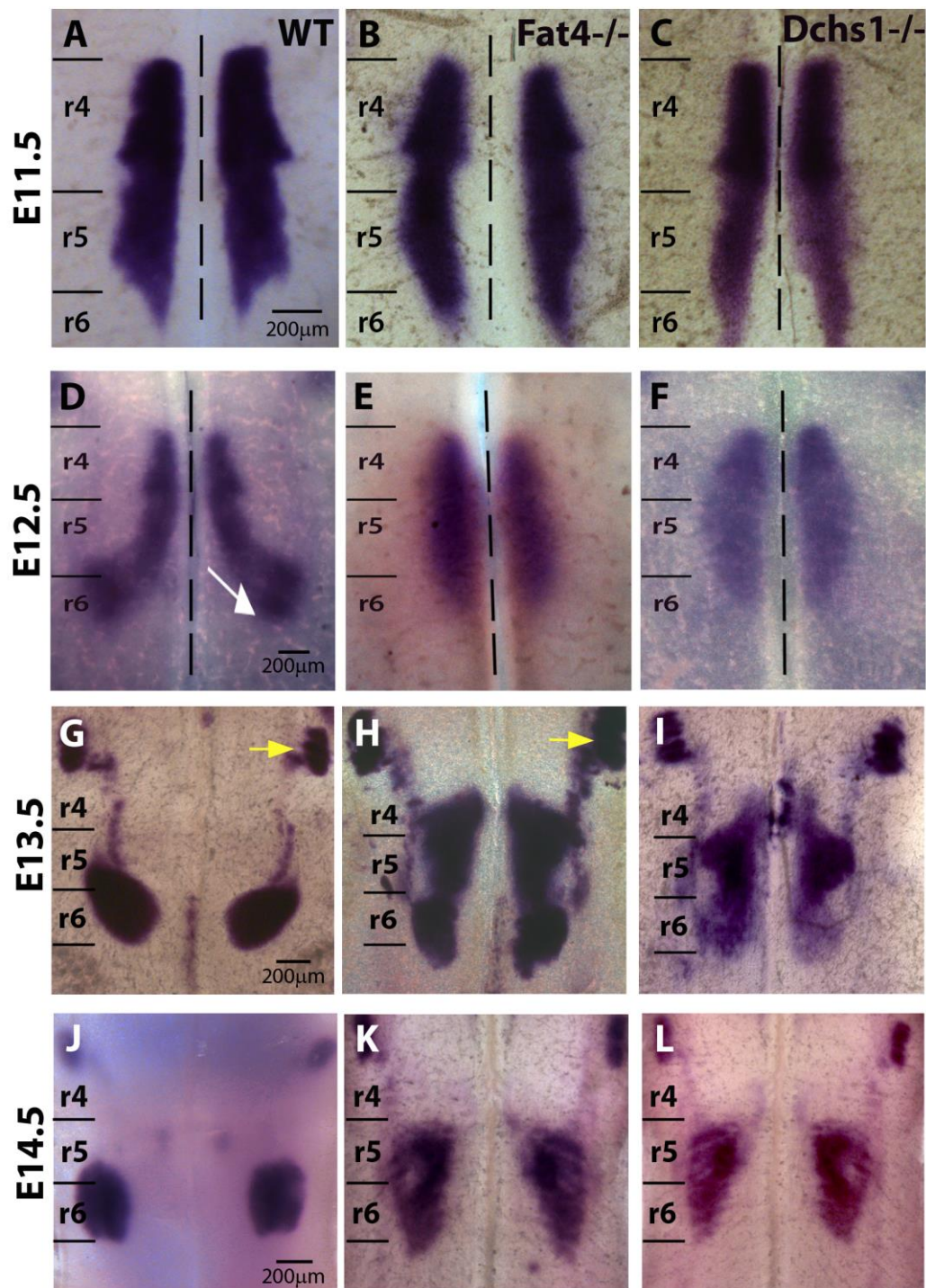
Figure 4.1. *Fat4* **and** *Dchs1* **control lateral tangential migration of FBNs.** Wholemount *in situ* hybridisation for *Islet-1* in E11.5-E14.5 hindbrains (A-L) viewed from the ventricular surface (A-F) and the pial surface (G-L). FBNs in the wildtype (A), *Fat4*^{-/-} (B) and *Dchs1*^{-/-} (C) E11.5 hindbrains show normal initiation of caudal migration into r5/r6. At E12.5, FBNs undergo lateral tangential migration in the wildtype hindbrain (white arrow, D) which fails to occur in the *Fat4*^{-/-} (E) and *Dchs1*^{-/-} (F) mutants and the FBNs are arrested at the midline (midline is dashed A-

F). E13.5 *in situ* hybridisation shows that the FBNs reach r6 and condense lateral to the midline in the wildtype hindbrain (G) whereas in the *Fat4*^{-/-} (H) and *Dchs1*^{-/-} (I) mutants the FBNs can still be found in r4 and r5 with a subset in r6, close to the midline. Position of the trigeminal was used as an internal control of caudal migration (yellow arrows, G and H). At E14.5, *in situ* hybridisation revealed condensed nuclei in the lateral hindbrain of the wildtype embryos (J) whereas in the *Fat4*^{-/-} (K) and *Dchs1*^{-/-} (L) hindbrains, a loose cluster of FBNs spanning r5-r6 is seen close to the midline. r= rhombomere.
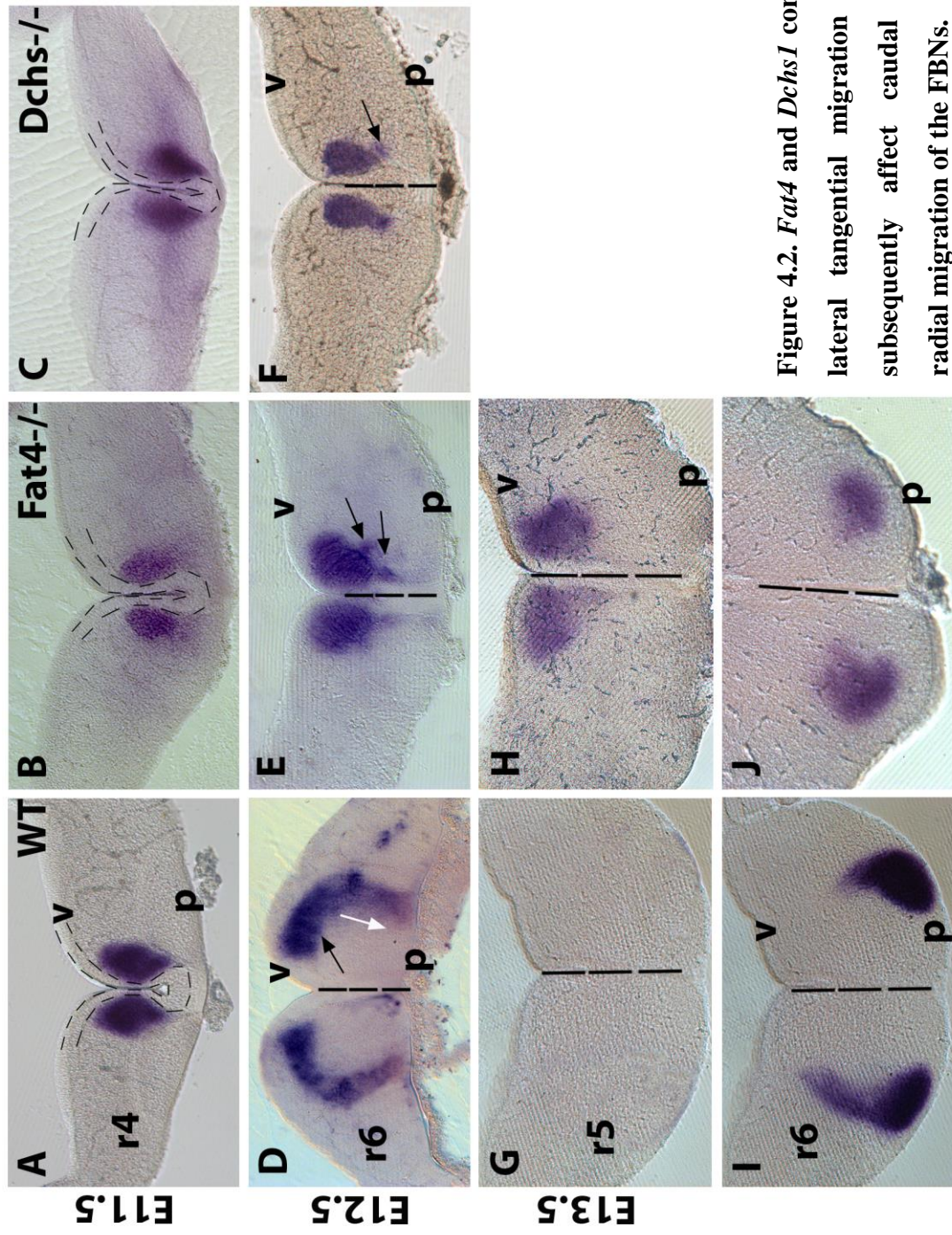
Figure 4.2. *Fat4* and *Dchs1* control lateral tangential migration and subsequently affect caudal and radial migration of the FBNs.

Figure 4.2. *Fat4* **and** *Dchs1* **control lateral tangential migration and subsequently affect caudal and radial migration of the FBNs.** Transverse sections of wholemount *in situ* hybridisations for *Islet-1* in E11.5-E13.5 hindbrains (A-J). At E11.5, FBNs are at the midline of the wildtype (A) *Fat4*$^{-/-}$ (B) and *Dchs1*$^{-/-}$ (C) hindbrains and the ventricular layer is outlined in black (A-C). In r6 at E12.5, wildtype FBNs can be seen undergoing lateral tangential migration at the ventricular surface depicted by a black arrow for migration and midline indicated as dashed (D). The wildtype FBNs are also moving into the pial surface as they migrate radially (white arrow, D). The FBNs in the *Fat4*$^{-/-}$ (E) and *Dchs1*$^{-/-}$ (F) hindbrains are arrested at the midline and there are hints of radial migration (black arrows, E, F). At E13.5 in r5, the FBNs are not visible in the wildtype hindbrain (G) in contrast to the FBNs observed in r5 of the *Fat4*$^{-/-}$ hindbrain (H). In r6 of E13.5 wildtype hindbrains, FBNs can be seen at the pial surface, condensing lateral to the midline (I). A cluster of FBNs in the *Fat4*$^{-/-}$ hindbrain (J) can be seen at the pial front, closer to the midline. p= pial, r= rhombomere, v= ventricular.

4.2.2 Fat4 and Dchs1 act as a receptor-ligand pair

Fat4 and Dchs1 have been characterised as a receptor-ligand pair, respectively, in a few studies in the vertebrate system (Ishiuchi et al. 2009; Mao et al. 2011). *Fat4* and *Dchs1* are expressed in the same tissues, in an overlapping fashion, and upon inactivation result in identical phenotypes in several organs (Mao et al. 2011; Ishiuchi et al. 2009; Saburi et al. 2008).

To investigate if Fat4 and Dchs1 behave as a dedicated receptor and ligand pair in the hindbrain, FBN migration was characterised in double $Fat4^{-/-}Dchs1^{-/-}$ mutant mice. Wholemount *in situ* hybridisation was performed on E12.5 hindbrains using *Islet-1* as a marker for FBNs. The *in situ* hybridisation analysis revealed that loss of both *Fat4* and *Dchs1* does not exacerbate the FBN migration phenotype observed in $Fat4^{-/-}$ and $Dchs1^{-/-}$ mutants (Fig.4.3 A, B). *In situ* hybridisation was also performed on E13.5 hindbrains in $Fat4^{-/-}Dchs1^{-/-}$ double mutants. The analysis revealed a similar phenotype to that observed in the single mutants at E13.5, where there is a delay in the caudal migration of the FBNs (Fig.4.3 C, D). These results support the possibility that Fat4 and Dchs1 operate as a receptor-ligand pair in this tissue, therefore loss of one of these proteins would render the other protein essentially non-functional.
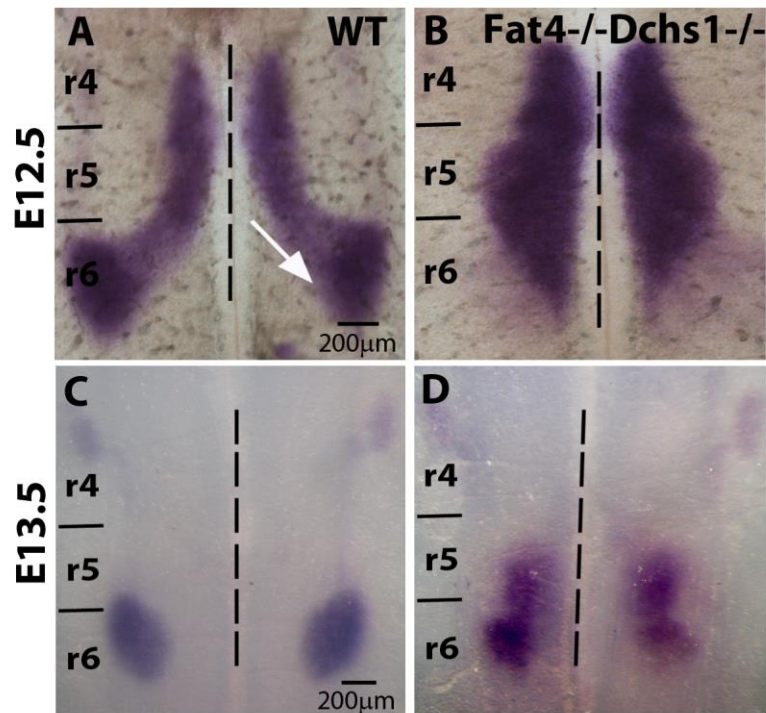
Figure 4.3. Fat4 and Dchs1 behave as a receptor-ligand pair. Wholemount *in situ* hybridisation to *Islet-1* in E12.5 hindbrains viewed from the ventricular surface (A, B) and E13.5 hindbrains viewed from the pial surface (C, D). At E12.5, FBNs in the wildtype hindbrain move away from the midline and undergo lateral tangential migration (white arrow, A) whilst FBNs in the *Fat4*$^{-/-}$ *Dchs1*$^{-/-}$ double mutant hindbrains appear completely arrested at the midline (midline indicated as dashed, B). At E13.5, FBNs in the wildtype hindbrain condense at the pial surface lateral to the midline, in r6 (C). Analysis of the E13.5 hindbrain of the *Fat4*$^{-/-}$ *Dchs1*$^{-/-}$ double mutant reveals a subset of the FBNs arrested in r5 whilst some are present in r6 close to the midline (D). r= rhombomere.

4.2.3 Migration of other branchiomotor neurons and axons is not affected in *Fat4*$^{-/-}$ and *Dchs1*$^{-/-}$ mutants

The branchiomotor neurons encompass the trigeminal, glossopharyngeal, vagus and the cranial accessory neurons. These neurons move mediolaterally between E10-E11.5 but do not migrate caudally. The glossopharyngeal and vagus neurons do not form a nucleus, unlike the trigeminal neurons, and appear as a single line of continuous neurons extending from r6-r7 (Keynes & Lumsden 1989; Gilland & Baker 1993). To investigate if loss of *Fat4* or *Dchs1* affects migration of these neurons, whole-mount *in situ* hybridisations were carried out on E11.5 hindbrains, using *Islet-1* as a marker for the trigeminal neurons and *Sema3A* as a marker for the glossopharyngeal and vagus neurons.

The *in situ* hybridisation analysis revealed that the trigeminal neurons are able to move mediolaterally and form a nucleus in the *Fat4*$^{-/-}$ and *Dchs1*$^{-/-}$ mutants (yellow arrows, Fig.4.4 A-C). In addition, both the glossopharyngeal and the vagus neurons are also able to move mediolaterally in the *Fat4*$^{-/-}$ and *Dchs1*$^{-/-}$ mutants (yellow and orange arrows, Fig.4.4 D-F). This demonstrates that only FBNs are affected by loss of *Fat4* and *Dchs1*.

A few Fz-PCP mutants display minor axonal migration defects (Song et al. 2006). To investigate if *Fat4* and *Dchs1* also regulate axonal migration, wholemount axonal labelling was carried out on E11.5 wildtype, *Dchs1*$^{-/-}$ and *Fat4*$^{-/-}$ embryos using a monoclonal neurofilament antibody. Wholemounts were imaged on a dissection microscope and the confocal microscope to reveal the axonal branching of the trigeminal, facial, glossopharyngeal and vagus neurons (Fig.4.5). In the wildtype hindbrains, the trigeminal axons branch out and innervate the frontonasal prominence and also innervate the eye and the first branchial arch (white arrow, Fig.4.5 A, D). These axons appear normal in the *Fat4*$^{-/-}$ and *Dchs1*$^{-/-}$ mutant embryos (white arrow, Fig.4.5 A-F). The axons of the FBNs are split into two main branches innervating the first and second branchial arch in wildtype embryos (black and yellow arrows, Fig.4.5 A, D). The axonal branching of the FBNs is normal in the *Fat4*$^{-/-}$ and *Dchs1*$^{-/-}$ mutant embryos (Fig.4.5 B, C, E, and F). The glossopharyngeal and vagus axons exit very close to each other and innervate muscles in branchial arch 3 and branchial arches 4 and 6, respectively, in wildtype embryos (pink arrow,

Fig.4.5 A). These axons are not affected in the *Fa4⁻/⁻* and *Dchs1⁻/⁻* mutants (Fig.4.5 B, C). These results reveal that axonal migration of branchiomotor neurons is not defective in *Fat4⁻/⁻* and *Dchs1⁻/⁻* mutants.
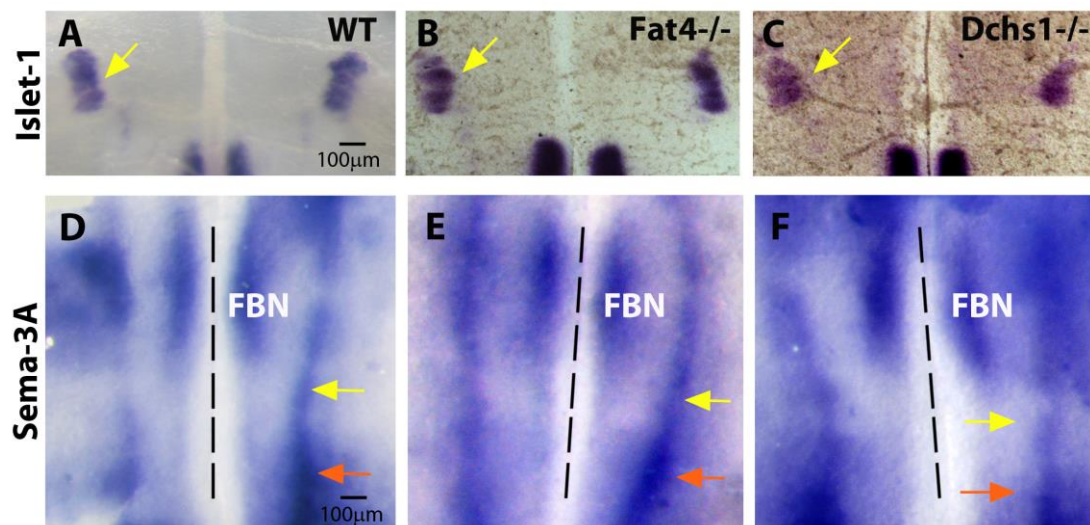
Figure 4.4. Loss of *Fat4* and *Dchs1* does not affect migration of other branchiomotor neurons. Wholemount *in situ* hybridisation to *Islet-1* (A-C) and *Sema-3A* (D-F) in E11.5 hindbrains (A-F) viewed from the ventricular surface. The lateral migration of trigeminal neurons (yellow arrow, A-C) appears normal in *Fat4*^{-/-} (B) and *Dchs1*^{-/-} (C) hindbrains and is comparable to the trigeminal neuron migration in the wildtype hindbrains (A). The glossopharyngeal and vagus neurons (yellow arrow and orange arrow respectively, D-F) appear as a single continuous column of neurons just below the FBNs and can be seen lateral to the midline (midline is dashed, D-F) in the wildtype (D) as well as the *Fat4*^{-/-} (E) and *Dchs1*^{-/-} (F) hindbrains. FBN= facial branchiomotor neuron.
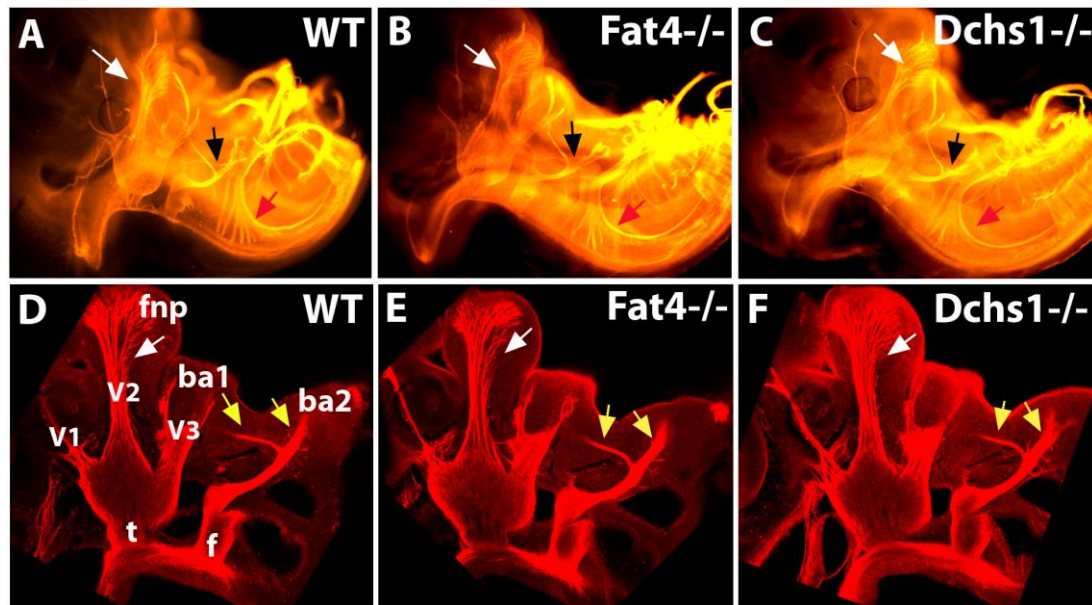
Figure 4.5. Axonal pathfinding is not affected by loss of *Fat4* and *Dchs1*. Wholemount immunochemistry using anti-neurofilament antibody to E11.5 heads, viewed at low magnification under a Zeiss stage microscope (A-C) and at higher magnification on a Leica Confocal (D-F). The neurofilament staining revealed the branching of the trigeminal axons (white arrow, A-C), the two branches of the FBN axons (black arrow, A-C) and the grouped cluster of glossopharyngeal and vagus axons (pink arrow, A-C). The axons in the wildtype hindbrain (A) appeared similar to the axons in the *Fat4*^{-/-} (B) and *Dchs1*^{-/-} (C) hindbrains. In the confocal z-stack, the trigeminal axons can be seen as three branches V1-3, innervating the eye, the frontonasal process and the first branchial arch, respectively (white arrow, D-F). The FBN axon splits into two branches innervating the first and the second branchial arches (yellow arrows, D-F). The wildtype (D), *Fat4*^{-/-} (E) and *Dchs1*^{-/-} (F) axons innervate the target musculature and take the appropriate exit points. ba= branchial arch, f= facial axons, fnp= frontonasal process, t= trigeminal axons.

4.2.4 Specification of the hindbrain and FBN identity is not affected by loss of *Fat4* and *Dchs1*

In order for appropriate migration to occur, FBNs require a set of intrinsic cues at different stages of their migration and also require extrinsic cues presented by the rhombomeres (Guthrie & Lumsden 1992; Garel et al. 2000). In order to assess whether the FBN migration defect is caused by mis-patterning of the hindbrain, *in situ* hybridisation analysis was performed on E10.5 hindbrains using *Hoxb1* and *EphrinA4* as markers for r4 and r3, r5, respectively.

The *in situ* hybridisation analysis revealed normal expression of *Hoxb1* in r4 of the *Fat4*$^{-/-}$ and *Dchs1*$^{-/-}$ mutant hindbrains (Fig.4.6 A-C). Furthermore, *EphrinA4* expression in r3 and r5 of the *Fat4*$^{-/-}$ and *Dchs1*$^{-/-}$ hindbrains was also comparable to that in the wildtype hindbrain (Fig.4.6 D-F). Given that FBNs arise in r4 and the identity of r4 is intact, it can be assumed that the FBNs are initially specified appropriately. Rhombomeres 3 and 5 also appear to be correctly specified suggesting that overall hindbrain patterning and rhombomere identity is unaffected in *Fat4*$^{-/-}$ and *Dchs1*$^{-/-}$ mutant mice.

To investigate if the intrinsic transcriptional regulation of FBN migration is intact, *in situ* hybridisations were performed using a set of markers that are expressed at different stages of FBN migration. *Tbx20* is expressed in the FBNs at E12.5 in the entire migratory stream and is essential for migration (Song et al. 2006). *Ret* is expressed by the FBNs as they migrate into r5 and r6 (Müller et al. 2003). *Cadherin-8* and *Neogenin* mark the FBNs at a later stage of migration as they enter r6 and start condensing on the pial surface of the hindbrain at E12.5 (Garel et al. 2000; Müller et al. 2003).
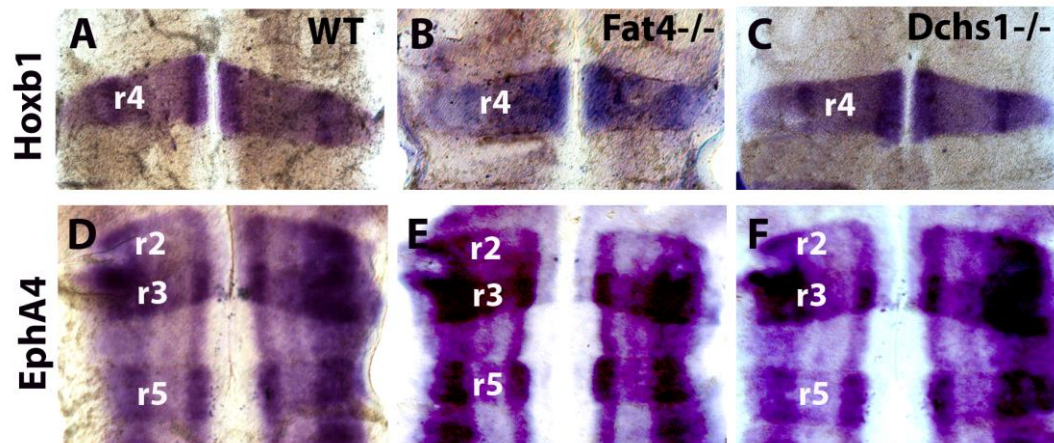
Figure 4.6. Rhombomere identity is intact upon loss of *Fat4* and *Dchs1*. Wholemount *in situ* hybridisation to *Hoxb1* (A-C) and *EphA4* (D-F) in E10.5 wildtype (A, D), *Fat4⁻/⁻* (B, E) and *Dchs1⁻/⁻* (C, F) hindbrains. In the *Fat4⁻/⁻* (B) and *Dchs1⁻/⁻* (C) hindbrains, rhombomere 4 is correctly specified. Similarly, compared to the wildtype hindbrain (D), rhombomere 3 and 5 are appropriately specified in the *Fat4⁻/⁻* (E) and *Dchs1⁻/⁻* (F) hindbrains. r= rhombomere.

In situ hybridisation to *Tbx20* on wildtype, *Fat4⁻ᐟ⁻* and *Dchs1⁻ᐟ⁻* mutant hindbrains revealed that despite the arrest of FBNs in r4 and r5 in the mutants, *Tbx20* is expressed in the FBNs of wildtype and mutant hindbrains (Fig.4.7 A, B, C). *Ret* is expressed in the FBNs in r5 and r6 in the wildtype embryos (Fig.4.7 D) and is also expressed by the FBNs in the *Fat4⁻ᐟ⁻* and *Dchs1⁻ᐟ⁻* mutants (Fig.4.7 E, F).

Cadherin-8 is expressed in the condensing FBNs on the pial surface in the wildtype hindbrains (Fig.4.7 G). In the *Fat4⁻ᐟ⁻* and *Dchs1⁻ᐟ⁻* mutants, *Cadherin-8* expression can be seen in the FBNs that have reached the rostral edge of r6 (white arrow, Fig.4.7 H, I).

Neogenin also marks the condensing FBNs on the pial surface of the hindbrain in wildtype embryos (Fig.4.7 J). FBNs in the *Fat4⁻ᐟ⁻* and *Dchs1⁻ᐟ⁻* mutants do not express *Neogenin* at E12.5 (Fig.4.7 K, L). However, since the FBNs in the mutants do not reach caudal r6 by E12.5, *in situ* hybridisation was also performed at E13.5. *Neogenin* expression switches on in the FBNs located in caudal r6 of the *Fat4⁻ᐟ⁻* and *Dchs1⁻ᐟ⁻* mutants by E13.5 (Fig.4.7 M-O). These results suggest that the transcriptional integrity of the FBNs is intact and they have not been mis-specified in the *Fat4⁻ᐟ⁻* and *Dchs1⁻ᐟ⁻* mutants.
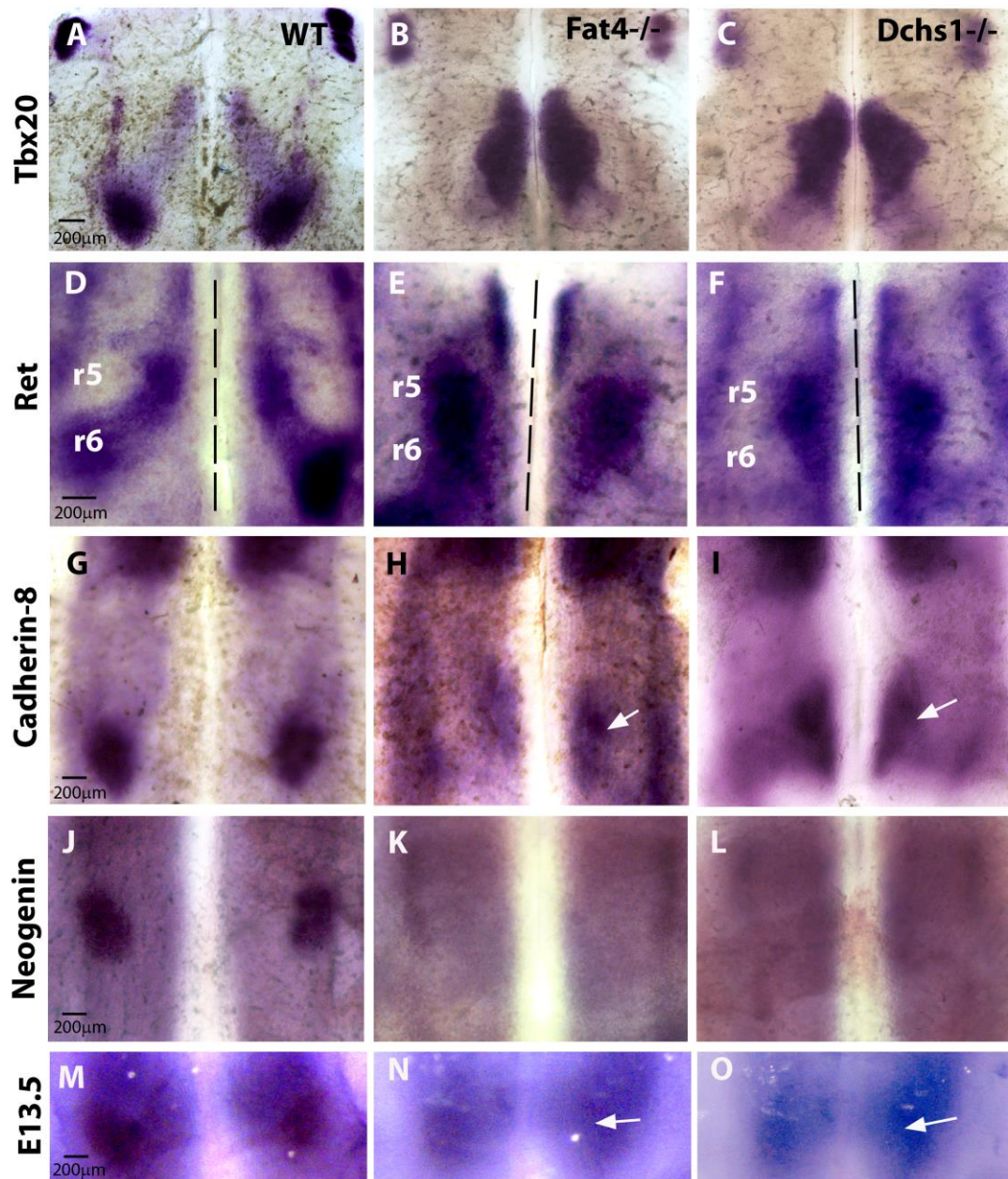
Figure 4.7. FBN transcriptional machinery is not compromised by loss of *Fat4* and *Dchs1*. Wholemount *in situ* hybridisation to *Tbx20* (A-C), *Ret* (D-F), *Cadherin-8* (G-I) and *Neogenin* (J-O). E12.5 hindbrains visualised on the ventricular surface (A-L) and E13.5 hindbrains visualised on the pial surface (M-O). *Tbx20* is expressed in the entire migratory stream of the FBNs in the wildtype hindbrain (A) as well as in the arrested FBNs in the *Fat4*$^{-/-}$ (B) and *Dchs1*$^{-/-}$ (C) hindbrains. *Ret* is expressed in the wildtype FBNs as they enter r5 and r6 (D), and in the FBNs in the *Fat4*$^{-/-}$ (E) and *Dchs1*$^{-/-}$ (F) hindbrains, despite the mediolateral arrest of the FBNs. *Cadherin-8* is expressed in the condensing FBN nuclei in r6 of the wildtype hindbrain (G) and in the subset of FBNs that are found at the midline in r6 of the *Fat4*$^{-/-}$ (white arrow, H)

and *Dchs1*^{-/-} (white arrow, I) hindbrains. At E12.5, *Neogenin* is expressed in the wildtype FBN nuclei in r6 (J), however the expression is absent in the FBNs of the *Fat4*^{-/-} (K) and *Dchs1*^{-/-} (L) hindbrains. At E13.5, *Neogenin* expression is still present in the wildtype FBN nuclei (M) and the expression switches on in the FBNs of the *Fat4*^{-/-} (white arrow, N) and *Dchs1*^{-/-} (white arrow, O) hindbrains.

4.3 Discussion

Analysis of the *Fat4*^{-/-} and *Dchs1*^{-/-} mutant mouse hindbrain revealed that the loss of either gene results in an identical phenotype. The FBNs have a defect in mediolateral migration and a delay in the caudal migration. Fat4 and Dchs1 are responsible for guiding mediolateral migration of FBNs and upon their loss FBNs are unable to move away from the midline. The mediolateral movement does not occur and FBNs settle in r5-r6 as a cluster of neurons. Fat4 and Dchs1 are not required for the initiation of caudal migration which is normal in the *Fat4*^{-/-} and *Dchs1*^{-/-} mutant mice. The ability to initiate caudal migration also demonstrates that the ability of the FBNs to migrate *per se* has not been intrinsically compromised in the mutants.

FBN migration comprises of three distinct types of movement; caudal, lateral and radial, which are regulated by independent signalling networks. For example, *Reelin* controls radial migration whereas Fz-PCP controls caudal migration (Rossel et al. 2005; Vivancos et al. 2009). This is the first time a signalling pathway involved in regulating mediolateral tangential migration of the FBNs has been uncovered. Fz-PCP components do not affect this axis of migration thus establishing the Fat pathway as a novel modulator of mediolateral tangential migration of FBNs.

Given the identical hindbrain phenotype of the *Fat4*^{-/-} and *Dchs1*^{-/-} mutants as well as the similar phenotype of the *Fat4*^{-/-} *Dchs1*^{-/-} double mutant, it is suggestive of Fat4 and Dchs1 functioning as a receptor-ligand pair in the hindbrain. The lack of either the ligand (Dchs1) or the receptor (Fat4) would render the other protein non-functional and as a result the FBNs cannot be guided towards their final position. The identical phenotypes observed in the hindbrain in the *Fat4*^{-/-} and *Dchs1*^{-/-} mutants are not restricted to the hindbrain and have been observed in the kidneys, salivary glands, somites, sterna and membranous bones of the mice (Mao et al. 2011; Saburi et al. 2008 + unpublished data). These results provide further evidence that Fat4 and Dchs1 are likely to act as a receptor ligand pair in several tissues and function in the same linear pathway.

Presumably if other *Fat* and *Dchs2* genes were involved in regulating FBN migration by interacting with Fat4 or Dchs1 then it would be expected that the double *Fat4*^{-/-} *Dchs1*^{-/-} mutants would have a more severe phenotype than the single

mutants due to redundancy in the pathway. The other *Fats/Dchs2* could compensate for loss of *Fat4* or *Dchs1*. However, given that the *Fat4* and *Dchs1* null mutant phenotype is as severe as the double *Fat4$^{-/-}$ Dchs1$^{-/-}$* mutant phenotype, it is more likely that Fat4 and Dchs1 exclusively participate in regulating FBN migration along the lateral axis. This does not, however, eliminate the possibility that other *Fats* or *Dchs2* are not involved since they could converge at the same point downstream in the pathway or regulate another process in a parallel pathway. Given that *Fat1* is expressed in the developing neuroepithelium and *Fat3* is also present in a variety of structures in the CNS makes them attractive candidates for interacting with Fat4 and Dchs1 to regulate neuronal migration (Mitsui et al. 2002; Cox et al. 2000). In contrast, *Fat2* is exclusively expressed in the cerebellum while *Dchs2* is found in a restricted region of the neural tube floor plate which makes them unlikely candidates for regulating FBN migration (Nakayama et al. 2002; Rock et al. 2005 + unpublished data).

Loss of *Fat4* and *Dchs1* only affects migration of the FBNs and not the other branchiomotor neurons. One possible reason for this could be that other branchiomotor neurons move mediolaterally and settle in their final positions by E11.5 whereas the FBNs start the mediolateral migration after E11.5. Therefore, it is possible that Fat4 and Dchs1 expression is temporally controlled and might switch on after E11.5. Movement of the other branchiomotor neurons is governed by an alternative mechanism to that of Fat4/Dchs1 signalling. This is further illustrated by the findings from the *Tbx20$^{-/-}$* mutant mouse where the mediolateral movement of the trigeminal is hindered thus uncovering another mechanism for controlling mediolateral migration of other branchiomotor neurons (Song et al. 2006).

Axon pathfinding generally functions independently of cell body migration (Jacob et al. 2001). The same set of receptors or proteins can facilitate the two different processes by a different combination of receptors and ligands working together. For instance, Neuropilin-1, a receptor, works together with SEMA-3A to guide facial motor axons and have no role in guiding facial cell body positioning (Jacob et al. 2001; Schwarz et al. 2004). Neuropilin-1 does, however, interact with VEGF164 to regulate the FBN cell body position (Jacob et al. 2001; Schwarz et al. 2004; Meléndez-Herrera & Varela-Echavarría 2006). However, a recent study in zebrafish highlighted the role of migration of the leading FBN and its dependence on its

trailing axon (Wanner & Prince 2013). The authors demonstrated that ablating the axon of the leading FBN results in a subsequent block of the FBNs in r5 (Wanner & Prince 2013). This study reflects the importance that axons can have on early cell body migration of FBNs. Some Fz-PCP mutant mice as well as the *Tbx20*$^{-/-}$ mutant have also been reported to have minor axon guidance defects (Song et al. 2006). Examination of the axons of all branchiomotor neurons in the *Fat4*$^{-/-}$ and *Dchs1*$^{-/-}$ mutants revealed that axon migration is normal in these mice.

The facial nerve innervates the muscles of facial expression, the stapedius and the posterior belly of the disgastric muscle (Chandrasekhar 2004; Guthrie 2007). The *Fat4*$^{-/-}$ and *Dchs1*$^{-/-}$ mutant mice are perinatal lethal hence it is not possible to conclude whether the migratory arrest and distortion of the FBN position would affect the functional output of the innervated muscles.

Analysis of hindbrain patterning revealed that loss of *Fat4* and *Dchs1* does not affect the overall patterning of the hindbrain and the specification of the FBNs by *Hoxb1* is intact. Expression of different genes is switched on in the FBNs as they migrate through the rhombomeres. The results presented suggest that the intrinsic machinery regulating FBN migration is not compromised by loss of *Fat4* and *Dchs1*. *Tbx20* and *Ret* are expressed in the *Fat4*$^{-/-}$ and *Dchs1*$^{-/-}$ FBNs located within r4 and r5. As a marker of late FBN migration, *Cadherin-8* expression was analysed. Surprisingly, despite the abnormal position of the FBNs at the rostral edge of r6, *Cadherin-8* expression was visible in the FBNs close to the midline. This suggests that reaching r6 is sufficient to switch on *Cadherin-8* expression in the FBNs.

Conversely, *Neogenin* expression was not observed in the FBNs of *Fat4*$^{-/-}$ and *Dchs1*$^{-/-}$ mutants at E12.5, despite a subset of FBNs present at the rostral edge of r6. However, *Neogenin* expression became apparent by E13.5 when the FBNs in the mutants had migrated into caudal r6 of the hindbrain. Since *Neogenin* is a marker of radial migration, it is likely that the delay in *Neogenin* expression upon loss of *Fat4* and *Dchs1* is due to the delay in radial migration of the FBNs. At E12.5, the section analysis of the mutants confirmed that there was a delay in the radial migration following the lateral migration arrest of the FBNs.

Overall, this analysis suggests that the FBNs possess the correct set of intrinsic cues to migrate in the absence of *Fat4* and *Dchs1*.

Loss of *Fat4* and *Dchs1* not only results in the arrest of lateral migration of FBNs but also results in a subsequent delay in the caudal and radial migration. The initiation of the caudal migration of the FBNs is unaffected in the mutants and a subset of the FBNs migrate radially and reach close to the pial surface thereby it is likely that these effects are secondary to the defect in lateral migration of the FBNs.

This analysis does not eliminate the possibility that Fat signalling could intersect with the Fz-PCP pathway in regulating caudal migration at a later stage (e.g. after FBNs leave r5).

These results have demonstrated that *Fat4* and *Dchs1* are unlikely to regulate FBN migration via a transcriptional pathway and led to further investigation in order to assess whether the FBN migration defect is caused by a disruption of PCP.

5 CHARACTERISATION OF FBN POLARITY; A GRADIENT MODEL

5.1 Introduction

Previous analysis of the FBN phenotype indicates that Fat signalling could regulate FBN migration via PCP. In *Drosophila* Fat signalling establishes PCP by graded expression of Ds and Fj (Yang et al. 2002; Matakatsu & Blair 2004). For instance, complementary gradients of Ds and Fj in the *Drosophila* wing and eye result in a graded activation of Ft across the tissue which imparts polarity to the cells (Yang et al. 2002; Matakatsu & Blair 2004).

In *Drosophila*, to investigate if the graded expression of Fj and Ds and the graded activity of Ft is essential to establish PCP in a given tissue, patches of clones, negative for Ft, Ds or Fj are randomly generated in a tissue to disrupt their gradients and determine the effect on polarisation of cells or disruption in polarity.

To determine if Fat4 and Dchs1 regulate FBN migration via PCP and if the mechanism is conserved between *Drosophila* and mouse, the following analyses were carried out. Expression of Fat4 and Dchs1 was determined in the hindbrain to investigate if gradients are present. To determine if FBNs are polarised during migration, polarity was examined by analysing the cell shape and position of the Golgi complex of the FBNs in wildtype, *Fat4* and *Dchs1* null embryos. Lastly, to assess if gradients play a role in regulating FBN migration, mosaic embryos were generated by randomly inactivating *Dchs1* from within the hindbrain to study the effect on FBN migration.

5.2 Results

5.2.1   Graded RNA expression of *Fat4* and *Dchs1* in the hindbrain

Wholemount *in situ* hybridisations and section analysis were carried out on E10.5-E12.5 hindbrains to determine *Fat4* and *Dchs1* expression (Fig.5.1 A-H). Sections and flatmounts of the hindbrain at E10.5 and E11.5 revealed diffuse Fat4 expression in the hindbrain (Fig.5.1 A, B). By E12.5 *Fat4* expression is high in the lateral hindbrain (Fig. 5.1 C). This was confirmed by section analysis which revealed *Fat4* is expressed in the ventricular and pial layers in the lateral hindbrain (Fig.5.1 H). Hints of *Fat4* expression were also detected where the FBNs are presumed to be present (black arrow, Fig.5.1 C).

Fat4 expression was quantified using a line plot tool from ImageJ. A line was drawn from the midline to the lateral edge of the hindbrain in flatmounts and sections at E12.5 to measure the intensity of pixels across the line (black line, Fig.5.1 C, H). The relative levels of expression were quantified and plotted as a graph of pixel intensity across the mediolateral axis of the hindbrain (black line, Fig.5.1 J, L). The analysis revealed that *Fat4* is expressed at lower levels in the medial hindbrain and at higher levels in the lateral hindbrain (Fig.5.1 J, L).

Diffuse expression of *Dchs1* was observed in the ventricular layer of the hindbrain in E10.5 sections and all across the hindbrain in E11.5 flatmounts (Fig.5.1 D, E). At E12.5, *Dchs1* expression becomes slightly stronger medially and can also be observed in the FBNs (black arrow, Fig.5.1 F). This expression pattern confirmed in the sections and high levels of *Dchs1* expression was also detected in the midline in the ventricular layer with lower levels laterally (arrowed, Fig.5.1 G). Although, *Dchs1* expression was diffuse compared to the graded expression of *Fat4*, line plot analysis of the wholemounts revealed that *Dchs1* expression is overall slightly higher in the medial hindbrain relative to the lateral hindbrain (Fig.5.1 I). Line plot analysis of the sections also revealed the same pattern of *Dchs1* expression with high levels of *Dchs1* at the midline and lower levels of *Dchs1* laterally in the ventricular layer (Fig.5.1 K). Taken together, the wholemount and section analysis indicates that there is a possible RNA gradient of *Fat4* and *Dchs1* mediolaterally across the hindbrain, especially at the level of r4-r6 at the ventricular surface (Fig.5.1 C, H, F, and G).
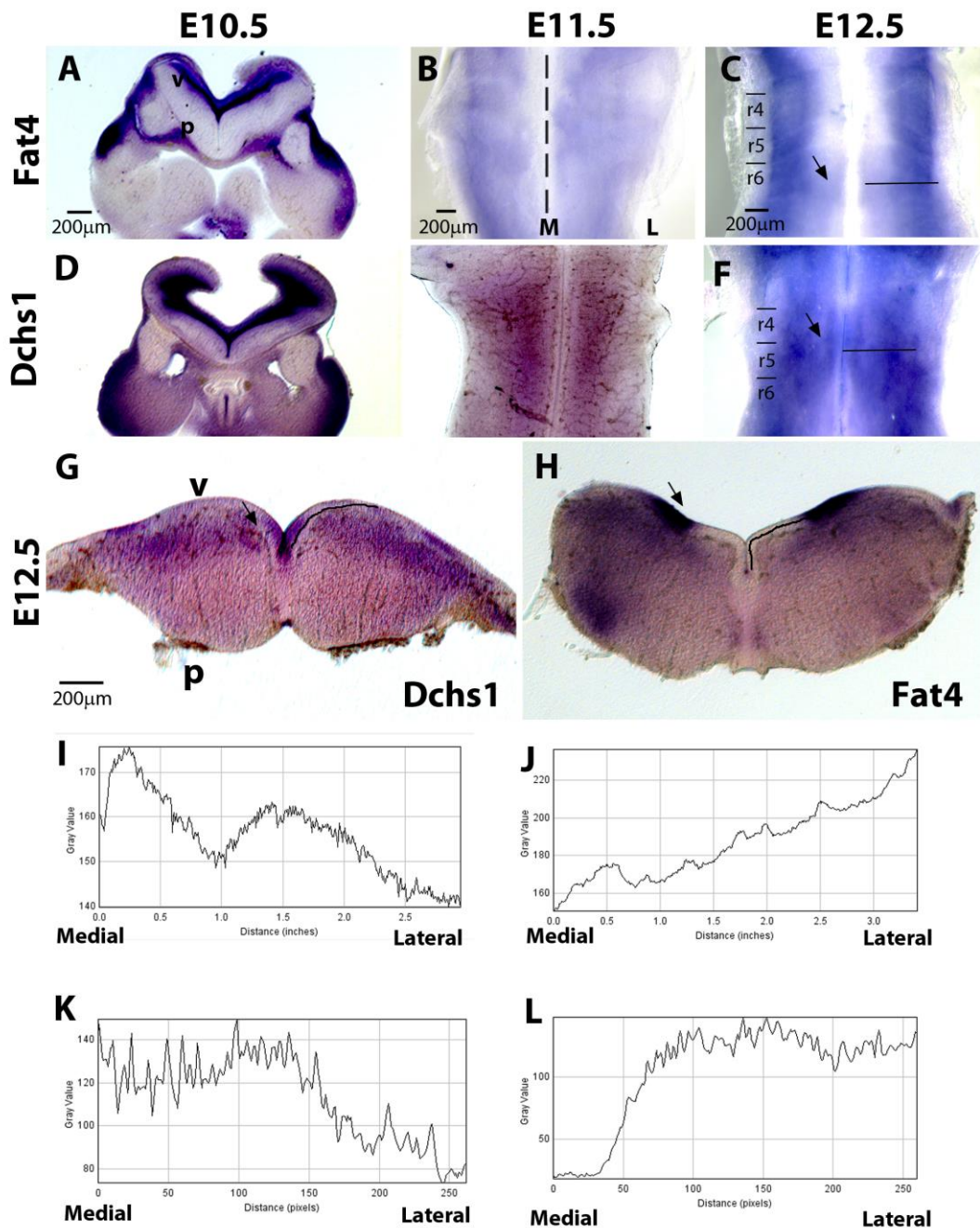
Figure 5.1. Graded expression of *Fat4* and *Dchs1* in the hindbrain. Transverse sections of the head from wholemount *in situ* hybridisation for *Fat4* (A) and *Dchs1* (D) at E10.5 show hints of diffuse expression in the ventricular layer of the hindbrain. Wholemount *in situ* hybridisation for *Fat4* (B, C) and *Dchs1* (E, F) at E11.5 (midline dashed, B, E) and at E12.5 (C, F) viewed from the ventricular surface. At E11.5, *Fat4* expression is observed throughout the hindbrain (B) and by E12.5 it is distinctly expressed at higher levels laterally (C). There are hints of *Fat4*

expression where the FBNs are present at E12.5 (black arrow). At E11.5, *Dchs1* expression is diffuse across the medial hindbrain (E) but by E12.5 there are hints of expression in the FBNs (black arrow) and stronger medial expression (F). Transverse sections of the hindbrain at E12.5 reveal that *Dchs1* is expressed in the midline and is expressed at lower levels lateral to the midline at the ventricular surface (black arrow, G). *Fat4* expression in transverse sections at E12.5 confirm that it is expressed higher laterally at the ventricular surface (black arrow, H) with some expression noted in the pial surface. The RNA levels were quantified (I-L) across a line drawn along the mediolateral axis of the hindbrain at E12.5 in wholemounts (black line, C, F) and in sections (black line, G, H). *Dchs1* expression is overall higher medially based on the wholemount (F, I) and section analysis (G, K). *Fat4* expression is higher laterally based on wholemount (C, J) and section analysis (H, L). L= lateral, M= medial, r= rhombomere, v= ventricular, p= pial.

5.2.2 Fat4 and Dchs1 are expressed as complementary gradients in the hindbrain

In *Drosophila*, Ft and Ds undergo various post translational modifications which can determine their interaction and stability at adjacent cell surfaces (Feng & Irvine 2009; Simon et al. 2010). To confirm the RNA gradients at the protein level, double wholemount immunolabelling was carried out with antibodies against Fat4, Dchs1 and Islet-1 in E12.5 hindbrains by our collaborator Dr Yaopan Mao (Postdoc in Ken Irvine's lab, Rutgers University) (Fig.5.2 A-D). To assess the levels of background staining, immunolabelling was also carried out with the anti-Fat4 and anti-Dchs1 antibodies on the respective mutant hindbrains as a negative control (Fig.5.2 B, D) which revealed that the staining observed in wildtype tissues was not non-specific.

The immunolabelling revealed that although Dchs1 is expressed diffusely across the hindbrain, it is higher medially and also expressed in the FBNs (Fig.5.2 A, A'). Dchs1 expression is higher in r4 when compared to r6 (Fig.5.2 A). The Dchs1 gradient is more defined at the protein level compared to the RNA expression.

Fat4 is expressed at higher levels in the lateral hindbrain and recapitulates the RNA gradient observed (Fig.5.2 C'). Fat4 expression is higher in r6 when compared to r4 and is also expressed in the leading edge of the FBNs as they migrate into the region of high Fat4 expression (Fig.5.2 C). The expression of Fat4 and Dchs1 was quantified across r4-r7 in the rostro-caudal and medio-lateral axes which confirmed that Fat4 and Dchs1 are expressed as a complementary gradient in the mediolateral and rostro-caudal axes (Fig.5.2 E-H).
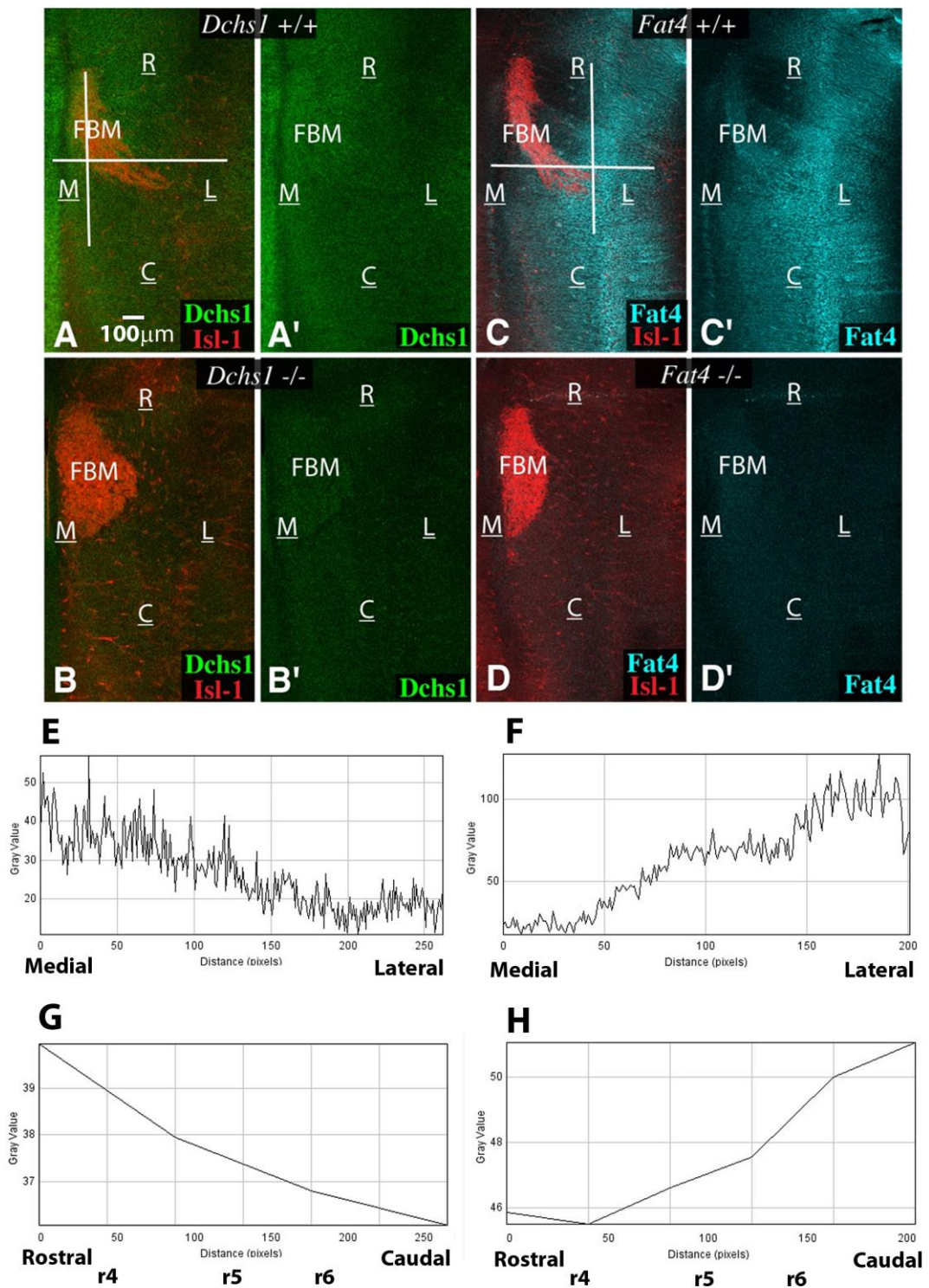
Figure 5.2. Opposing Gradients of Fat4 and Dchs1 expression may regulate lateral migration of FBNs. Wholemount immunochemistry on hindbrains from E12.5 mouse embryos, stained for Islet-1 to mark FBNs (red, A-D) and Dchs1 (green, A, A') or Fat4 (cyan, C, C'). Antibody stains were done on mutant embryos, as a control for background staining (B, B', D, D'). Dchs1 expression is higher

medially and lower laterally whilst Fat4 expression is higher laterally and lower medially (A, C). There are also differences in expression levels in the rostral to caudal axis of the hindbrain. Expression quantification across the dashed line in the mediolateral axis (A, C) confirmed that Dchs1 is higher medially (E) while Fat4 is higher laterally (F). Same analysis in the rostro-caudal axis revealed that Dchs1 is higher rostrally (G) while Fat4 is higher caudally (H). C= caudal, FBN= facial branchiomotor neurons, L= lateral, M= medial, R= rostral.

5.2.3   Loss of *Fat4* and *Dchs1* results in loss of polarity of the FBNs

It has been established that during migration of neurons, the Golgi complex and centrosome translocate to the front of the migrating cell and can therefore be used as a readout of cell polarity (Bellion et al. 2005). Cell shape can also be used a measure of polarity in a given axis.

 In order to determine if the FBNs become polarised during caudal migration wholemount-immunohistochemistry was carried out on E11.5 hindbrains using antibodies against Islet-1 and Giantin to visualise FBNs and the Golgi complex, respectively.

Wholemount-immunochemistry to E11.5 hindbrains revealed the cell body of individual FBNs at the midline, along with the localisation of the Golgi complex, in the form of a round dot, belonging to each neuronal cell body (Fig.5.3 A-C). In order to assess the polarisation of the FBNs, the position of the Golgi complex within each neuron was measured as an angle relative to the long axis of its corresponding nucleus and relative to the midline. These angles were then counted and plotted onto a rose plot into bins of 20 degrees. Each concentric circle represents increments of 5%. The analysis revealed that in the wildtype hindbrain, the Golgi complex of the FBNs are not polarised in the caudal axis as expected due to the direction of migration at this stage (Fig.5.3 A). Similarly, the FBNs in the *Fat4*$^{-/-}$ and *Dchs1*$^{-/-}$ hindbrains revealed no polarisation in the caudal axis (Fig.5.3 B, C).

Wholemount-immunohistochemistry was carried out on E12.5 hindbrains and the same analysis as described above was performed. In the wildtype hindbrain, the FBNs move away from the midline as organised streams of neurons (Fig.5.3 D). Analysis of the angles of the Golgi complex revealed that the FBNs are oriented in a biased direction, namely the caudal-lateral axis of the hindbrain, reflecting the migratory route being taken (Fig.5.3 D). The FBNs in the *Fat4*$^{-/-}$ and *Dchs1*$^{-/-}$ hindbrains are arrested at the midline with no visible streams of neurons migrating away (Fig.5.3 E, F). The Golgi of the FBNs are randomly oriented in the *Fat4*$^{-/-}$ and *Dchs1*$^{-/-}$ mutants and lack any directional bias (Fig.5.3 E, F).

 In order to statistically confirm whether the FBNs in the wildtype hindbrain are more polarised than the FBNs in the *Fat4*$^{-/-}$ and *Dchs1*$^{-/-}$ mutant hindbrains, the

Rayleigh test was performed on angle distribution of the Golgi complex of the FBNs. The test revealed that the FBNs in the wildtype were highly polarised with a p-value of $p<10^{-12}$, whereas the *Fat4*$^{-/-}$ mutants had a value of $p=0.13$ and the *Dchs1*$^{-/-}$ mutants had a value of $p=0.09$ revealing a more uniform distribution of the Golgi complex. The Mardia-Watson-Wheeler test was also performed to determine whether the difference between the Golgi angle distribution of the wildtype and *Fat4*$^{-/-}$ or *Dchs1*$^{-/-}$ mutant FBNs is significantly different from one another. The paired test revealed a significant difference between wildtype and *Fat4*$^{-/-}$ FBN polarity with a p value of $p<10^{-14}$. Similarly, a significant difference was observed between the wildtype and *Dchs1*$^{-/-}$ FBN polarity with a p value of $p<10^{-12}$.
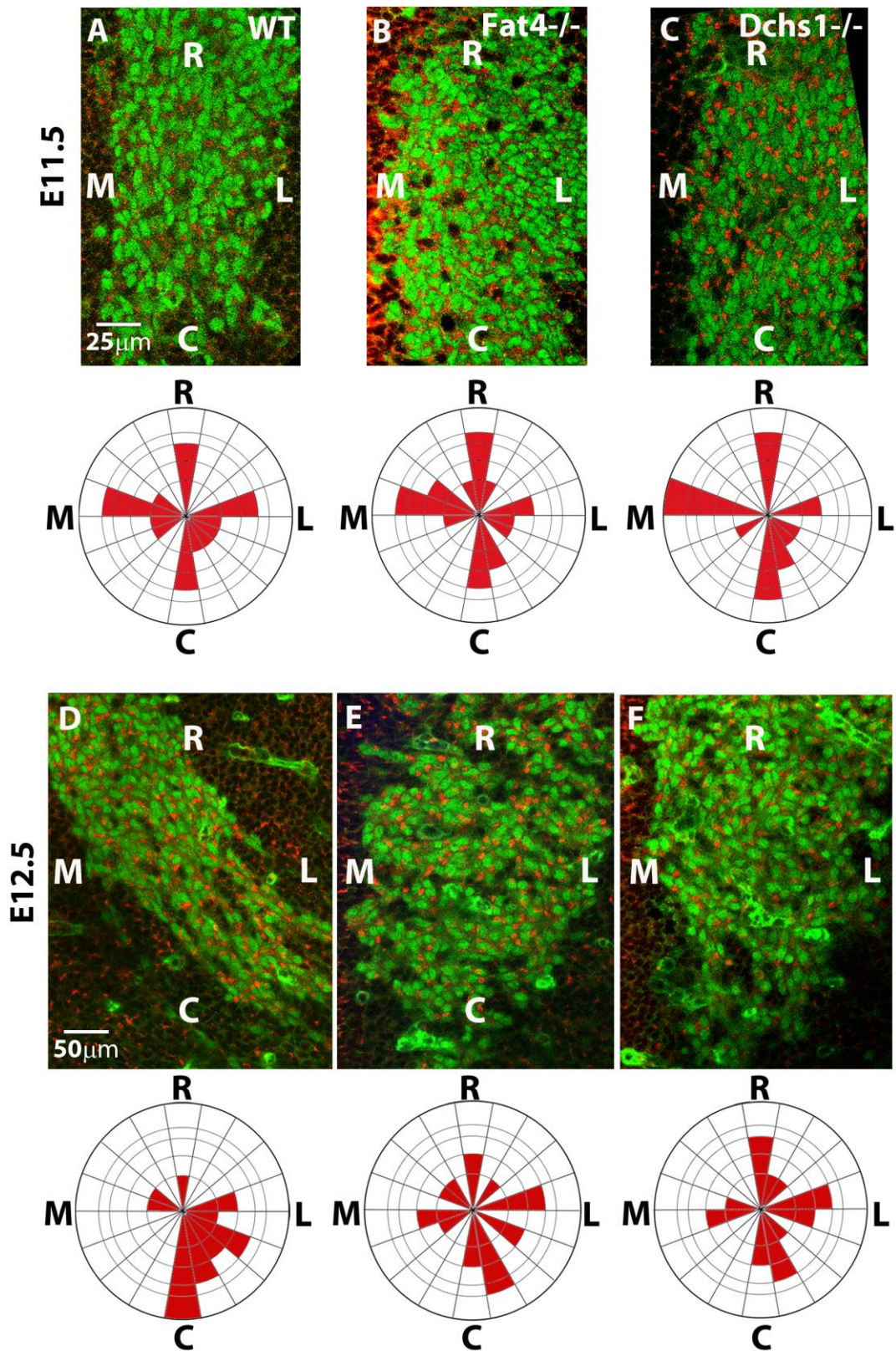
Figure 5.3. The FBNs fail to polarise in *Fat4-/-* and *Dchs1-/-* mutants. Wholemount immunochemistry showing the orientation of the Golgi complex (red) in migrating FBNs (green) at E11.5 in wildtype (A), *Fat4*^{-/-} (B) and *Dchs1*^{-/-} (C)

embryos. The polarity of the neurons is quantified in the rose plots below each image. In the wildtype hindbrain, the FBNs have no obvious polarity (A) and neither do the FBNs in the *Fat4*$^{-/-}$ (B) and *Dchs1*$^{-/-}$ (C) hindbrains. At E12.5, FBNs in the wildtype hindbrain can be seen undergoing lateral tangential migration and are accordingly polarised in the caudal-lateral axis of the hindbrain (D). In the *Fat4*$^{-/-}$ (E) and *Dchs1*$^{-/-}$ (F) hindbrains, the FBNs are arrested at the midline and fail to polarise in any particular axis of the hindbrain. C= caudal, L= lateral, M= medial and R= rostral.

5.2.4 Analysis of cell shape of FBNs

As an alternative measure of polarity, the cell shape of the FBNs was investigated by wholemount-immunohistochemistry using phalloidin to stain F-actin at cell membranes of the FBNs and anti-Islet-1 to stain the FBN cell body. In the wildtype hindbrains, FBNs have an elongated morphology along the direction of migration (Fig.5.4 A). However, there is a difference in the relative elongation of the FBNs at the back of the migratory stream versus the leading edge (Fig.5.4 A, white boxes). This difference was quantitatively measured by analysing the eccentricity of an object using Cell Profiler software. Eccentricity is a measure of how elliptical an object is. A true ellipse or an elongated FBN is given a score of 1 and a round FBN is scored as 0.

Analysis of the wildtype FBNs confirmed that the FBNs at the back of the stream are less elongated when compared to the front of the migratory stream (Fig.5.4 A, C). Analysis of the $Dchs1^{-/-}$ hindbrain showed that the FBNs are less elongated at the back and front of the neuronal stream when compared to wildtype FBNs in the same position of the migratory stream (Fig.5.4 B, C). Furthermore, the FBNs in $Dchs1^{-/-}$ hindbrain are particularly more rounded in the front half of the migratory stream (Fig.5.4 C).
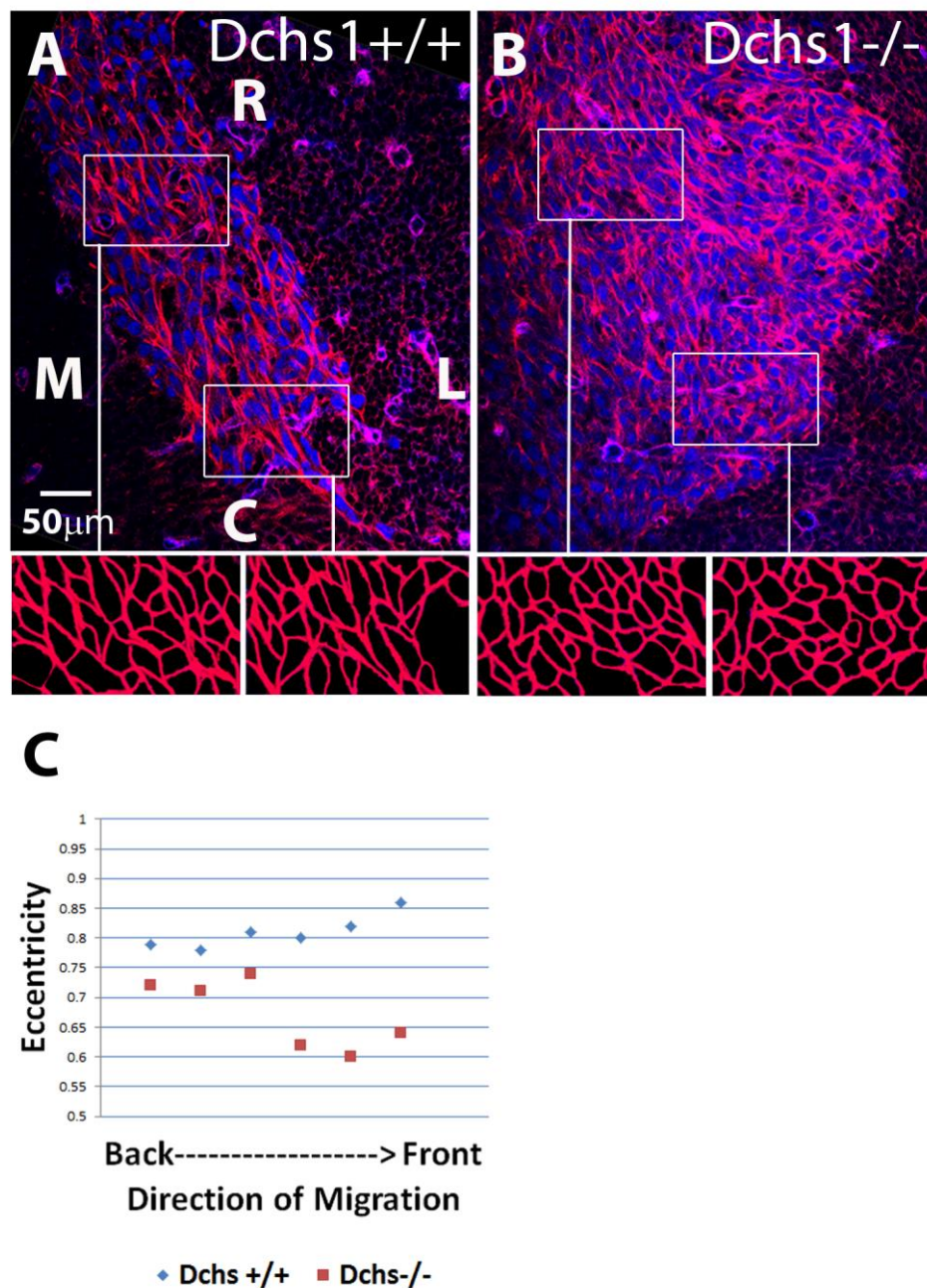
Figure 5.4. Loss of Fat signalling results in loss of polarised cell shape of the FBNs. Wholemount immunochemistry showing F-actin at cell membrane by phalloidin staining (red) and migrating FBNs (blue) in E12.5 wildtype (A) and *Dchs1*^{−/−} (B) hindbrains. The outlines of the FBN cell shape at the leading edge and in the centre of the neuronal stream are shown in the sketches below (white boxes used for magnified area, A, B). The cell shape of the FBN is quantified (C) where 0 is a circle and 1 is an ellipse. The wildtype FBNs are elongated at the leading edge (A, C) whilst the *Dchs1*^{−/−} FBNs are less elongated in the entire FBN migratory stream (B, C). C= caudal, L= lateral, M= medial and R= rostral.

5.2.5   Analysing polarity in the Neuroepithelium

Fat4 and Dchs1 are expressed as gradients in the hindbrain and regulate polarised lateral migration of the FBNs. To determine if the neuroepithelium shows any polarity (apart from apical-basal) and if Fat4/Dchs1 gradients could also polarise the neuroepithelium, the same images used for E12.5 FBN and Golgi analysis were analysed for neuroepithelium cell polarity.

The immunostaining allowed visualisation of neuroepithelial cell membranes (Fig.5.5 A-D). The Golgi complex of the neuroepithelial cells appears as a small dot at the edge of the cell membrane (Fig.5.5 A-D white arrows). The neuroepithelial cells are very rounded and compact hence it is not possible to differentiate between the cell membranes of adjacent cells. Due to this caveat, Golgi was scored as either being positioned on medial/lateral membrane of a cell or rostral/caudal surface of a cell with the assumption that there is only one Golgi per cell. Therefore, anything that was scored as medial could also be interpreted as lateral and hence the Golgi angles were plotted as a mirror image (Fig.5.5 A-D). Analysis of the wildtype hindbrains revealed that the Golgi are present on both the medial-lateral and rostro-caudal axes of the neuroepithelial cells (Fig.5.5 A, C). Similarly, no polarisation or bias was observed in the neuroepithelium of *Fat4*$^{-/-}$ and *Dchs1*$^{-/-}$ hindbrains (Fig.5.5 B, D) and the rose plots illustrated a uniform distribution of the Golgi complex position (Fig.5.5 A-D).
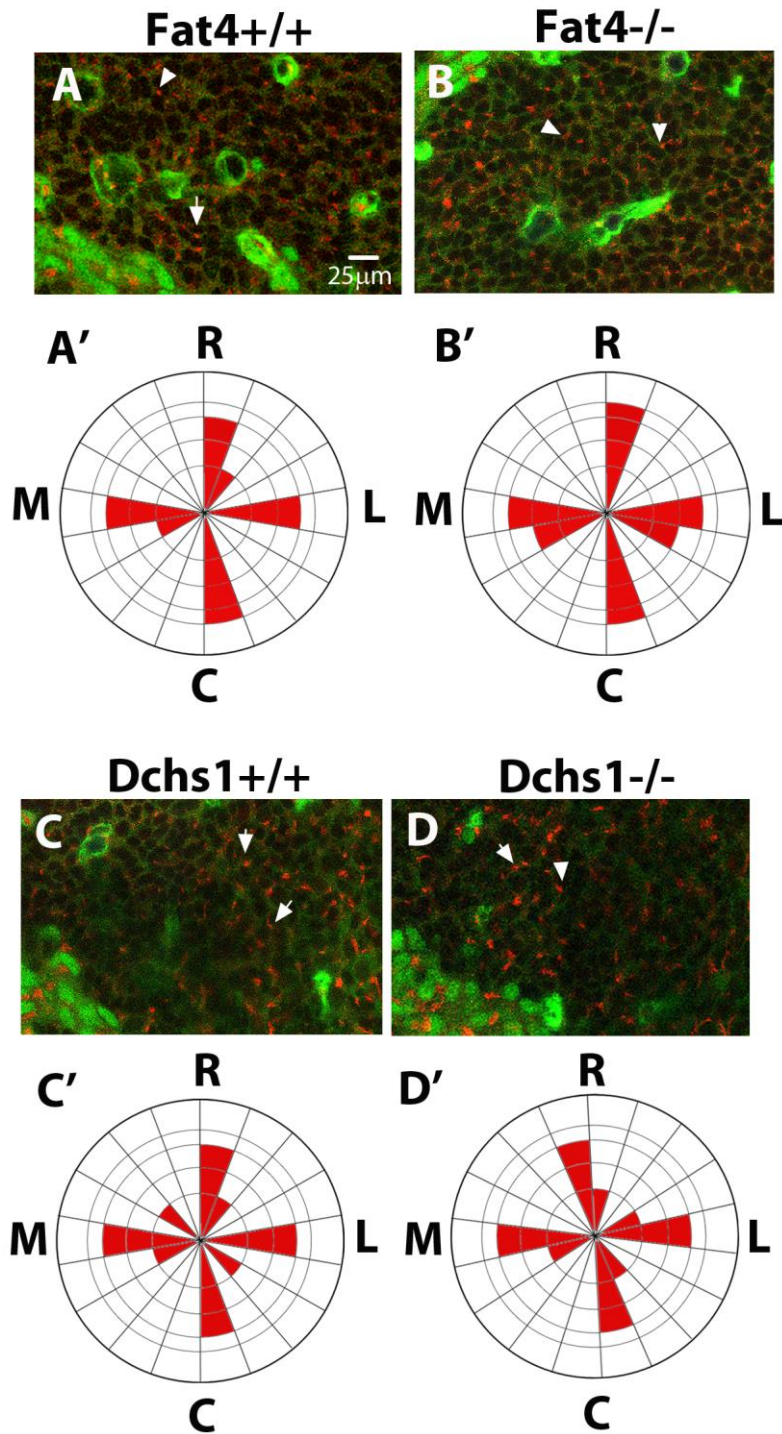
Figure 5.5. Polarity analysis of the neuroepithelium. Wholemount immunochemistry showing the polarity of the Golgi (red) and the cell membrane of the neuroepithelial cells (green) at E12.5 in wildtype (A, C), *Fat4*^{-/-} (B) and *Dchs1*^{-/-} (D) hindbrains. The Golgi complex was observed on all axes of the neuroepithelial cells (white arrowheads, A-D) and the position was plotted as a mirror image on the rose plots (A'-C'). C= caudal, L= lateral, M= medial and R= rostral.

5.2.6 Mosaics shed light on cell-cell communication and gradient disruption

In *Drosophila*, the role of gradients of Ds has been determined by creating a patch of mutant cells that lack expression of Ds which disrupt the Ds gradient. The polarity of cells around the clone of mutant cells is then analysed to assess reversal of polarity or loss of polarity. Given that Fat4 and Dchs1 appear as gradients across the hindbrain and are responsible for polarising the FBNs, a mouse line was generated specifically to disrupt the Dchs1 gradient to determine its importance in polarised FBN migration.

The mT/mG mouse line constitutively expresses membrane-Tomato hence all cell membranes can be visualised with red fluorescence. However, upon Cre activation the tomato cassette is excised and the adjacent GFP cassette becomes actively transcribed (Muzumdar et al. 2007). The mT/mG reporter line was crossed to a *Dchs1*$^{fl/fl}$ line to generate *Dchs1*$^{fl/fl}$ *ROSA* $^{mT/mG}$ homozygous mice. This line was later crossed with a Tamoxifen induced Cre (CreER^{TM}) *Dchs1*$^{+/-}$ line which was predicted to switch on GFP and inactivate *Dchs1* simultaneously from all the cells that are Cre positive. The percentage of Cre positive cells depends on the tamoxifen dose. Using this line, mosaic tissue was generated which was used to assess the effect of disruption of the Dchs1 gradient across the hindbrain. Tamoxifen was administered at doses of 1 mg, 0.75 mg and 0.6 mg.

Wholemount-immunochemistry was carried out using anti-Islet-1 and anti-Giantin antibodies on E12.5 hindbrains. The *Fat4*$^{+/-}$ and *Dchs1*$^{+/-}$ heterozygous mice do not have any defects in migration or polarisation of FBNs therefore a heterozygous background was used as a control for this experiment. Wholemount analysis of the CreER^{TM} *Dchs1*$^{fl/+}$*ROSA* $^{mT/mG}$ control E12.5 hindbrains revealed normal migration of FBNs (Fig.5.6 A). Analysis in the GFP and Tomato channels revealed mosaicism of the tissue (Fig.5.6 A') and the Golgi staining revealed polarity comparable to that of wildtype hindbrains showing the typical bias along the caudal-lateral axis of the hindbrain (Fig.5.6 A'').

Various doses of Tamoxifen were administered and a dose dependant response was observed in the CreER^{TM} *Dchs1*$^{fl/-}$*ROSA* $^{mT/mG}$ mosaic hindbrains (Fig.5.6 B-D). At the highest dose of 1 mg Tamoxifen the FBNs were arrested at the midline and looked identical to the *Dchs1*$^{-/-}$ phenotype (Fig.5.6 B). Analysis was carried out on

higher magnification images to determine mosaicism in the tissue (Fig.5.6 B') and to measure the Golgi complex orientation, which revealed a generalised disruption in polarity (Fig.5.6 B''). The identical phenotype was observed in the mosaic hindbrains at a dose of 0.75 mg Tamoxifen, revealing FBNs at the midline and disruption of the FBN polarity (Fig.5.6 C-C''). The lowest dose of 0.6 mg Tamoxifen resulted in a slightly less severe FBN migration phenotype. Nevertheless, FBNs still appeared largely arrested in their lateral migration and a loss of FBN polarity was also observed (Fig.5.6 D-D'').

In order to assess the level of inactivation of *Dchs1* from the tissue and gauge the mosaicism of the tissue at different Tamoxifen doses, GFP positive cells were counted in the hindbrain neuroepithelium and in the FBNs (Fig.5.6 F). At the highest dose of 1 mg Tamoxifen, approximately 40% cells were GFP positive both in the neuroepithelium and in the FBNs. At a lower dose of 0.75 mg, up to 25% GFP positive cells were observed in the neuroepithelium and in the FBNs. Lastly, at the lowest dose of 0.6 mg, 18-20% GFP positive cells were observed across the tissue. Overall, a similar level of mosaicism was observed in the neuroepithelium as well as in the FBNs (Fig.5.6 F).

The level of Dchs1 inactivation should correlate with GFP activation as this should occur mutually exclusively in the same cell. However, due to not being able to test the efficiency of the Cre because of a lack of available anti-Dchs1 antibody, Q-PCR was carried out to assess levels of *Dchs1* transcripts at the various doses of Tamoxifen (Fig.5.6 G). Since a heterozygous background was used to generate mosaics, it was expected that *Dchs1* transcription would always be below 50%. The 1 mg dose resulted in total *Dchs1* transcript levels at just 20% compared to wildtype levels, and at the 0.75 mg dose, *Dchs1* levels were at 35%. Lastly, at the 0.6 mg dose *Dchs1* levels were at 40% (Fig.5.6 G). Comparing the Q-PCR results with the GFP cell counts revealed a slight discrepancy between the percentage of GFP positive cells and the percentage cells estimated for Dchs1 inactivation.
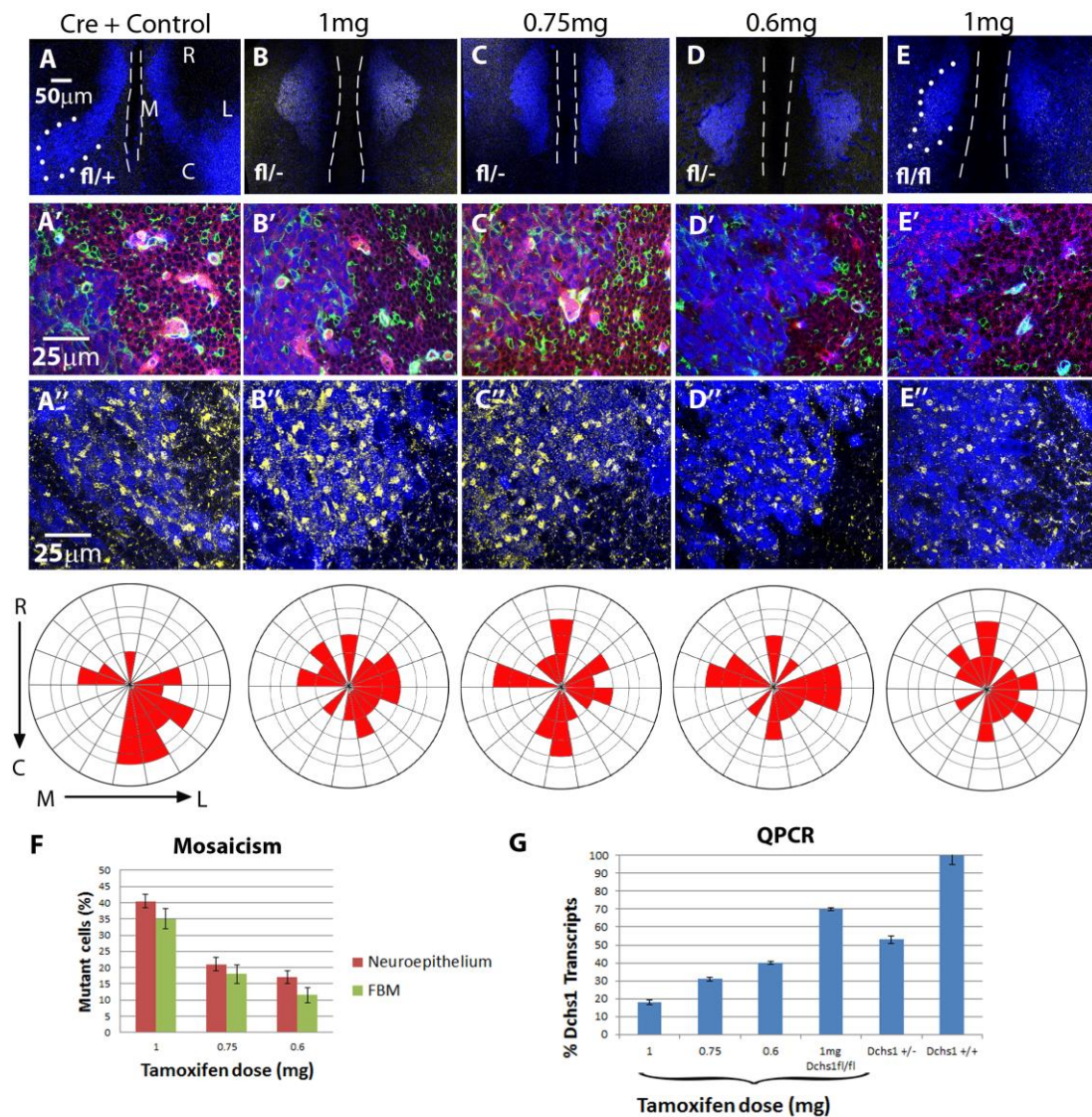
Figure 5.6. Dchs1 gradient is essential for polarised FBN migration.
Wholemount immunochemistry on the hindbrains of E12.5 Cre^{TM} $Dchs1^{fl/fl}$ $^{fl/-}$ $^{fl/+}$ $ROSA$ $^{mT/mG}$ embryos stained to mark the FBNs (blue) and the Golgi complex (yellow) (A-E). High magnification images show the constitutively active tomato expression interspersed with GFP expression, representing the null cells to show mosaicism of the tissue at all doses of tamoxifen (A'-E'). In the control hindbrains, tamoxifen treatment did not disrupt FBN migration or Golgi orientation (A-A''). At doses 1mg and 0.75 mg, FBNs were completely arrested at the midline and Golgi orientation was severely disrupted in $Cre^{TM}Dchs1^{fl/-}ROSA$ $^{mT/mG}$ embryos (B-B'', C-C''). At the low dose of 0.6 mg of tamoxifen treatment FBNs were less affected but largely disrupted in their movement and Golgi orientation (D-D''). In the $Dchs1^{fl/fl}$ background, a dose of 1 mg tamoxifen results in a significant disruption of FBN

migration as well as Golgi orientation (E-E''). GFP cell count analysis revealed similar level of GFP activation in both the FBNs and the neuroepithelium at all tamoxifen doses (F). There were 40% GFP positive cells at 1 mg, 22% GFP cells at 0.75 mg and 18% GFP cells at 0.6 mg (F). QPCR analysis revealed Dchs1 transcript levels of 20% at 1 mg dose, 30% at 0.75 mg and 40% at 0.6 mg in $Dchs1^{fl/-}$ background whilst 70% transcript levels were present at 1 mg dose in $Dchs1^{fl/fl}$ embryos (G). C= caudal, L= lateral, M= medial and R= rostral.

Fat signalling could regulate polarised migration of FBNs by a transcriptional pathway or by PCP signalling therefore mosaics were generated in a *Dchs1*^{fl/fl} background to keep Dchs1 levels above 50% in order to truly assess the role of PCP by disruption of Dchs1 gradient in the hindbrain (Fig.5.6 E). Given that in a heterozygous mouse when Dchs1 transcript levels are at 50%, there is no FBN phenotype, a 1 mg dose of Tamoxifen was administered in the *Dchs1*^{fl/fl} background to generate mosaics with above 50% *Dchs1* transcript levels (Fig.5.6 E). Wholemount immunohistochemistry revealed that at 1 mg dose in the CreER^{TM} *Dchs1*^{fl/fl}*ROSA* ^{mT/mG} hindbrains, FBNs were largely arrested in their migration and a disruption in FBN polarity was also observed (Fig.5.6 E-E''). Furthermore, QPCR analysis revealed that these embryos had 70% *Dchs1* transcript levels compared to wildtype embryos (Fig.5.6 G). This result was indicative of Fat regulation of FBN migration via PCP.

5.2.7 Gain of function of *Fat4* and *Dchs1* in vitro

The disruption of Dchs1 gradient across the hindbrain results in loss of polarisation of FBNs. To determine whether Fat4 or Dchs1 could play an instructive role in regulating the polarised response of FBNs, hindbrain explants were electroporated with *Fat4* or *Dchs1* full length constructs to observe a gain of function response by either inducing an ectopic gradient or by flattening the gradient of Fat4 and Dchs1. A *GFP-PCAX* construct was co-electroporated to visualise the region of electroporation and hindbrain explants were cultured for 48 hours and stained with anti-Islet-1, anti-Giantin and anti-GFP antibodies (Fig.5.7 A-C).

In the control hindbrain, GFP was electroporated to assess the effects of electroporation and explant culture on migration of the FBNs (Fig.5.7 A). Controls were repeated with GFP localisation observed in the midline, caudally, rostrally and laterally with no effect on FBNs themselves. However, the migration of FBNs was slow in culture (Fig.5.7 A, representative image shown for control). The Golgi complex orientation was also analysed in the controls on the electroporated and non-electroporated contralateral sides which revealed that only 50-60% of the FBNs were polarised in the caudal and lateral direction compared to a wildtype control that is

not cultured (Fig.5.7 A', A''). There is no difference in FBN polarity between the GFP electroporated and non-electroporated side of the hindbrain (Fig.5.7 A-A'').

Hindbrains were co-electroporated with GFP and Fat4 constructs and the GFP localisation was assumed to be indicative of Fat4 localisation. GFP expression was observed in different areas of the hindbrain such as laterally (overlapping with endogenous Fat4 expression), medially (potentially flattening the gradient) and caudally/rostrally in ectopic positions where Fat4 expression is not normally observed (Fig.5.7 B, representative image chosen). Electroporations with Fat4 revealed no obvious differences in the migration of the FBNs, however on a few occasions the FBNs appeared to migrate further caudally or a larger cluster of FBNs appeared to turn laterally in r5 compared to the non-electroporated side (Fig.5.7 B). However, it was not possible to eliminate the likelihood that these differences could be due to culture conditions. The Golgi orientation was also analysed in the Fat4 electroporated hindbrains, which showed slight differences in the polarity between the contra-lateral sides of about 10-15%. However, no bias or randomisation could be interpreted due to the variation within in the controls (Fig.5.7 B', B'', see table A.6 in Appendix).

Similar observations were made when hindbrains were co-electroporated with GFP and Dchs1. GFP localisation was observed in patches at the midline (overlapping with endogenous Dchs1 expression), laterally (potentially flattening the gradient) and caudal to the FBNs as well as rostral to the FBN migratory stream (Fig.5.7 C, representative image chosen). There was no effect on the migration of the FBNs although some variation in Golgi orientation was observed between the contralateral sides (Fig.5.7 C-C''). However, due to the variation in Golgi orientation of control FBNs, no conclusions could be made about effect on FBN polarity (Fig.5.7 C'') (see table A.6 for list of explants analysed).

The occasional extended caudal migration of the FBNs in Fat4 electroporated hindbrains suggested that Fat4 may be instructive when misexpressed in r7. However, lack of rhombomere marker identity in the analysis made it difficult to confirm this. To investigate this double *in situ* hybridisation was carried out against *Islet-1* (purple) to mark FBNs and *Cyp26b1* (light blue) to mark the boundary of

r6/r7. This analysis revealed that FBN migration was normal in both the control and Fat4 electroporated hindbrains (Fig.5.7 E, G).

Given the very minor changes, if any, in the migratory behaviour and polarity of the FBNs, one possibility is that Fat4 and Dchs1 are expressed at very low levels. Fat4 full length constructs are very large (~15kb) and may not be optimally expressed in the explant system employed in the studies here. In order to assess whether the constructs were expressed in the *in vitro* assays, hindbrains were electroporated with GFP and Fat4 and sent to our collaborator (Dr. Yaopan Mao) to carry out wholemount-immunohistochemistry with anti-Fat4 antibody. This analysis revealed that GFP was localised laterally in the hindbrain, overlapping with endogenous Fat4 expression (Fig.5.7 H). However, the Fat4 staining revealed no difference in levels of protein in the electroporated versus the non-electroporated contralateral side of the hindbrain (Fig.5.7 I). Therefore, based on these experiments it was not possible to conclude whether Fat4 and Dchs1 provide instructive or permissive cues to the FBNs.
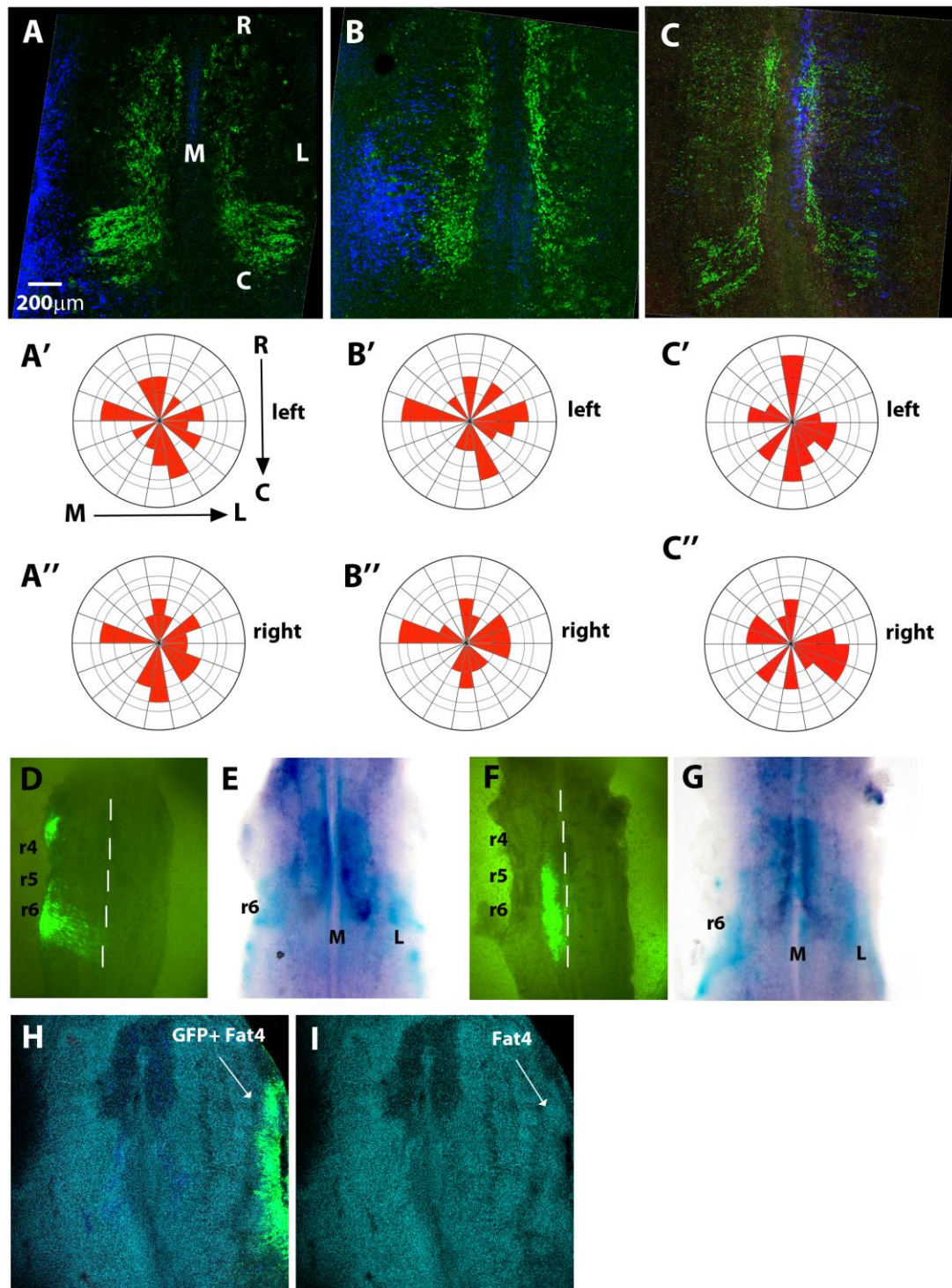
Figure 5.7. Fat4 and Dchs1; uncoupling instructive and permissive cues. Hindbrain explants electroporated with a GFP-PCAX construct (A, D, E), co-electroporated with GFP and Fat4 (B, F-I) and co-electroporated with GFP and Dchs1 (C). GFP electroporated hindbrains were stained for GFP (blue) and FBNs (green) which revealed no effect on FBN migration (A) but polarity of the Golgi complex was affected in cultures on both electroporated and non-electroporated side

of the hindbrain (A', A''). Electroporations with Fat4 and Dchs1 constructs had mild to moderate effects on FBN migration which could be attributed to the culture environment (B, C, and F). Similarly, the FBN polarity was variable and often similar on electroporated and non-electroporated sides of the hindbrain (B', B'', C', C''). Double wholemount *in situ* hybridisation was carried out after GFP (D, E) and GFP + Fat4 electroporation (F, G) to *Islet-1* (purple) to mark FBNs and *Cyp26b1* (blue) to mark r5 and r6. No difference in FBN migration was noted between GFP only and GFP + Fat4 co-electroporated hindbrains (E and G). Hindbrains electroporated with GFP + Fat4 (H, I) were stained for GFP (green) and Fat4 (cyan). GFP expression can be seen in the lateral hindbrain (H), however, no increase in levels of Fat4 expression was observed (H, I). C= caudal, L= lateral, M= medial, r= rhombomere and R= rostral.

5.3 Discussion

The analysis here shows that Fat4 and Dchs1 are expressed in gradients and loss of Dchs1 and Fat4 disrupts FBN polarity. Analysis of Dchs1 mosaic embryos shows that the gradient of Dchs1 is required for normal FBN migration and polarity. The data argues that Fat4/Dchs1 regulate FBN migration through PCP rather than a cell adhesive function.

Analysis of FBN polarity at E11.5 revealed no polarisation as the FBNs migrate caudally in wildtype or $Fat4^{-/-}$ and $Dchs1^{-/-}$ hindbrains. Although this was surprising, a few studies in zebrafish have reported that during caudal migration cellular polarity cannot be observed using the position of the centrosome or Golgi complex as a readout of polarity, however polarised cell protrusions can be observed in the FBNs (Jessen et al. 2002).

At E12.5, two readouts were used for assessing polarity of FBNs; cell shape and orientation of the Golgi complex within the FBNs. The FBNs are elongated in the direction of the migration and about 80% of the FBNs have the Golgi complex oriented along the lateral-caudal axis of the hindbrain. Loss of $Fat4$ and $Dchs1$ results in a loss of FBN polarity as well as loss of the elongated cell shape thus illustrating the essential role of Fat signalling in regulating polarised FBN migration.

The analysis of the neuroepithelium in the wildtype and mutant hindbrains did not reveal any polarity. One possibility could be that the neuroepithelium is undergoing changes in size in various axes at this stage of development hence Golgi complex orientation may not be the appropriate readout of polarisation.

To determine if gradients are important, mosaic embryos were analysed to assess the effect of disruption of the graded Dchs1 expression within the hindbrain. This analysis revealed that a continuous Dchs1 gradient is required for polarised FBN migration. Although $Dchs1^{+/-}$ mice (i.e. with 50% Dchs1 transcript levels) do not display a FBN migration defect, FBN polarisation and migration is significantly disrupted in mosaic embryos with 70% Dchs1 transcript levels. This analysis highlights that graded activity of Dchs1 is crucial to the polarisation and migration of FBNs and is indicative of Fat-PCP signalling.

It would be expected that if FBN migration is governed by Fat signalling through a direct transcriptional pathway or via alterations in cell adhesion, then minor disruptions to overall Dchs1 levels would not severely affect FBN polarity and migration as observed in the mosaic embryos.

Fat4 and Dchs1 expression is complementary in the hindbrain and this, in part, can be compared to Ft-Ds activity in *Drosophila.* Although Ft is uniformly expressed in *Drosophila* tissues, Fj and Ds interaction results in a graded activity of Ft across the tissue which is complementary to Ds expression (Yang et al. 2002; Ma et al. 2003). This parallel of opposing activity gradients suggests a potential conservation of mechanism.

Based on Fat4 and Dchs1 expression in the hindbrain, it is proposed that that they interact in the following manner. The cells in the medial hindbrain have higher levels of Dchs1 at their cell surface and low levels of Fat4 at the adjacent cell surface (Fig.5.8). The heterophilic interaction of Fat4 and Dchs1 across the cell surfaces results in a graded activation of Dchs1 and Fat4 across the hindbrain (Fig.5.8) This asymmetry is propagated from cell-cell via heterophilic interactions of Fat4 and Dchs1 which impart directional polarity to the FBNs either directly or indirectly (Fig.5.8).

Although asymmetry of Fat4 and Dchs1 protein can be observed at the tissue level their localisation at the cellular level has not been studied in this system. Recent evidence from *Drosophila* has emerged showing subtle asymmetry in localisation of Ft and Ds at adjacent cell membranes in the wing (Brittle et al. 2012; Ambegaonkar et al. 2012), providing insight into polarity propagation from cell-cell by the Fat-PCP pathway.
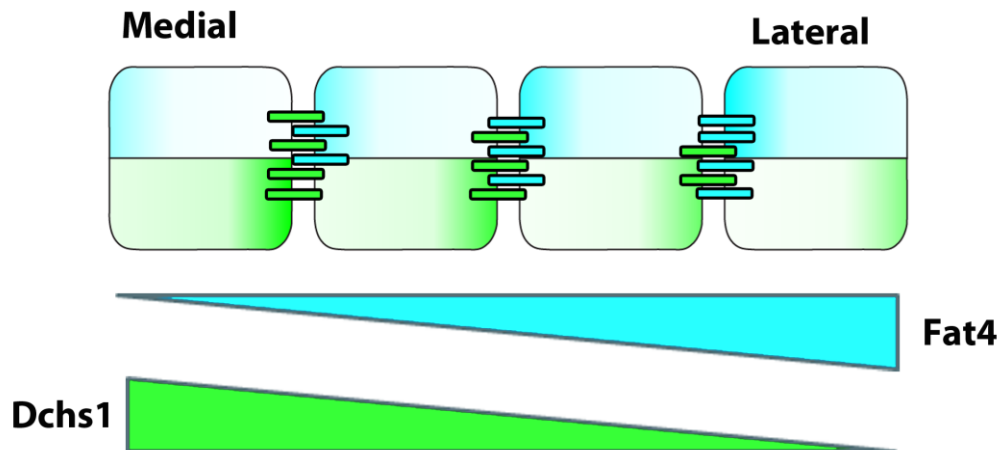
Figure 5.8. Model of Fat4 and Dchs1 gradients in the hindbrain. Sketch diagram representing the gradients of Fat4 and Dchs1 across the hindbrain. Each cell is represented by a square and varying levels of Fat4 (blue) and Dchs1 (green) are present in each cell across the hindbrain. Heterophilic interactions of Fat4 and Dchs1 occur on the adjacent cell surface represented by blue and green coloured bars. The nature of Fat4 and Dchs1 interaction and thereby their activity changes across the tissue due to relative levels of Fat4 and Dchs1 in each cell. This is proposed to impart polarity to the FBNs. The triangles below the cells represent the gradients of Dchs1 (green) and Fat4 (blue) across the medio-lateral axis of the hindbrain.

Gain of function analysis of Fat4 and Dchs1 was carried out to investigate any instructive role of Fat4 and Dchs1 in regulating FBN migration by either reversing the gradient or making it uniform. Due to several caveats, these experiments were inconclusive. It is possible that the explant assays are not optimal for expressing the large full length Fat4 and Dchs1 constructs or the timing of the electroporation is not optimal. An alternative approach would be to electroporate *in vivo* at E10.5 to ensure an optimal timeframe for protein expression and stabilisation before the FBN defect arises. The studies described in this chapter strongly suggest the role of Fat-PCP signalling in regulating polarised migration of FBNs.

6 FAT4 AND DCHS1 HAVE CELL AUTONOMOUS AND NON-CELL AUTONOMOUS ROLES IN REGULATING LATERAL MIGRATION OF FBNS

6.1 Introduction

FBN migration is regulated by both intrinsic and environmental signals. For example, intrinsic cues include *Tbx20* whilst extrinsic factors include *Wnt5a* and *VEGF-164* (Jacob et al. 2001; Schwarz et al. 2004; Song et al. 2006; Vivancos et al. 2009). Fat4 and Dchs1 are expressed in complementary patterns in the hindbrain and FBNs. The chimeric studies indicate that gradient of Dchs1 may regulate FBN migration but the analysis did not reveal whether Dchs1 is required intrinsically within the FBNs or in the neuroepithelium.

Several studies have been carried out in zebrafish to uncouple the cell autonomous and non-cell autonomous roles of Fz-PCP components during FBN migration (Wada et al. 2006; Sittaramane et al. 2009; Walsh et al. 2011). Mutation in zebrafish *trilobite* gene, mapped to the *Vangl* locus, revealed that trilobite function is required both cell and non-cell autonomously (Jessen et al. 2002). Wildtype FBNs transplanted into the *trilobite* mutant hindbrain were unable to undergo caudal migration, highlighting the non-cell autonomous role of trilobite in the hindbrain. Conversely, a subset of the *trilobite* mutant FBNs were unable to migrate out of r4 in a wildtype host revealing the cell-autonomous roles of trilobite (Jessen et al. 2002). A similar study in zebrafish highlighted the non-cell autonomous function of *Celsr1-3* genes and *Fz3a* which prevent FBNs from migrating radially instead of tangentially (Wada et al. 2006). Genetic approaches in mice have also indicated that *Celsr1* is required non-cell autonomously whilst *Celsr2* and *Celsr3* act cell-autonomously in a partially redundant fashion to regulate caudal FBN migration (Qu et al. 2010).

In order to understand the cell-autonomous and non-cell autonomous requirements of Fat4 and Dchs1 in the FBNs and the hindbrain, conditional mouse lines were generated. To inactivate *Fat4* and *Dchs1* in the FBNs, a Cre line was generated under the control of the *Islet-1* promoter which is expressed exclusively in motor

neurons (Yang et al. 2006). Similarly, to inactivate *Fat4* and *Dchs1* in the neuroepithelium the *Hoxa3* promoter was used which is expressed in r5 and r6 of the neuroepithelium, but not in r4 where the FBNs are born (Macatee et al. 2003). Both the conditional lines were crossed to a Lac-Z (R26R) reporter line to visualise where Cre induced inactivation had occurred.

6.2 Results

6.2.1 Analysis and characterisation of the Cre lines

The *Islet-1^{cre}* line has been used previously to analyse cell autonomous roles of *Celsr* genes in FBN migration (Qu et al. 2010). The *Hoxa3^{cre}* line inactivates gene function within r5 and r6 but not r4 (Gary Gaufo, personal communication) and was chosen to inactivate *Fat4* and *Dchs1* within the neuroepithelium. In the first instance, the tissue-specificity of these Cre lines was confirmed by crossing *Fat4$^{fl/fl}$* and *Dchs1$^{fl/fl}$* lines to a LacZ reporter mouse (R26R$^{LacZ/LacZ}$). These homozygous lines were then crossed to either *Islet-1^{cre} Fat4$^{+/-}$* or *Islet-1^{cre} Dchs1$^{+/-}$* and *Hoxa3^{cre} Fat4$^{+/-}$* or *Hoxa3^{cre} Dchs1$^{+/-}$* mice. E12.5 hindbrains were immunostained using anti-β-galactosidase antibody to detect LacZ expression which marked the area of inactivation of *Fat4* and *Dchs1* in the hindbrain, and anti-Islet-1 antibody to visualise the FBNs.

As heterozygous *Fat4$^{+/-}$* and *Dchs1$^{+/-}$* mice have no phenotype in the hindbrain, *Fat4$^{fl/+}$* and *Dchs1$^{fl/+}$* under the control of *Islet-1^{cre}* or *Hoxa3^{cre}* were used as control embryos and compared to *Fat4$^{fl/-}$* and *Dchs1$^{fl/-}$* Cre positive embryos. In the *Islet-1^{cre}Fat4$^{fl/+}$* and *Islet-1cre Dchs1$^{fl/+}$* control hindbrains the expression of LacZ was observed in the FBNs only. The β-galactosidase staining overlapped with the Islet-1 staining in the FBNs (Fig.6.1 A-D). This pattern of staining confirmed that the Cre is activated specifically within the FBNs under the control of the *Islet-1^{cre}* promoter (Fig.6.1).

In the *Hoxa3^{cre}Fat4$^{fl/+}$* and *Hoxa3^{cre}Dchs1$^{fl/+}$* control hindbrains the expression of LacZ was observed in the neuroepithelium in r5 and r6 of the hindbrain and was completely absent in the FBNs (Fig.6.2 A-D). This confirmed that the Cre is activated specifically within the neuroepithelium under the control of the *Hoxa3^{cre}* promoter (Fig.6.2).

Based on the mating strategy undertaken, in the *Hoxa3^{cre}Fat4$^{fl/-}$* and *Hoxa3^{cre} Dchs1$^{fl/-}$* lines, the FBNs are heterozygous for either *Fat4* or *Dchs1* whilst the neuroepithelium is null. Conversely in the *Islet1^{cre} Fat4$^{fl/-}$* and *Islet-1^{cre}Dchs1$^{fl/-}$* lines, the FBNs are null for either *Fat4* or *Dchs1* whilst the neuroepithelium is heterozygous. Each analysis includes n≥3.

6.2.2   Dchs1 and Fat4 have cell autonomous roles within the FBNs

To analyse FBN migration, immunohistochemistry analysis of the *Islet-1^{cre}Fat4$^{fl/-}$* and *Islet-1^{cre}Dchs1$^{fl/-}$* E12.5 hindbrains was carried out using an anti-Islet-1 antibody to visualise the FBNs. The polarity of the FBNs was simultaneously analysed by immunostaining for the Golgi complex using an anti-Giantin antibody. In the control hindbrains (Fig.6.1 A-D, E, H), FBN migration is normal and analysis of Golgi polarity revealed that the Golgi complex is predominantly polarised along the caudal-lateral axis, as expected from the previous analysis in heterozygous mice. However, in *Islet-1^{cre}Fat4$^{fl/-}$* and *Islet-1^{cre}Dchs1$^{fl/-}$* hindbrains, FBN tangential migration is disrupted. Loss of *Dchs1* from the FBNs has a more significant effect on migration.

Analysis of the *Islet-1^{cre}Dchs1$^{fl/-}$* hindbrains revealed a very striking arrest in migration, similar to that observed in *Dchs1$^{-/-}$* null embryos (Fig.6.1 G). The FBNs are completely arrested at the midline and do not have a leading edge (Fig.6.1 J). The angle of the Golgi complex was plotted onto a rose plot which revealed a severe loss of Golgi polarisation compared to the control FBNs (Fig.6.1 J'). The Rayleigh test revealed that the Golgi angle distribution of FBNs in the *Islet-1^{cre}Dchs1$^{fl/-}$* hindbrains is significantly more uniform and not polarised with a value of p=0.145 compared to a value of $p<10^{-12}$ for control FBNs. The Mardia-Watson-Wheeler test confirmed that the Golgi angle distribution of FBNs between the control and *Islet-1^{cre}Dchs1$^{fl/-}$* FBNs is significantly different with a value of $p<10^{-12}$.

In contrast, loss of *Fat4* function within the FBNs has a milder effect on FBN migration. FBNs in the *Islet-1^{cre}Fat4$^{fl/-}$* hindbrain were able to move away from the midline (Fig.6.1 F, I). However, they had not moved as far laterally or caudally as the FBNs in control hindbrains (Fig.6.1 E, F, H, I). The FBNs in the *Islet-1^{cre}Fat4$^{fl/-}$* hindbrain also did not migrate as a compact stream of neurons and appeared scattered at the leading edge when compared to the streamlined leading edge of the control FBNs (Fig.6.1 E, F, H, I).

Analysis of the FBN polarity indicated a moderate disruption in Golgi orientation compared to control FBNs. The Mardia-Watson-Wheeler test confirmed that the Golgi angle distribution between the controls and *Islet-1^{cre}Fat4$^{fl/-}$* FBNs is significantly different with $p<10^{-12}$. However, the Rayleigh test indicated that the

FBNs in the *Islet-1^{cre}Fat4^{fl/-}* hindbrains show some polarised behaviour with a value of $p<4\times10^{-5}$ (Fig.6.1 I, I'), although they are less polarised when compared to the control FBNs which have a value of $p<10^{-12}$ (Fig.6.1 H, H', I, I').

In order to assess the effect of loss of *Fat4* and *Dchs1* on FBN migration at E13.5, *in situ* hybridisation was carried out to E13.5 hindbrains of the *Islet-1^{cre}* conditional mutants using an *Islet-1* antisense probe to visualise the FBNs. (Fig.6.3 A-C). In the control hindbrains normal migration of the FBNs was observed, as expected from previous analysis of heterozygous mice, and FBNs could be seen condensing laterally within r6 (Fig.6.3 A). Loss of *Dchs1* from the FBNs results in a continued arrest of lateral migration of FBNs and a delay in the caudal migration as seen previously in the *Dchs1* null mice (Fig.6.3 C). In contrast, loss of *Fat4* from the FBNs results in a largely normal migration of FBNs at this stage as they could be seen condensing laterally as slightly elongated nuclei in caudal r5 and r6 (Fig.6.3 B).
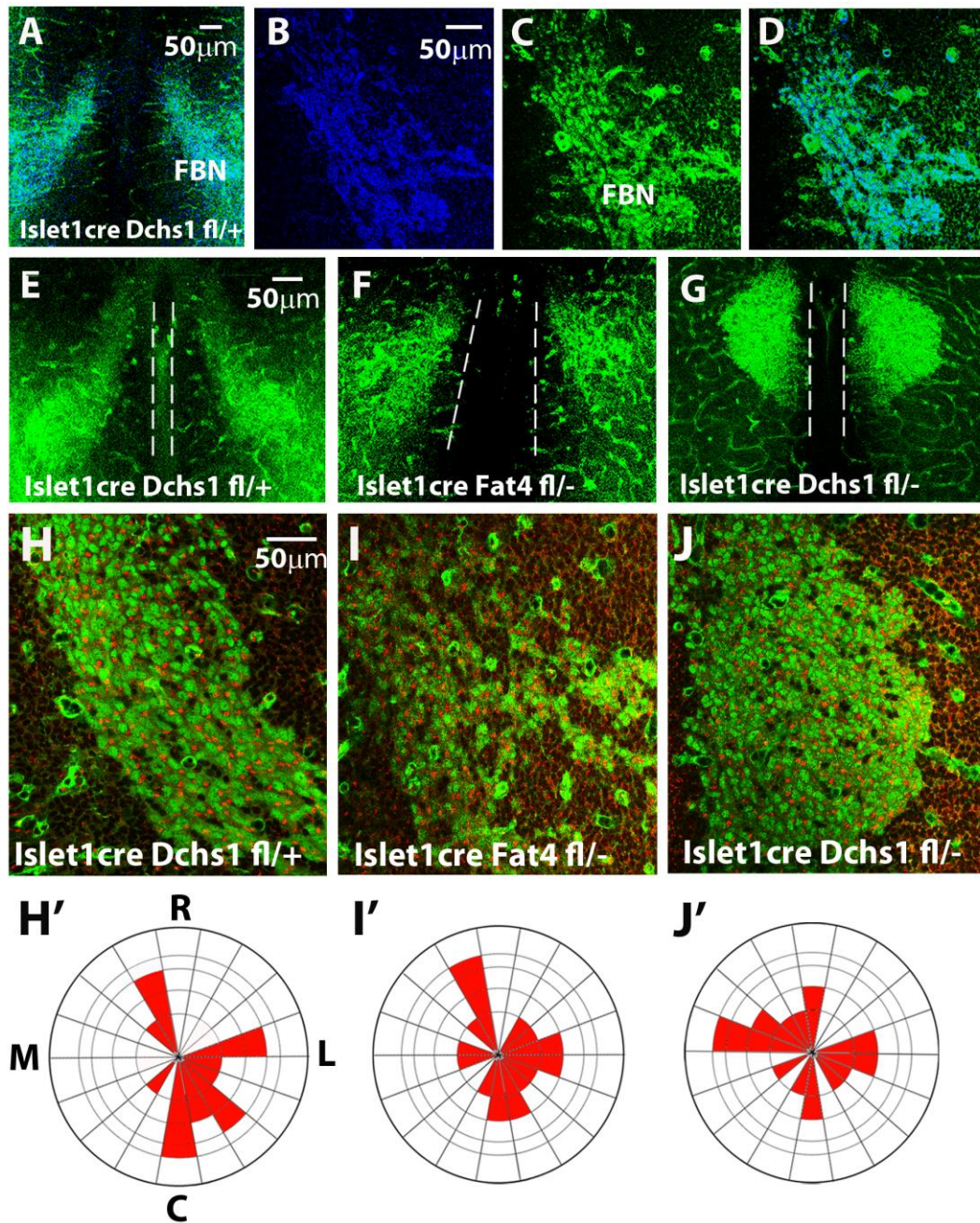
Figure 6.1. Fat4 and Dchs1 have a cell autonomous role in FBN migration.
Wholemount staining of E12.5 hindbrains for β-galactosidase showing Islet-1[Cre] reporter activity (blue, A, B, D), FBNs (green, A, C-J) and the Golgi complex (red, H-J). Low magnification image of control hindbrain reveals overlap of FBN and β-galactosidase staining (A). High magnification views of β-galactosidase staining (B), the FBNs (C) and overlay (D) of (B and C) confirming that the *Islet-1^{cre}* promoter is active exclusively in the FBNs. In the *Islet-1^{cre}Fat4^{fl/-}* hindbrains, FBNs appear scattered next to the midline (F). The polarity of the Golgi complex in the FBNs is also moderately disrupted (I, I') compared to the control FBNs (H, H'). In the *Islet-*

1^{cre}Dchs1^{fl/-} hindbrains, the FBNs are completely arrested at the midline (G) and there is a loss of polarity in the FBNs (J, J'). Midline marked with white dashes (E-G). C= caudal, FBN= Facial branchiomotor neurons, L= lateral, M= medial, R= rostral.

6.2.3 Dchs1 and Fat4 are required non-cell autonomously in the neuroepithelium

Immunohistochemistry was carried out to E12.5 *Hoxa3^{cre}Fat4$^{fl/-}$* and *Hoxa3^{cre}Dchs1$^{fl/-}$* hindbrains using anti-Islet-1 antibody and anti-Giantin antibody to visualise the FBNs and the Golgi complex, respectively. This revealed that loss of either *Fat4* or *Dchs1* in the neuroepithelium results in a complete arrest of the FBNs at the midline, reminiscent of the null phenotypes (Fig.6.2 E-G). The FBNs had no obvious leading edge and were unable to undergo lateral migration (Fig.6.2 E-G).

Analysis of the Golgi complex distribution revealed that the FBNs are not polarised in the *Hoxa3^{cre}Fat4$^{fl/-}$* and *Hoxa3^{cre}Dchs1$^{fl/-}$* hindbrains compared to the FBNs in the controls (Fig.6.2 H-J). The Rayleigh test revealed that the FBNs of the control embryos are highly polarised with a p value of $p<10^{-12}$ compared to the uniform Golgi angle distribution of *Hoxa3^{cre}Fat4$^{fl/-}$* embryos with a p value of p= 0.35 and *Hoxa3^{cre}Dchs1$^{fl/-}$* embryos with a value of p=0.45. The Mardia-Watson-Wheeler test confirmed that there is a significant difference between the Golgi angle distribution of the control FBNs compared to that of the *Hoxa3^{cre}Fat4$^{fl/-}$* and *Hoxa3^{cre}Dchs1$^{fl/-}$* FBNs with a value of $p<10^{-12}$ for both (Fig.6.2 H-J).

In situ hybridisation was carried out to E13.5 hindbrains to investigate later stages of FBN migration using an antisense *Islet-1* probe to visualise the FBNs. The *in situ* hybridisation analysis of the *Hoxa3^{cre}* positive control hindbrains revealed the normal position of the FBNs at the pial surface, condensing in lateral r6 (Fig.6.3 D). In contrast, in *Hoxa3^{cre}Fat4$^{fl/-}$* and *Hoxa3^{cre}Dchs1$^{fl/-}$* hindbrains there is an arrest of FBN migration along the caudal and lateral axis and the FBNs could be seen spanning r5 and r6 (Fig.6.3 E, F). Although the FBNs were unable to undergo the lateral migration they had undertaken their radial migration in r6 as they could be viewed from the pial surface (Fig.6.3 D-F).
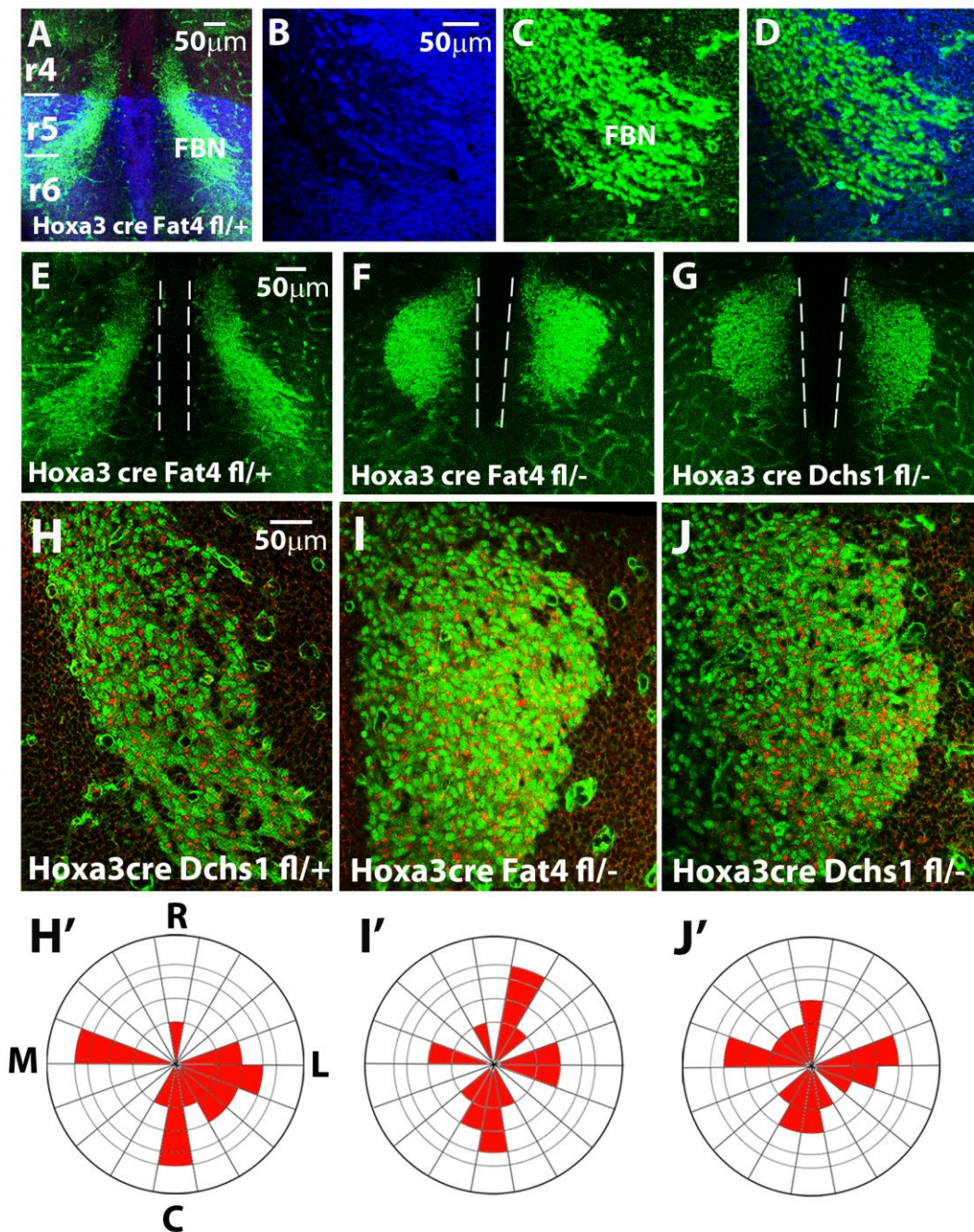
Figure 6.2. Fat4 and Dchs1 have a non-cell autonomous role in FBN migration.
Wholemount staining of E12.5 hindbrains for β-galactosidase showing Hoxa3[cre]
reporter activity (blue, A, B, D), FBNs in green (A, C-J) and the Golgi complex in
red (H-J). Low magnification image of control hindbrain reveals β-galactosidase
staining in the neuroepithelium in r5 and r6 (A). At higher magnification, β-
galactosidase staining can be seen in the neuroepithelium with negative patches (B)
where the FBNs are located (C). Overlay (D) of (B and C) confirms that the *Hoxa3[cre]*
reporter is only active in the neuroepithelium of r5 and r6 and not in the FBNs. In the

Hoxa3^{cre} Fat4$^{fl/-}$ and *Hoxa3^{cre}Dchs1$^{fl/-}$* hindbrains, the FBNs are completely arrested at the midline (F, G). Golgi analysis at higher magnification revealed loss of polarity of the FBNs in both *Hoxa3^{cre}Fat4$^{fl/-}$* and *Hoxa3^{cre}Dchs1$^{fl/-}$* mutants compared to the polarised orientation of the Golgi complex within the FBNs of the controls (H-J). Midline marked with white dashes (E-G). C= caudal, FBN= Facial branchiomotor neurons, L= lateral, M= medial, R= rostral, r= rhombomere.
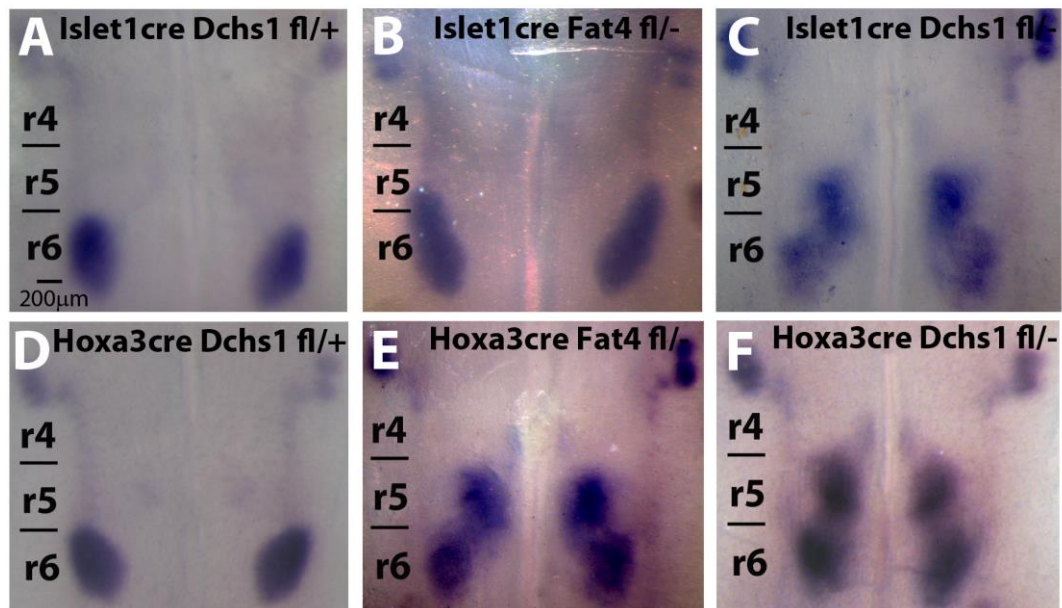
Figure 6.3. Conditional loss of *Fat4* and *Dchs1* results in a continued arrest of FBN migration. Wholemount *in situ* hybridisation to *Islet-1* in E13.5 hindbrains, viewed from the pial surface (A-F). In the controls, FBNs can be seen as condensed nuclei in r6, present lateral to the midline (A, D). In the *Islet-1^{cre}Fat4$^{fl/-}$* hindbrain (B) FBN migration appears similar to the FBN migration in controls (A, D). The FBNs in the *Islet-1^{cre}Dchs1$^{fl/-}$* mutants, however, appear arrested in their caudal and lateral migration and can be seen spanning r5-r6 (C). In both the *Hoxa3^{cre}Fat4$^{fl/-}$* and *Hoxa3^{cre}Dchs1$^{fl/-}$* mutant hindbrains, the FBNs are arrested in their caudal and lateral migration and appear close to the midline compared to the FBNs in the control hindbrain (D-F). r= rhombomere.

6.3 Discussion

To understand the cell autonomous and non-cell autonomous roles of *Fat4* and *Dchs1* in the hindbrain, promoter specific Cre lines were utilised.

Analysis of the *Islet-1^{cre}* lines revealed a different cell autonomous requirement for *Dchs1* and *Fat4* in the FBNs. Loss of *Dchs1* from the FBNs results in a complete arrest of the FBNs at the midline, reminiscent of the *Dchs1* null phenotype. More over this defect in migration persists at E13.5 and is also similar to what was observed in *Dchs1* null hindbrain at E13.5. Clearly *Dchs1* has a requirement within the FBNs to regulate lateral tangential migration within r5 and r6.

On the contrary, loss of *Fat4* from the FBNs results in a slightly aberrant pattern of FBN migration at E12.5 which is almost normal by E13.5. This analysis argues that *Fat4* function within the FBNs is either required only during a critical window when the FBNs initiate their lateral turn or *Fat4* doesn't play an essential role in the FBNs at all. However, given that the pattern of FBN migration at E12.5 appears aberrant, this argues for the model that *Fat4* is minimally required in the leading edge of the FBNs to direct the streamlined lateral turn of the FBNs. Since there is a dominant gradient of *Fat4* in the neuroepithelium which would not become disrupted by loss of *Fat4* in the leading edge of the FBNs, it would appear that the FBNs are able to re-align their trajectory by the cues presented by *Fat4* in the neuroepithelium hence they appear largely normal by E13.5.

Analysis of the *Hoxa3^{cre}* conditional mutants revealed that loss of either *Fat4* or *Dchs1* from the neuroepithelium results in a complete arrest of FBNs at the midline at E12.5. The FBN migration continues to be affected along the lateral and caudal axis at E13.5, recapitulating the null phenotypes.

Taking these results into account, the following models are proposed for how *Dchs1* and *Fat4* might be interacting and imparting polarity on the FBNs for tangential migration. The simplest model would be if both Dchs1 and Fat4 were required in the neuroepithelium and their graded expression resulted in variable heterophilic interaction on adjacent cell surfaces. Subsequently, this would result in cell-cell propagation of the activity of Fat4 and Dchs1 at each cell interface and could present

cues to the FBNs for directed lateral migration. This model however is not plausible since Dchs1 is required within the FBNs as well.

The second and favoured model is that Dchs1 is present as a continuous gradient across the neuroepithelium and the FBNs. Dchs1 and Fat4 heterophilic interactions occur across the neuroepithelium. Loss of *Dchs1* from the FBNs behaves as a patch of *Dchs1* negative clones would in a *Drosophila* tissue. The cells at the midline which have a high level of Dchs1 and the cells lateral to the FBNs which have low levels of Dchs1 would not be able to propagate the polarised activity of Fat4 and Dchs1 along the medio-lateral axis due to the patch of Dchs1 negative cells.

On the other hand, loss of *Fat4* from the neuroepithelium would largely abolish its gradient since that is where the most dominant Fat4 expression is present whereas loss of *Fat4* from the FBNs has a minimal effect. A likely reason for this could be because Fat4 is only present in the leading edge of the FBNs and might be required for a compact turn of the FBNs whereas the high amount of Fat4 in the neuroepithelium is necessary to guide the FBNs for the lateral turn of the migration. This would explain why loss of *Fat4* from the FBNs results in a scattered appearance of FBNs initially. Furthermore, loss of *Fat4* from the leading edge of the FBNs would not perturb the more lateral Fat4 gradient within the neuroepithelium. Moreover, Dchs1 within the FBNs would be able to heterphilically bind to Fat4 in the surrounding neuroepithelium to polarise the FBNs in the absence of Fat4 from the FBNs. This model proposed is in line with the results observed from the conditional Cre lines as well the *Dchs1* mosaic hindbrains.

7 INTERACTION WITH FZ-PCP AND MODULATORS OF FAT-PCP

7.1 Introduction

Studies in *Drosophila* have identified a few modulators of the Fat signalling pathway such as the Golgi kinase *four-jointed (fj)*, the transcriptional corepressor *atrophin* and an unconventional myosin *dachs* (Zeidler et al. 2000; Simon 2004; Fanto 2003; Mao et al. 2006). Fj modulates the binding affinity and interaction between Ft and Ds (Brittle et al. 2010; Strutt et al. 2004). It is important for modulating growth as well as PCP and is expressed in a complementary gradient to Ds in some tissues where it functions to enhance the vector of polarity (Brittle et al. 2010). Although *fj* mutants have minor polarity phenotypes in most tissues, analysis of mosaic tissue has revealed more significant defects due to perturbation of the Fj gradient (Zeidler et al. 2000; Simon 2004; Yang et al. 2002; Brittle et al. 2010).

The mammalian orthologue *Fjx1* is expressed in epithelial tissues in complementary patterns to *Fat4* and *Dchs1*, which are expressed in mesenchymal tissues during development (Rock et al. 2005; Mao et al. 2011). One study also reported that loss of *Fat4* coupled with loss of *Fjx1* exacerbated the polycystic kidney phenotype providing evidence that *Fat4* and *Fjx1* can behave in a synergistic manner in mice (Saburi et al. 2008). Another study highlighted the importance of Fjx1 in regulating dendrite growth and branching of hippocampal neurons (Probst et al. 2007). Furthermore, there is evidence suggesting that Fjx1 is secreted in the mouse in contrast to the Golgi tethered active form of Fj in *Drosophila* (Strutt et al. 2004; Rock et al. 2005b). However, overall there is limited evidence for the role of *Fjx1* in mammalian development. Here, the role of *Fjx1* was characterised in tangential FBN migration to determine if it could behave as a modulator of Fat-PCP signalling.

In *Drosophila*, Fat-PCP and Fz-PCP pathways can act independently of each other to establish PCP, for example in the abdomen (Donoughe & DiNardo 2011). Conversely, Fat-PCP functions upstream and imparts polarity to Fz-PCP components in the ommatidia of the eye (Yang et al. 2002). The interaction observed between Fat-PCP and Fz-PCP components is complex and varies from one tissue to another. In the mammalian system, studies of Fz-PCP and Fat-PCP mutants have revealed

several overlapping phenotypes in a range of tissues such as during convergent extension of the inner ear, together with kidney and lung branching morphogenesis (Montcouquiol et al. 2003; Saburi et al. 2008; Mao et al. 2011). However, to date it is unknown if the two pathways function independently or intersect.

FBN migration presents an interesting opportunity to study the relationship between the Fz-PCP and Fat-PCP pathways given they both play a role in regulating tangential migration.

7.2 Results

7.2.1 *Fjx1*; a possible modulator of the activity gradient of *Fat4* and *Dchs1*

Fjx1 is expressed in the same tissues as *Fat4* and *Dchs1* during embryonic development, making it plausible that its function in *Drosophila* could be conserved in mammals (Rock et al. 2005). To assess potential roles of *Fjx1* in the hindbrain, wholemount *in situ* hybridisation was carried out on wildtype E12.5 hindbrains to determine the expression of *Fjx1*. This stage was chosen for analysis as this is when the *Fat4* and *Dchs1* null phenotypes arise and polarity of the FBNs is disrupted. *Fjx1* is expressed at high levels in the midline of the hindbrain and in the lateral neuroepithelium (Fig.7.1 A). *Fjx1* is also expressed in the region where the FBNs migrate (Fig.7.1 A, white arrow). This expression was confirmed by section analysis at the level of r4 and r6 (Fig.7.1 A', A''). *Fjx1* expression appears to overlap with *Dchs1* and *Fat4* expression in the hindbrain suggesting that it could modulate their activity in regulating FBN migration (Fig.7.1 A).

To investigate if *Fjx1* is required for FBN migration, *in situ* hybridisation was carried out on E12.5 *Fjx1*$^{-/-}$ hindbrains using an antisense *Islet-1* probe to visualise the FBNs. Loss of *Fjx1* has no effect on FBN migration and the migration is comparable to the wildtype FBNs (Fig.7.1 B, C).

Since *Fjx1* has been shown to act synergistically with *Fat4* and *Fjx1* in the kidneys (Saburi et al. 2012), double *Fat4*$^{-/-}$*Fjx1*$^{-/-}$ mice were generated to determine whether any synergy could be observed in regulation of FBN migration. Wholemount *in situ* hybridisation analysis at E12.5 in the double *Fat4*$^{-/-}$*Fjx1*$^{-/-}$ hindbrains revealed FBNs were arrested at the midline, spanning r4-r5 and were unable to migrate laterally or further caudally (Fig.7.1 D). This result is similar to what was observed in the *Fat4* null mice.

To determine if there are any defects in the polarity of the Golgi complex of the FBNs, wholemount immunohistochemistry was carried out on E12.5 hindbrains of *Fjx1*$^{-/-}$ and *Fat4*$^{-/-}$*Fjx1*$^{-/-}$ embryos (Fig.7.1 E-G). FBNs in the *Fjx1*$^{-/-}$ hindbrains appear polarised along the caudal-lateral axis (Fig.7.1 E, F rose plots). However, the FBNs in the double *Fat4*$^{-/-}$*Fjx1*$^{-/-}$ mutant hindbrains are at the midline and not polarised along any particular axis (Fig.7.1 G, rose plot). The Rayleigh test confirmed that the

Golgi complex orientation of the FBNs in $Fat4^{-/-}Fjx1^{-/-}$ hindbrains lacks a directional bias with a p value of p=0.21 whereas the wildtype and $Fjx1^{-/-}$ FBNs have a value of p<10^{-10}. Similarly, the Mardia-Watson Wheeler test shows that Golgi complex angle distribution is significantly different in the FBNs of the $Fat4^{-/-}Fjx1^{-/-}$ mice when compared to the wildtype FBNs with a value of p<10^{-12} whereas no difference was observed between wildtype and $Fjx1^{-/-}$ FBNs with a value of p=0.1.

In addition, the Mardia-Watson Wheeler test was also performed on the $Fat4^{-/-}$ and $Fat4^{-/-}Fjx1^{-/-}$ null embryos to determine if any subtle differences are present in Golgi angle distribution but a value of p=0.3 revealed that the Golgi angle distribution of the $Fat4^{-/-}$ and $Fat4^{-/-}Fjx1^{-/-}$ FBNs is not significantly different. Therefore, the double $Fat4^{-/-}Fjx1^{-/-}$ phenotype is reminiscent of the $Fat4$ null phenotype and does not appear exacerbated (Fig.7.1 D, G).
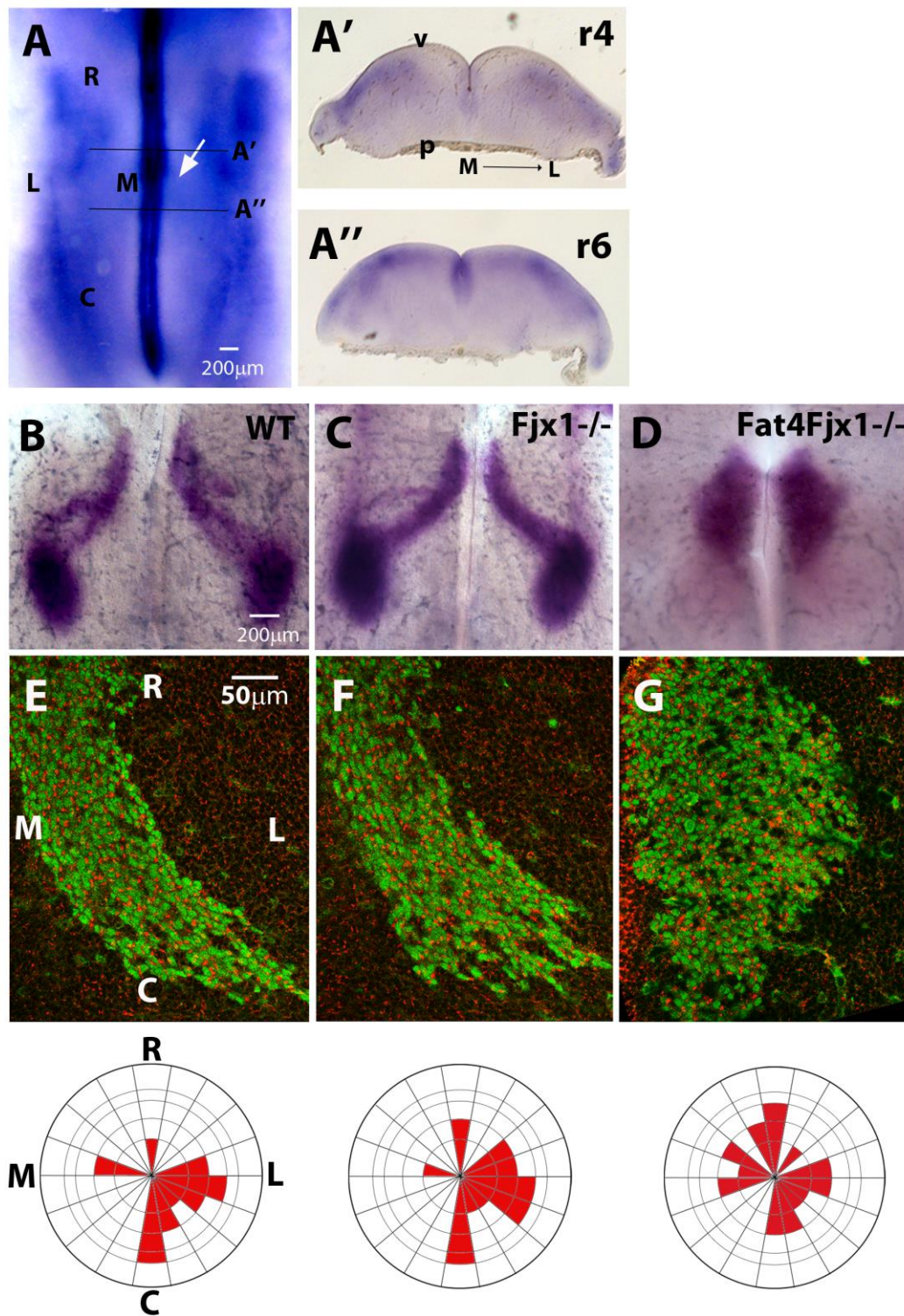
Figure 7.1. Expression of *Fjx1*; a possible modulator of Fat signalling. Wholemount *in situ* hybridisation of E12.5 hindbrains viewed on the ventricular surface showing *Islet-1* (B-D) and *Fjx1* expression(A) in wildtype (A, B), *Fjx1*^{−/−} (C) and *Fjx1*^{−/−}*Fat4*^{−/−} (D) embryos. Wholemount *in situ* hybridisation analysis revealed normal FBN migration in the wildtype (B) and *Fjx1*^{−/−} (C) hindbrains. FBN migration

was disrupted in the *Fjx1*^{-/-}*Fat4*^{-/-} embryos (D). Wholemounts and transverse sections of E12.5 hindbrains reveal *Fjx1* expression in the midline and the lateral hindbrain with hints of expression in the FBNs (white arrow, A-A''). Wholemount immunohistochemistry of E12.5 hindbrains showing the FBNs (green) and the Golgi complex (red) (E-G) in wildtype (E), *Fjx1*^{-/-} (F) and *Fjx1*^{-/-}*Fat4*^{-/-} (G) embryos. Loss of *Fjx1* has no effect on polarised migration of FBNs (F) whereas in the *Fjx1*^{-/-}*Fat4*^{-/-} hindbrains the FBNs are arrested at the midline with no obvious polarity (G). The polarity of the Golgi is shown in the Rose plots below (E-G). C= caudal, L= lateral, M= medial, p= pial, R= rostral and v= ventricular.

7.2.2 Vangl2 and Fat4 regulate FBN migration along orthogonal axes

In Fz-PCP mouse mutants, caudal migration of FBNs is arrested, however the FBNs are able to undergo lateral migration within r4 or r5 by E13.5 (Vivancos et al. 2009; Qu et al. 2010). In contrast, FBNs in the *Fat4* and *Dchs1* null mice are unable to migrate laterally but can migrate caudally into r5 and r6 (Fig.7.2 A). Since Dchs1 and Fat4 are expressed as complementary gradients in r4-r6, it was hypothesised that Fat4 and Dchs1 may regulate the ectopic lateral tangential migration of the FBNs within r4/r5 in Fz-PCP mutants. If so, the simultaneous loss of both Fat signalling and *Vangl2* should result in a complete arrest of the FBNs at the midline in r4. To test this hypothesis, double *Fat4$^{-/-}$Vangl2$^{Lp/Lp}$* mutant mice were generated by our collaborator Dr. Yaopan Mao.

Wholemount immunostaining was carried out with anti-Islet-1 antibody on E13.5 hindbrains, when the FBNs have undertaken the lateral migration, to visualise the trigeminal neurons and the FBNs (Fig.7.2 B-D, FBNs indicated with a white arrow). The trigeminal neurons arise in r2 of the hindbrain and migrate laterally within r2 by E11.5. Trigeminal neuron migration is unaffected in the *Vangl2$^{Lp/+}$* and *Vangl2$^{Lp/Lp}$* mice as well as in the *Fat4* nulls (see Fig.4.1) (Vivancos et al. 2009) hence they were used as an internal control to determine the relative lateral migration of the FBNs.

The analysis of *Fat4$^{+/+}$Vangl2$^{Lp/+}$* and *Vangl2$^{Lp/Lp}$* hindbrains revealed the trigeminal neurons had migrated laterally in r2 and the FBNs had migrated laterally within r4 (Fig.7.2 B, C). However, in the double *Fat4$^{-/-}$ Vangl2$^{Lp/Lp}$* hindbrains, the FBNs were observed closer to the midline in r4 (Fig.7.2 D). The distance from the midline to the trigeminal neurons and from the midline to the FBNs was measured (Fig.7.2 E, midline indicated as white dashes B-D). This revealed that the trigeminal neurons and FBNs can migrate laterally in *Fat4$^{+/+}$Vangl2$^{Lp/+}$* and *Vangl2$^{Lp/Lp}$* hindbrains whereas in the double *Fat4$^{-/-}$Vangl2$^{Lp/Lp}$* mutants the FBNs are arrested at the midline in r4 (Fig.7.2 E).
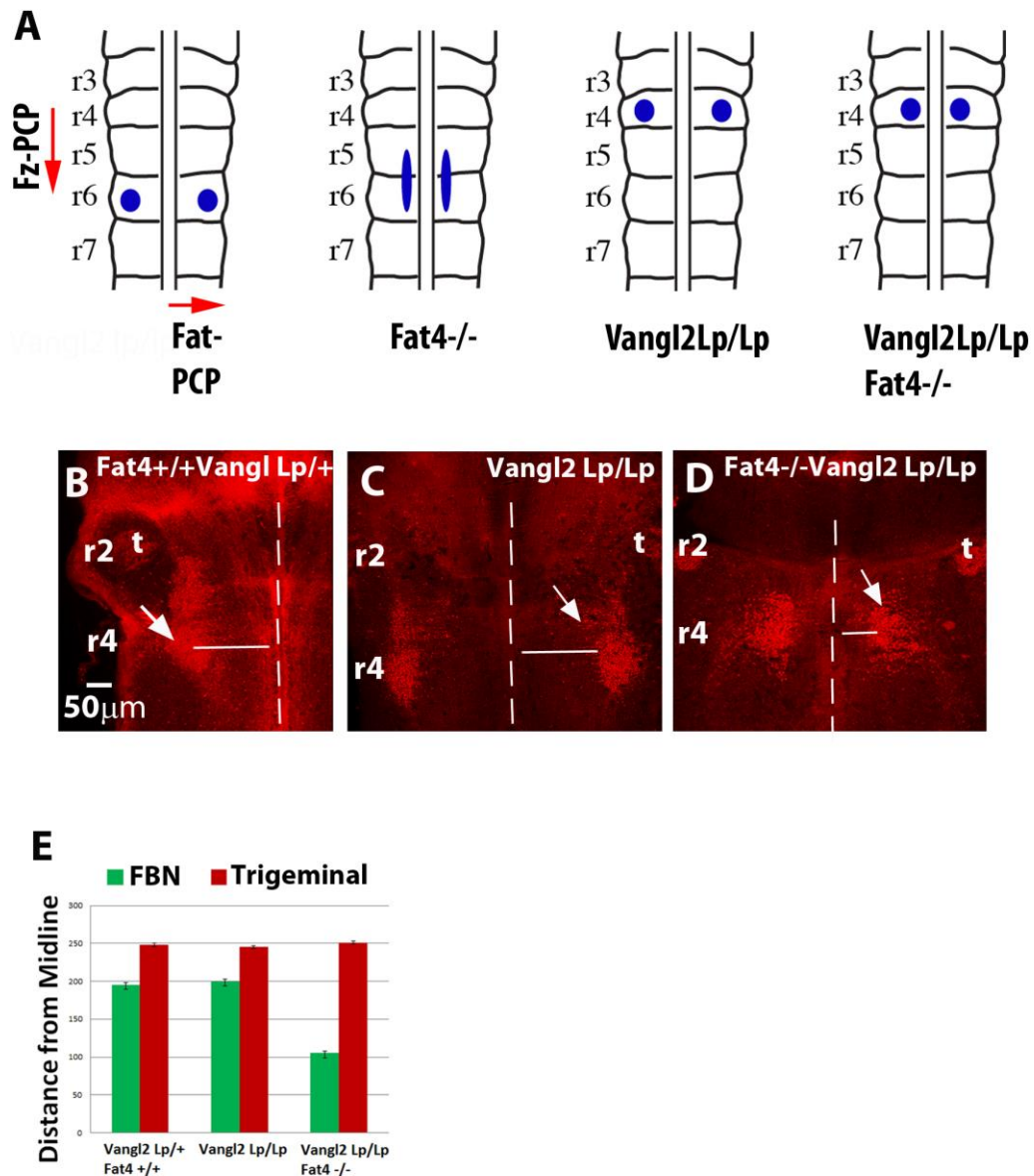
Figure 7.2. Fz-PCP and Fat-PCP regulate tangential migration on orthogonal axes. Sketch diagram of the hindbrain depicting normal migration of the FBNs and the perpendicular axes on which Fat-PCP and Fz-PCP act (A). The loss of Fat signalling causes a delay in caudal migration and a defect in lateral migration (A). Loss of *Vangl2* from the hindbrain results in arrest of the FBNs in r4 with ectopic lateral migration (A). Loss of both *Fat4* and *Vangl2* results in a complete arrest of FBNs at the midline in r4 (A). Wholemount immunochemistry of E13.5 hindbrains viewed from the pial surface show Islet-1 expression (in red) to mark FBNs (white arrow, B-D) and trigeminal neurons (t, B-D). The distance of the FBNs from the midline and the distance of the trigeminal neurons from the midline was measured

(white dashes, B-D) and represented on a graph (E). In the $Fat4^{+/+}Vangl2^{Lp/+}$, $Vangl2^{Lp/Lp}$ and the $Fat4^{-/-}Vangl2^{Lp/Lp}$ hindbrains, the position of the trigeminal neurons is comparable and no defect in migration is observed (B-D, E). In both the $Fat4^{+/+}Vangl2^{Lp/+}$ and the $Vangl2^{Lp/Lp}$ hindbrains, FBNs are present in lateral r4 and their distance from the midline is comparable revealing no defect in lateral migration (B, C, E). In the double $Fat4^{-/-}Vangl2^{Lp/Lp}$ hindbrains, FBNs are close to the midline in r4 and are arrested in lateral and caudal migration (D, E). FBN= facial branchiomotor neurons, r= rhombomere and t= trigeminal neurons.

7.3 Discussion

The studies carried out reveal that *Fjx1* is expressed in r4-r6 of the hindbrain and overlaps with *Fat4* and *Dchs1* expression, including the region in r6 where the FBNs are migrating laterally. Loss of *Fjx1* has no effect on polarised FBN migration, and based on the FBN migration and Golgi distribution analysis it appears that the simultaneous loss of *Fat4* and *Fjx1* does not cause an exacerbation of the *Fat4* null phenotype.

Loss or overexpression of *fj* in *Drosophila* results in very minor PCP defects whereas generation of mutant and overexpression clones result in more severe PCP defects (Zeidler et al. 2000; Simon 2004). Fj modulates Ds and Ft activity which results in a graded activation of Ft across a tissue, however, the gradient of Fj provides directional information in a partially redundant fashion with the Ds gradient (Simon 2004; Ma et al. 2003).

Loss of *Fjx1* in the hindbrain has no effect on FBN migration, however, if Fjx1 has a role in modulating the interaction of Fat4 and Dchs1 in the hindbrain then perhaps a disruption of *Fjx1* expression rather than a complete loss of Fjx1 may provide evidence for this. If there is a conservation of *Fjx1* function in the mouse then based on *Fjx1* expression it could be hypothesised that Fjx1 steepens the graded activity of Fat4 and Dchs1 in r6 as the FBNs turn laterally. The caveat to studying the function of Fjx1 in this system is that Fat4 and Dchs1 are already expressed in a graded fashion which may mean that Fjx1 is completely redundant in this system. Therefore, in order to study any activity Fjx1 may have, both the gradients of Fat4 and Dchs1 would have to be abolished by overexpression in a wildtype and then in a *Fjx1* null background to determine if there is an exacerbation of the FBN phenotype, if any, in the *Fjx1* null background.

In the *Vangl2*$^{Lp/Lp}$ hindbrains, FBNs are unable to migrate caudally but are able to undergo lateral migration within r4 (Fig.7.2 A). Based on the complementary gradients of Dchs1 and Fat4 in r4-r6 of the hindbrain, it was proposed that Fat4 and Dchs1 are responsible for guiding lateral migration of FBNs in r4 in Fz-PCP mutants.

Analysis of E13.5 hindbrains of *Fat4$^{-/-}$Vangl2$^{Lp/Lp}$* embryos confirmed that in fact loss of both *Fat4* and *Vangl2* results in a complete arrest of the FBNs at the midline in r4 compared to the *Vangl2$^{Lp/Lp}$* hindbrain where the FBNs condense laterally in caudal r4. It is clear from this study that Fz-PCP and Fat-PCP pathways are largely temporally uncoupled in their regulation of FBN tangential migration and function on orthogonal axes. This is the first time that the activities of these two pathways have been uncoupled in the same system in mammalian development. The results also suggest that Fat-PCP can function globally across r4-r6 to regulate FBN lateral migration and is consistent with the expression analysis of Fat4 and Dchs1.

Interestingly, in the double *Fat4$^{-/-}$Vangl2$^{Lp/Lp}$* mutant hindbrain, the cluster of FBNs at the midline could be seen in rostral r4 whereas in the *Vangl2$^{Lp/Lp}$* hindbrain the FBNs had condensed in caudal r4. This could mean that either the FBNs accumulating at the midline are unable to go anywhere which results in passive displacement of the FBNs into rostral r4 or that Fat-PCP and Fz-PCP synergistically regulate caudal migration of FBNs as proposed earlier.

Another possibility is that loss of *Vangl2* and *Fat4* might affect the length of the neural tube since loss of both genes results in a slightly wider neural tube and a reduced length to width ratio which would affect the length of the hindbrain (Wang et al. 2006; Saburi et al. 2008). This can be verified by measuring the length of a segment of the neural tube, for example, the distance between the otic vesicle and the forelimb can be measured and compared between the *Vangl2$^{Lp/Lp}$* and the double *Fat4$^{-/-}$Vangl2$^{Lp/Lp}$* embryos to see if the hindbrain is shorter in the double mutants. This could explain why the FBNs and trigeminal neurons are closer to each other in the double mutants.

The model proposed based on the results presented here is that Fz-PCP regulates caudal tangential migration of FBNs whilst Fat-PCP regulates lateral tangential migration of FBNs (Fig.7.2 A). The respective phenotypes that arise due to loss of Fat and Fz-PCP signalling are illustrated as sketches (Fig.7.2 A). This is a novel demonstration of Fat-PCP and Fz-PCP working on orthogonal axes in vertebrates to regulate polarised behaviour within the same tissue.

8   GENERAL DISCUSSION AND FUTURE WORK

8.1   General Discussion

This study has revealed the importance of Fat signalling in several aspects of craniofacial development; namely its requirement in the development of salivary glands, polarisation of the hair cells of the utricle, differentiation of osteoblasts of the facial bones and tangential migration of the FBNs.

Fat4 and Dchs1 function in the same pathway as a receptor/ligand pair and loss of either or both results in identical phenotypes in the hindbrain, the osteoblasts and the salivary glands. Similarly, the defects previously reported in the *Fat4* and *Dchs1* null embryos are identical in the kidney, sternum and lungs (Mao et al. 2011). Analysis in the mouse has revealed that Fat4 and Dchs1 undergo heterophilic interactions at adjacent cell surfaces and can modify each other's protein levels and localisation post-translationally (Ishiuchi et al. 2009; Mao et al. 2011). Although this does not provide evidence for whether Fat4 is a receptor and Dchs1 is a ligand, it is clear that the nature of their interaction is conserved between the mouse and *Drosophila*.

Fat4 and Dchs1 are expressed in an overlapping fashion in several tissues such as the lung and kidney mesenchyme but neither are expressed as an obvious gradient in these tissues (Rock et al. 2005; Mao et al. 2011). It has been proposed that Fat4 regulates OCD in the kidney tubules which poses an interesting question; if Fat4 or Dchs1 are not expressed as gradients and neither is Fjx1, then how do they orchestrate polarised cell divisions?

In contrast to the kidney, Fat4 and Dchs1 are expressed as complementary gradients in the hindbrain. The complementary graded expression of Fat4 and Dchs1 is at odds with what is observed in *Drosophila* tissues where Fj and Ds are expressed as opposing gradients and Ft is uniformly expressed (Yang et al. 2002; Ma et al. 2003; Casal et al. 2006). However, Fat-PCP propagates polarity across a tissue by the graded activation of Ft which occurs in an opposing fashion to the expression of Ds and can be compared to the opposing gradients of Fat4 and Dchs1 in the hindbrain.

Fat4 and Dchs1 are necessary for the polarised lateral migration of the FBNs. The graded expression of Dchs1 is required for the polarised migration of FBNs as revealed by chimeric analysis. In heterozygous embryos with 50% transcript levels of Dchs1, the FBNs are able to polarise and migrate appropriately, however, upon disruption of the Dchs1 gradient with 70% Dchs1 transcript levels, the FBN are arrested in their migration and do not have a polarised cell morphology or Golgi complex orientation. These results indicate that a Dchs1 gradient itself may be important for the migration of FBNs.

Dchs1 is required both cell autonomously and non-cell autonomously whereas there is a greater requirement of Fat4 non-cell autonomously as revealed by the conditional knockout experiments undertaken with *Islet-1^{cre}* and *Hoxa3^{cre}* mouse lines. Taken together with the expression data and chimeric analysis, a model of Fat-PCP signalling emerges based on drawing parallels from the *Drosophila* model.

The graded expression of Fat4 and Dchs1 results in formation of varying amount of Fat4/Dchs1 heterodimers on adjacent cell surfaces across the hindbrain. This interaction can result in direct or indirect polarisation of the FBNs providing cues for polarised migration across the hindbrain. Although this model has been tested by disrupting the Dchs1 gradient, it has not been tested whether the gradients of Fat4 and Dchs1 are permissive or instructive. Furthermore, it is not currently known whether Fat4 and Dchs1 localise asymmetrically within each cell as recently observed in the *Drosophila* wing, which can provide robustness to long range polarity propagation (Brittle et al. 2012; Ambegaonkar et al. 2012).

Given that Fat4 and Dchs1 are expressed as complementary gradients, the requirement of Fjx1 in the hindbrain might be redundant at best. The expression of *Fjx1* overlaps with that of Fat4 and Dchs1 but does not appear as an obvious gradient in the hindbrain. If the function of Fjx1 is conserved in vertebrates then based on the expression pattern it can be predicted that it could steepen the gradient of Fat4 and Dchs1 as the FBNs turn laterally in r6, since Fjx1 expression is high in the region. However, the high Fjx1 expression observed in the midline, which overlaps with Dchs1 expression, is puzzling. Moreover, Fjx1 appears to be secreted in the mouse tissues whereas it has been shown to be more active in a Golgi bound form in

Drosophila making it difficult to decipher its precise role based on localisation (Rock et al. 2005b; Strutt et al. 2004).

Fat4/Dchs1 signalling is clearly responsible for the polarised lateral migration of the FBNs but the Fz-PCP pathway is responsible exclusively for the caudal migration of FBNs. Loss of Fz-PCP components results in an arrest of the caudal migration of the FBNs (Vivancos et al. 2009; Qu et al. 2010). The simultaneous loss of the Fz-PCP component *Vangl2* and *Fat4* results in a complete arrest of caudal and lateral migration of FBNs within r4. This reveals a distinct and temporally uncoupled role of the Fat-PCP and Fz-PCP pathways in polarising the FBNs on perpendicular axes. Moreover, this reveals Fat4/Dchs1 as a global system for regulating lateral migration of FBNs across r4-r6. This is a novel finding in terms of FBN migration as well since no defects affecting lateral migration of FBNs have been reported to date.

Expression analysis in the chick reveals that Fat4 and Dchs1 are expressed in a similar fashion in the chick hindbrain and the FBNs in the chick only undergo lateral migration (unpublished data, Francis-West lab). This makes it tempting to speculate that the role of Fat4/Dchs1 in regulating lateral migration could be conserved across some vertebrate species.

It is interesting to note that the Fz-PCP and Fat-PCP signalling only affect the migration of the FBNs and do no play a role in lateral migration of all other branchiomotor neurons. It is not clear why these pathways specifically act upon this particular group of neurons. Loss of *Tbx20* not only affects FBN migration but also disrupts the migration of trigeminal neurons providing evidence that parallel pathways exist that regulate lateral migration of other branchiomotor neurons (Song et al. 2006). One possible reason for the requirement of parallel pathways to regulate the migration of these neurons could be to control the temporally distinct phases of their migration. FBNs migrate in the caudal axis from E10.5 onwards and only migrate laterally at E12.5 whereas all other branchiomotor neurons complete their lateral migration by E11.5 and do not undergo caudal migration.

Although Fat signalling is largely involved in craniofacial development through either PCP or transcriptional signalling there is evidence for slightly divergent roles of Fat signalling in vertebrates. A role for Fat4 and Dchs1, which does not fit into the category of PCP or growth control via the Hippo pathway, was highlighted by a

study on the cerebral cortex of mice. Localisation of Fat4 and Dchs1 was reported at cell-cell contacts more apical to the adherens junctions in the embryonic cerebral cortex, reminiscent of *Ft* and *Ds* localisation in *Drosophila* (Ishiuchi et al. 2009). The study revealed that Fat4 forms a complex with Pals1 and Mupp1 to regulate apical membrane organisation and architecture in the cerebral cortex. Loss of *Fat4* does not affect recruitment of Pals1 and Mupp1, rather results in collapse of neuronal apical membrane organisation (Ishiuchi et al. 2009). This role of Fat signalling might have implications for interaction with the cytoskeleton to maintain architecture and/or could have implications for Fat signalling regulating apical-basal polarity in a subset of cells.

Although it is likely that Fat-PCP is required for polarised FBN migration, the Hippo transcriptional pathway has not been addressed or ruled out in these studies rather the lack of involvement has been inferred based on the analysis and the lack of Hippo signalling involvement in neuronal migration in general. Typically responsible for regulating proliferation and differentiation through the downstream targets Yap/Taz, it is unlikely that the pathway is directly involved in regulating polarised tangential migration of FBNs. Moreover, the FBNs appear to be specified and differentiate appropriately and no effect on proliferation or cell death was evident in these studies upon loss of *Fat4* or *Dchs1* (based on observation). Although a recent study in *Drosophila* has revealed the involvement of the Hippo pathway in regulating border cell migration by interacting with the actin cytoskeleton, Fat signalling has not been implicated in this process (Lucas et al. 2013).

Interestingly Fat-Hippo pathway has been implicated during kidney development. The study shows non-cell autonomous effects of Fat4 on suppressing Yap/Taz activity in the nephron progenitors and this effect was also propagated by the extracellular domain of Fat4 (Das et al. 2013). It is not clear how Fat4 regulates the activity of Yap/Taz in this tissue. Moreover, in *Drosophila*, Ft has not been reported as yet to affect Hippo targets non-cell autonomously which is in contrast to the findings in the vertebrate kidney (Lawrence et al. 2008; Das et al. 2013).

The results presented in this study reflect a novel and varied role for Fat signalling in craniofacial development. It also provides the first evidence of complementary

graded expression of Fat4 and Dchs1 in epithelial tissues of vertebrates. Furthermore, this is the first time evidence of disruption of lateral polarised migration of FBNs has been revealed and that Fat4/Dchs1 regulate this migration across r4-r6. Furthermore, the study reflects a differential cell-autonomous and non-cell autonomous requirement for Fat4 and Dchs1 in the hindbrain and also reveals that the gradient of Dchs1 is necessary for polarised FBN migration. A hypothetical model can be proposed for Fat-PCP signalling based on the FBN migration system. Although rigorous testing of this model is needed and several questions remain unanswered, these results provide some evidence of conservation of activity of Fat4 and Dchs1 between *Drosophila* and vertebrates.

8.2 Future work

The opposing activity readout of Fat4 and Dchs1 is analogous to their interaction in *Drosophila* tissues. Although they have been proposed as a receptor-ligand pair, evidence based on the activity of the Ds ICD with its interaction with the Ft ECD in regulating Hippo pathway targets proposes that this is not a linear relationship (Willecke et al. 2008). Furthermore, recent evidence has come to light identifying a novel branch of signalling downstream of Ds in regulating growth via the Hippo pathway (Degoutin et al. 2013). It is not possible to say if this is also the case in vertebrates.

Analysis of Ft/Ds ICD and ECD domains as undertaken in *Drosophila* must be carried out in the vertebrate system to understand the different requirement of the Fat4 and Dchs1 ICD and ECD which will elucidate their relationship with each other and further our understanding of the biphasic model of Ft/Ds relationship. The hindbrain provides an *in vitro* as well as an *in vivo* system for studying the activities of Fat4 and Dchs1 ECD and ICDs by introducing these constructs into *Fat4* or *Dchs1* null hindbrains and studying their respective effects on polarised FBN migration.

Another aspect of Fat-PCP signalling that is yet to be answered is what sets up the gradient of Fat4 and Dchs1 in the first instance and what is downstream of Fat-PCP signalling? In *Drosophila*, it has been shown that morphogens such as Wg and Hh

are responsible for the opposing gradients of Fj and Ds in different tissues (Thomas & Strutt 2012). Potential candidates in the hindbrain could be the Wnt and Shh family which are abundantly expressed across the neural tube (Ulloa and Marti 2010). To determine if these signalling pathways could act as morphogens to set up the gradient of Fat4 and Dchs1, beads soaked in Cyclopamine to inhibit Shh or Sfrp to inhibit Wnt signalling could be targeted in hindbrain explants and the effect on Fat4/Dchs1 expression can be observed.

It is also important to determine what is downstream of Fat4 and Dchs1. In *Drosophila*, the atypical myosin Dachs plays a role downstream of Fat-PCP and Fat-Hippo signalling in the wing to impart directional growth and polarity (Harumoto et al. 2010; Ambegaonkar et al. 2012). In a limited region of the eye, Ft and the transcriptional co-repressor Atrophin interact with each other to impart ommatidia polarity around the equator of the eye (Sharma & McNeill 2013). There is no vertebrate homologue of Dachs but Atrophin2 has been shown to interact with Fat4 in kidney tubule formation by OCDs (Saburi et al. 2012). This makes Atrophin a possible candidate since both the atrophin isoforms (Atn1/2) are expressed in the CNS during mouse development, however, the exact expression in the hindbrain or FBNs has not been determined (BGEM database + Zoltewicz et al. 2004).

The presence of gradients and chimeric analysis is suggestive of a Fat-PCP pathway governing the polarised migration of the FBNs, however, some conclusive strategies can be undertaken to provide further evidence for this. Reversing the gradient of both Fat4 and Dchs1 should abolish the lateral polarised migration of the FBNs. The only caveat to this analysis is that the FBNs might not repolarise and cross over the midline since the floor plate provides repulsive cues to axons and neurons (Jacob et al. 2001). This complication is avoided in *Drosophila* where the orientation of the hair bristle or rotation of ommatidia itself is a direct readout of polarity whereas the migrating neurons are constantly interacting with the environment which presents repulsive and attractive cues and the Golgi complex orientation is a secondary readout of polarity of the FBNs.

Conversely, if the gradients of Fat4 and Dchs1 determine the vector of polarity then the uniform overexpression of both Fat4 and Dchs1 gradients should abolish the polarised lateral migration of the FBNs.

The role of Fjx1 is unclear in the hindbrain despite the overlapping expression with Fat4 and Dchs1. Although hypothetically Fjx1could steepen the activity gradient of Fat4 and Dchs1 as the FBNs turn laterally, the only way of gauging the redundant, if any, role of Fjx1 would be to disrupt the gradient of Dchs1 and Fat4 in a *Fjx1* null background and determine if there is an exacerbation of the FBN phenotype. Conversely, disruption of expression of Fjx1 by generating chimaeras might reveal a subtle phenotype if the localisation of Fjx1 is necessary for its activity, however the caveat to this analysis if that Fjx1 is secreted in the mouse (Rock et al. 2005b). On the other hand, a more biochemical approach might provide insight as to whether Fat4 and Dchs1 are phosphorylated by Fjx1 as observed in *Drosophila* (Simon et al. 2010; Brittle et al. 2010).

To assess if the Hippo pathway could play a role in polarised tangential migration of FBNs, expression of the Hippo targets can be determined in the hindbrain in the first instance. It can be assessed if loss of *Fat4* upregulates activity of Yap by determining the levels of phosphorylated versus total yap in the hindbrain by immunostaining or western blot analysis. Another strategy would be to carry out an RNAi knockdown of Yap/Taz in *Fat4* null hindbrains to observe rescue effects. Similarly, knockdown of Hpo/Wts in wildtype hindbrain explants could be carried out to observe for FBN migration defects. A knockout genetic approach is not feasible as double Fat/Yap embryos do not survive beyond stage E8, however, conditional mouse lines of Yap/Taz could be generated under the Islet-1[cre] and Hoxa3[cre] promoters.

A biochemical approach might also prove insightful in revealing if Fat4 and Dchs1 regulate FBN migration via a transcriptional pathway by conducting a microarray analysis on E12.0 *Fat4* and *Dchs1* null hindbrains. This will provide a list of possible downstream targets affected in the hindbrain by loss of Fat signalling and therefore provide clues as to what else is affected downstream of Fat signalling.

Interestingly, the role of Hippo pathway has been shown in collective cell migration of the border cells in *Drosophila* ovary, however, the Hippo components interact with the cytoskeleton to maintain appropriate apical-basal architecture of the cells which results in their appropriate cell-cell contact dependent migration (Lucas et al. 2013). Apical-basal polarity determinants have not been analysed in the FBNs as

they migrate in the planar axis and the radial migration, which occurs in the apical-basal axis is dependent on radial glia.

It would be interesting to assess the role of Fat4/Dchs1 in regulating tangential migration of cortical neurons and the olfactory neurons as it has been recently established that Fz-PCP is needed for migration of olfactory bulb neurons (Hirota et al. 2012). This would elucidate if Fat signalling is globally required across the CNS for tangential migration of neurons.

The hindbrain system is ideal and the first of its kind in the vertebrates in which the model proposed for Fat-PCP can be tested by gain of function studies. Recently the cellular asymmetry of Ft and Ds in the *Drosophila* wing has also been proposed as an added mechanism to aid the robustness of long range polarity propagation (Brittle et al. 2012; Ambegaonkar et al. 2012). Therefore, it would be interesting to determine the localisation of Fat4 and Dchs1 in the FBNs and the neuroepithelium to see if loss of *Dchs1/Fat4* affects localisation of each other as they do in *Drosophila* and if chimeric analysis can provide evidence of redistribution of Fat4/Dchs1 at clone boundaries. This can also be achieved by electroporating or transfecting Fat4-GFP and Dchs1-GFP fusion proteins into the *Fat4/Dchs1* null hindbrains.

Fat signalling is a relatively new and undefined field in the vertebrate system and several key questions remain to be answered. However, the strategies proposed above will help add to the current knowledge. It is an important pathway to study because loss of it activity not only results in a range of developmental defects but has also been linked to the human disorder; Van Maldergem syndrome and been implicated in melanomas and breast cancer (Qi et al. 2009; Nikolaev et al. 2012; Cappello et al. 2013).

9 APPENDIX

Table A.1

In situ Hybridisation		N=
E10.5		
Fat4		2
Dchs1		1
Hoxb1	Fat4$^{-/-}$	2
	Dchs1$^{-/-}$	2
EphA4	Fat4$^{-/-}$	2
	Dchs1$^{-/-}$	2
E11.5		
Fat4		2
Dchs1		2
Islet-1	Fat4$^{-/-}$	3
	Dchs1$^{-/-}$	3
Sema3A	Fat4$^{-/-}$	2
	Dchs1$^{-/-}$	2
E12.5		
Fat4		3
Dchs1		3
Fjx1		4
Islet-1	Fat4$^{-/-}$	4
	Dchs1$^{-/-}$	5
	Fat4$^{-/-}$Dchs1$^{-/-}$	3
	Fjx1$^{-/-}$	2
	Fat4$^{-/-}$Fjx1$^{-/-}$	2
Tbx20	Fat4$^{-/-}$	2
	Dchs1$^{-/-}$	2
Ret	Fat4$^{-/-}$	2
	Dchs1$^{-/-}$	2
Cadherin-8	Fat4$^{-/-}$	2
	Dchs1$^{-/-}$	2
Neogenin	Fat4$^{-/-}$	2
	Dchs1$^{-/-}$	2

Table A.1

In situ Hybridisation		N=
E13.5		
Islet-1	Fat4$^{-/-}$	3
	Dchs1$^{-/-}$	3
	Fat4$^{-/-}$Dchs1$^{-/-}$	2
	Islet-1^{cre}Fat4$^{fl/-}$	2
	Hoxa3^{cre}Fat4$^{fl/-}$	2
	Islet-1^{cre}Dchs1$^{fl/-}$	2
	Hoxa3^{cre}Dchs1$^{fl/-}$	2
Neogenin	Fat4$^{-/-}$	1
	Dchs1$^{-/-}$	1
E14.5		
Islet-1	Fat4$^{-/-}$	2
	Dchs1$^{-/-}$	2
E15.5		
Fat4		2
Dchs1		2
Sense Fat4		2

Table A.2

Skeletal Preparations		N=
P0	Fat4$^{-/-}$	4
	Dchs1$^{-/-}$	3
	Fjx1$^{-/-}$	3
	Fat4$^{-/-}$Dchs1$^{-/-}$	3
E15.5	Dchs1$^{-/-}$	2
E16.5	Dchs1$^{-/-}$	3

Table A.3

Histology Analysis		N=
Palatine bone E15.5	*Fat4$^{-/-}$*	2
	Dchs1$^{-/-}$	1
ALP Assay E15.5	*Fat4$^{-/-}$*	2
	Dchs1$^{-/-}$	2
Salivary Gland P0	*Fat4$^{-/-}$*	1
	Dchs1$^{-/-}$	1
	Fat4$^{-/-}$Dchs1$^{-/-}$	2

Table A.4

Wholemount immunostaining analysis		N=
Utricle P0	$Fat4^{-/-}$	1
Axonal branching E11.5	$Fat4^{-/-}$	3
	$Dchs1^{-/-}$	4
FBN - Golgi analysis E11.5	$Fat4^{-/-}$	2
	$Dchs1^{-/-}$	2
FBN - Golgi analysis E12.5	$Fat4^{-/-}$	3
	$Dchs1^{-/-}$	3
	$Fjx1^{-/-}$	3
	$Fat4^{-/-}Fjx1^{-/-}$	3
	$Islet\text{-}1^{cre}Fat4^{fl/-}$	3
	$Hoxa3^{cre}Fat4^{fl/-}$	3
	$Islet\text{-}1^{cre}Dchs1^{fl/-}$	3
	$Hoxa3^{cre}Dchs1^{fl/-}$	3
	$Cre™Dchs1^{fl/-}$ 1mg	3
	$Cre™Dchs1^{fl/-}$ 0.75mg	3
	$Cre™Dchs1^{fl/-}$ 0.60mg	3
	$Cre™Dchs1^{fl/fl}$ 1mg	3
FBN - Cell Shape Analysis E12.5	$Dchs1^{-/-}$	3
FBN – β-Galactosidase Staining E12.5	$Islet\text{-}1^{cre}Fat4^{fl/+}$	2
	$Hoxa3^{cre}Fat4^{fl/+}$	3
	$Islet\text{-}1^{cre}Dchs1^{fl/+}$	2
	$Hoxa3^{cre}Dchs1^{fl/+}$	3
FBN - Islet Staining E13.5	$Vangl^{lp/+}$	1
	$Vangl^{lp/lp}$	2
	$Fat4^{-/-}Vangl^{lp/lp}$	3

Table A.5

OPT Volume Analysis		N=
Salivary Gland P0	$Dchs1^{-/-}$	3
	$Fat4^{-/-}$	3
	$Fat4^{-/-}Dchs1^{-/-}$	3

Table A.6

	ELECTROPORATION ANALYSIS				
	GFP Only				
	Electroporated		Non-Electroporated		
	Golgi Polarity %	Length at Midline and Distance from Midline (cm)	Golgi Polarity %	Length at Midline and Distance from Midline (cm)	Comments
A	40	3.80 / 1.5	45	3.9 / 1.4	GFP lateral to FBNs r5
B	40	3.9 / 1.4	45	3.8 / 1.3	GFP in lateral r4
C	45	4.1 / 1.35	40	4 / 1.4	GFP in lateral r5
D	50	4 / 1.3	55	4 / 1.4	GFP at midline r4-r5
E	50	4 / 1.3	50	3.9 / 1.5	GFP in medial r3
F	40	4 / 1.65	35	4.1 / 1.6	GFP in lateral r3
G	45	4 / 1.4	40	3.8 / 1.3	Scattered GFP r4-r6
H	40	4.2 / 1.4	40	4.1 / 1.5	GFP lateral to FBNs r4-r6
I	45	3.9 / 1.4	45	3.9 / 1.4	GFP in lateral r5-r6
J	45	3.9 / 1.6	40	4 / 1.5	GFP in medial r3
K	50	4.1 / 1.4	45	4 / 1.4	GFP at midline r4-r5
L	35	3.8 / 1.3	45	3.8 / 1.4	GFP lateral r4-r6
M	40	3.9 / 1.5	40	3.9 / 1.4	GFP medial and lateral r5-r6

	ELECTROPORATION ANALYSIS				
	Dchs1 + GFP				Comments
	Electroporated		Non-Electroporated		
	Golgi Polarity %	Length at Midline and Distance from Midline (cm)	Golgi Polarity %	Length at Midline and Distance from Midline (cm)	
A	45	3.81 / 1.15	45	3.87 / 1.2	GFP in extremely lateral r5-r6
B	25	3.9 / 1	35	3.82 / 1	GFP lateral to the FBNs r4-r6
C	35	4 / 2	45	4 / 2	GFP in r6
D	25	4 / 1.4	30	4.1 / 1.4	GFP on both sides r5
E	20	3.7 / 1.3	40	3.7 / 1.2	GFP lateral to the FBNs r4-r6
F	55	3.9 / 1.7	50	3.9 / 1.5	GFP in lateral r5
G	40	4 / 1.7	50	4.1 / 1.5	GFP in medial r3
H	40	3.9 / 1.3	45	3.9 / 1.4	GFP at midline r5-r6
I	35	4 / 1.5	40	4.1 / 1.6	GFP in lateral r5
J	40	3.7 / 1.5	45	3.8 / 1.4	GFP in lateral r4
K	35	3.6 / 1.3	40	3.7 / 1.2	GFP at midline r4-r5
L	50	3.9 / 1.3	45	4 / 1.5	GFP at midline r5-r6
M	45 (medial)	4.2 / 1.9	50 (medial and lateral)	4.3 / 2.1	GFP at midline and lateral r4-r5
N	45	3.1 / 2.55	35	3 / 2.2	GFP at midline r4-r6
O	35	3.7 / 1.7	40	3.6 / 1.8	GFP at midline r4-r6

	ELECTROPORATION ANALYSIS				
	FAT4 + GFP				
	Electroporated		**Non-Electroporated**		
	Golgi Polarity %	**Length at Midline and Distance from Midline (cm)**	**Golgi Polarity %**	**Length at Midline and Distance from Midline (cm)**	**Comments**
A	45	4 / 1.4	55	3.9 / 1.5	Faint GFP scattered
B	40	4.1 / 1.6	50	4 / 1.5	GFP in lateral r6
C	45	4.2 / 1.3	40	4 / 1.3	GFP at midline r3-r4
D	45	3.8 / 1.6	45	3.9 / 1.4	GFP in lateral r3
E	30	4.6 / 1.9	30	4.5 / 1.8	GFP at midline in r5
F	25	4.1 / 1.5	25	4 / 1.4	GFP at midline and lateral r4-r6
G	25 (medial)	7.1 / 1.65	20 (medial + lateral)	7 / 1.5	GFP at midline and lateral r4-r6/r7
H	20	4.7 / 2.1	35	4.6 / 1.7	GFP at midline r3-r5
I	40	4.1 / 1.3	35	4.4 / 1	GFP lateral r4-r5
J	40	4.3 / 1.7	45	4.2 / 1.6	GFP very lateral r4-r6
K	35	4.5 / 1	40	4.5 / 0.8	GFP lateral to FBNs r4-r6

ELECTROPORATION ANALYSIS					
	FAT4 + GFP				**Comments**
	Electroporated		**Non-Electroporated**		
	Golgi Polarity %	**Length at Midline and Distance from Midline (cm)**	**Golgi Polarity %**	**Length at Midline and Distance from Midline (cm)**	
L	25	5.7 1.3	25	5.6 1.4	GFP at midline r5-r6/r7
M	40	4.5 1.7	40	4.2 1.6	GFP at edges of hindbrain
N	30	4.3 1.7	35	4.2 1.6	GFP in lateral r5-r6
O	20	3.9 1.5	25	4 1.6	GFP at midline r4-r5
P	45	4.2 1.6	50	4.4 1.5	GFP lateral to FBNs r5-r6
Q	25	3.9 1.6	45	4.1 1.6	GFP at midline in r5
R	25	3.9 0.5	20	4 1.2	GFP at midline r4-r6
S	50	4.1 1.6	50	4.2 1.5	GFP in lateral r5

In situ Hybridisation Analysis		
Islet-1 &	GFP	N= 4
Cyp26b1	Fat4 + GFP	N= 7

* Golgi polarity was measured as a percentage of FBNs polarised in the axis of migration (caudal-lateral).

10 BIBLIOGRAPHY

Adler, P.N., 2002. Planar signaling and morphogenesis in Drosophila. *Developmental cell*, 2(5), pp.525–35.

Altman, J. & Bayer, S.A., 1985. Embryonic development of the rat cerebellum. III. Regional differences in the time of origin, migration, and settling of Purkinje cells. *The journal of comparative neurology*, 231(1), pp.42–65.

Ambegaonkar, A. a et al., 2012. Propagation of Dachsous-Fat planar cell polarity. *Current biology : CB*, 22(14), pp.1302–8.

Axelrod, J.D., 2001. Unipolar membrane association of Dishevelled mediates Frizzled planar cell polarity signaling. *Genes & development*, 15(10), pp.1182–1187.

Bell, E., Wingate, R. & Lumsden, A, 1999. Homeotic Transformation of Rhombomere Identity After Localized Hoxb1 Misexpression. *Science*, 284(5423), pp.2168–2171.

Bellion, A. et al., 2005. Nucleokinesis in tangentially migrating neurons comprises two alternating phases: forward migration of the Golgi/centrosome associated with centrosome splitting and myosin contraction at the rear. *The Journal of neuroscience : the official journal of the Society for Neuroscience*, 25(24), pp.5691–5699.

Black, M.M. & Baas, P.W., 1989. The basis of polarity in neurons. *Trends in neurosciences*, 12(6), pp.211–214.

Blair, S.S., 2012. Cell polarity: overdosing on PCPs. *Current biology : CB*, 22(14), pp.567–569.

Brittle, A., Thomas, C. & Strutt, D., 2012. Planar polarity specification through asymmetric subcellular localization of Fat and Dachsous. *Current biology : CB*, 22(10), pp.907–914.

Brittle, A.L. et al., 2010. Four-jointed modulates growth and planar polarity by reducing the affinity of dachsous for fat. *Current biology : CB*, 20(9), pp.803–810.

Bryant, P J & Schubiger, G., 1971. Giant and duplicated imaginal discs in a new lethal mutant of Drosophila melanogaster. *Developmental biology*, 24(2), pp.233–263.

Bryant, Peter J et al., 1988. Mutations at the fat Locus Interfere with Cell Proliferation Control and Epithelial Morphogenesis in Drosophila. *Developmental biology*, 129(2), pp.541–554.

Calamita, P. & Fanto, M., 2011. Slimming down fat makes neuropathic hippo: The Fat/Hippo tumor suppressor pathway protects adult neurons through regulation of autophagy. *Autophagy*, 7(8), pp.907–909.

De Calisto, J. et al., 2005. Essential role of non-canonical Wnt signalling in neural crest migration. *Development,* 132(11), pp.2587–2597.

Cappello, S. et al., 2013. Mutations in genes encoding the cadherin receptor-ligand pair Dchs1 and Fat4 disrupt cerebral cortical development. *Nature genetics*, doi:10.1038/ng.2765.

Casal, J., Lawrence, Peter A. & Struhl, G., 2006. Two separate molecular systems, Dachsous/Fat and Starry night/Frizzled, act independently to confer planar cell polarity. *Development*, 133(22), pp.4561–4572.

Casal, J., Struhl, G. & Lawrence, Peter A., 2002. Developmental compartments and planar polarity in Drosophila. *Current biology : CB*, 12(14), pp.1189–1198.

Castillejo-López, C., Arias, W.M. & Baumgartner, S., 2004. The fat-like gene of Drosophila is the true orthologue of vertebrate fat cadherins and is involved in the formation of tubular organs. *The Journal of biological chemistry*, 279(23), pp.24034–24043.

Chandrasekhar, A., 2004. Turning heads; Development of Vertebrate Branchiomotor Neurons. *Developmental Dynamics,* 229(1), pp.143–161.

Chen, W. et al., 2008. Asymmetric homotypic interactions of the atypical cadherin Flamingo mediate intercellular polarity signaling. *Cell*, 133(6), pp.1093–1105.

Cho, E. & Irvine, K.D., 2004. Action of fat, four-jointed, dachsous and dachs in distal-to-proximal wing signaling. *Development*, 131(18), pp.4489–4500.

Ciani, L. et al., 2003. Mice lacking the giant protocadherin mFAT1 exhibit renal slit junction abnormalities and a partially penetrant cyclopia and anophthalmia phenotype. *Molecular and cellular biology*, 23(10), pp.3575–3582.

Ciruna, B. et al., 2006. Planar cell polarity signalling couples cell division and morphogenesis during neurulation. *Nature*, 439, pp.220–224.

Clark, H.F. et al., 1995. Dachsous encodes a member of the cadherin superfamily that controls imaginal disc morphogenesis in Drosophila. *Genes & Development*, 9(12), pp.1530–1542.

Cox, B. et al., 2000. Cloning and Expression Throughout Mouse Development of mfat1 , a Homologue of the Drosophila Tumour Suppressor Gene fat. *Developmental Dynamics*, 217(3), pp.233–240.

Das, A. et al., 2013. Stromal-epithelial crosstalk regulates kidney progenitor cell differentiation. *Nature cell biology*, 15(9), pp.1035–1044.

Day, S.J. & Lawrence, Peter A., 2000. Measuring dimensions: the regulation of size and shape. *Development*, 127(14), pp.2977–2987.

Deans, M.R. et al., 2011. Control of neuronal morphology by the atypical cadherin Fat3. *Neuron*, 71(5), pp.820–832.

Deardorff, M. A. et al., 1998. Frizzled-8 is expressed in the Spemann organizer and plays a role in early morphogenesis. *Development*, 125(14), pp.2687–2700.

Degoutin, J.L. et al., 2013. Riquiqui and Minibrain are regulators of the Hippo pathway downstream of Dachsous. *Nature cell biology*, 15(8), pp.1–12.

Devenport, D. & Fuchs, E., 2008. Planar polarization in embryonic epidermis orchestrates global asymmetric morphogenesis of hair follicles. *Nature cell biology*, 10(11), pp.1257–1268.

Donoughe, S. & DiNardo, S., 2011. dachsous and frizzled contribute separately to planar polarity in the Drosophila ventral epidermis. *Development*, 138(13), pp.2751–2759.

Down, M. et al., 2005. Cloning and expression of the large zebrafish protocadherin gene, Fat. *Gene expression patterns : GEP*, 5(4), pp.483–490.

Dunne, J. et al., 1995. Molecular cloning and tissue expression of FAT, the human homologue of the Drosophila fat gene that is located on chromosome 4q34-q35 and encodes a putative adhesion molecule. *Genomics*, 30(2), pp.207–223.

Dupont, S. et al., 2011. Role of YAP/TAZ in mechanotransduction. *Nature*, 474(7350), pp.179–183.

Ericson, J. et al., 1992. Early stages of motor neuron differentiation revealed by expression of homeobox gene Islet-1. *Science*, 256(5063), pp.1555–1560.

Fanto, M. et al., 2003. The tumor-suppressor and cell adhesion molecule Fat controls planar polarity via physical interactions with Atrophin, a transcriptional co-repressor. *Development*, 130(4), pp.763–774.

Faux, C. et al., 2012. Neurons on the move: migration and lamination of cortical interneurons. *Neuro-Signals*, 20(3), pp.168–189.

Feng, Y. & Irvine, K.D., 2007. Fat and expanded act in parallel to regulate growth through warts. *Proceedings of the National Academy of Sciences of the United States of America*, 104(51), pp.20362–20367.

Feng, Y. & Irvine, K.D., 2009. Processing and phosphorylation of the Fat receptor. *Proceedings of the National Academy of Sciences of the United States of America*, 106(29), pp.11989–11994.

Franco, S.J. & Müller, U., 2011. Extracellular matrix functions during neuronal migration and lamination in the mammalian central nervous system. *Developmental neurobiology*, 71(11), pp.889–900.

Gao, B. et al., 2011. Wnt signaling gradients establish planar cell polarity by inducing Vangl2 phosphorylation through Ror2. *Developmental cell*, 20(2), pp.163–176.

Gao, C. & Chen, Y.-G., 2010. Dishevelled: The hub of Wnt signaling. *Cellular signalling*, 22(5), pp.717–727.

Gao, W.Q. & Hatten, M E, 1994. Immortalizing oncogenes subvert the establishment of granule cell identity in developing cerebellum. *Development*, 120(5), pp.1059–1070.

Garel, S., Garcia-Dominguez, M. & Charnay, P., 2000. Control of the migratory pathway of facial branchiomotor neurones. *Development*, 127(24), pp.5297–5307.

Gilardi-Hebenstreit, P. et al., 1992. An Eph-related receptor protein tyrosine kinase gene segmentally expressed in the developing mouse hindbrain. *Oncogene*, 7(12), pp.2499–2506.

Gilland, E & Baker, R, 1993. Conservation of Neuroepithelial and Mesodermal Segment in the Embryonic Vetebrate Head. *Acta Anat*, 148(2-3), pp.110–123.

Gilland, Edwin & Baker, Robert, 2005. Evolutionary patterns of cranial nerve efferent nuclei in vertebrates. *Brain, behavior and evolution*, 66(4), pp.234–254.

Glasco, D.M. et al., 2012. The mouse Wnt/PCP protein Vangl2 is necessary for migration of facial branchiomotor neurons, and functions independently of Dishevelled. *Developmental biology*, 369(2), pp.211–222.

Goodrich, L. V & Strutt, D., 2011. Principles of planar polarity in animal development. *Development*, 138(10), pp.1877–92.

Gros, J. et al., 2011. Wnt5a/Jnk and FGF/Mapk pathways regulate the cellular events shaping the vertebrate limb bud. *Current Biology*: *CB,* 20(22), pp.1993–2002.

Gubb, D. & Garcia-Bellido, A., 1982. A genetic analysis of the determination of cuticular polarity during development in Drosophila melanogaster. *Journal of Embryology and Experimental Morphology*, 68, pp.37–57.

Gumbiner, B.M., 2000. Regulation of cadherin adhesive activity. *The Journal of cell biology*, 148(3), pp.399–404.

Guo, N., Hawkins, C. & Nathans, J., 2004. Frizzled6 controls hair patterning in mice. *Proceedings of the National Academy of Science of the United States of America*, 101(25), pp.9277-9281.

Guthrie, S & Lumsden, a, 1992. Motor neuron pathfinding following rhombomere reversals in the chick embryo hindbrain. *Development*, 114(3), pp.663–673.

Guthrie, Sarah, 2007. Patterning and axon guidance of cranial motor neurons. *Nature reviews. Neuroscience*, 8(11), pp.859–871.

Happé, H. et al., 2011. Altered Hippo signalling in polycystic kidney disease. *The Journal of pathology*, 224(1), pp.133–142.

Harumoto, T. et al., 2010. Atypical cadherins Dachsous and Fat control dynamics of noncentrosomal microtubules in planar cell polarity. *Developmental cell*, 19(3), pp.389–401.

Van Hateren, N.J. et al., 2011. FatJ acts via the Hippo mediator Yap1 to restrict the size of neural progenitor cell pools. *Development*, 138(10), pp.1893–1902.

Hatten, Mary E, 2002. New directions in neuronal migration. *Science*, 297(5587), pp.1660–1663.

Hirano, S., Suzuki, S.T. & Redies, C., 2003. The cadherin superfamily in neural development: diversity, function and interaction with other molecules. *Frontiers in bioscience: a journal and virtual library*,1(8), pp.306–355.

Hirota, Y. et al., 2012. Roles of planar cell polarity signaling in maturation of neuronal precursor cells in the postnatal mouse olfactory bulb. *Stem cells,* 30(8), pp.1726–1733.

Hogan, J. et al., 2011. Two frizzled planar cell polarity signals in the Drosophila wing are differentially organized by the Fat/Dachsous pathway. *PLoS genetics*, 7(2), doi:10.1371/journal.pgen.1001305.

Hong, J.H. et al., 2005. TAZ, a transcriptional modulator of mesenchymal stem cell differentiation. *Science*, 309(5737), pp.1074–1078.

Hou, R. & Sibinga, N.E.S., 2009. Atrophin proteins interact with the Fat1 cadherin and regulate migration and orientation in vascular smooth muscle cells. *The Journal of biological chemistry*, 284(11), pp.6955–6965.

Höng, J.C. et al., 2004. Identification of new human cadherin genes using a combination of protein motif search and gene finding methods. *Journal of molecular biology*, 337(2), pp.307–317.

Ishikawa, H.O. et al., 2008. Four-jointed is a Golgi kinase that phosphorylates a subset of cadherin domains. *Science*, 321(5887), pp.401–404.

Ishiuchi, T. et al., 2009. Mammalian Fat and Dachsous cadherins regulate apical membrane organization in the embryonic cerebral cortex. *The Journal of cell biology*, 185(6), pp.959–967.

Jacob, J. & Guthrie, S, 2000. Facial visceral motor neurons display specific rhombomere origin and axon pathfinding behavior in the chick. *The Journal of neuroscience : the official journal of the Society for Neuroscience*, 20(20), pp.7664–7671.

Jacob, J., Hacker, a & Guthrie, S, 2001. Mechanisms and molecules in motor neuron specification and axon pathfinding. *BioEssays : news and reviews in molecular, cellular and developmental biology*, 23(7), pp.582–595.

Jessen, J.R. et al., 2002. Zebrafish trilobite identifies new roles for Strabismus in gastrulation and neuronal movements. *Nature cell biology*, 4(8), pp.610–615.

Karner, C.M. et al., 2009. Wnt9b signalling regulates planar cell polarity and kidney tubule morphogenesis. *Nature Genetics*, 41(7), pp.793–799.

Keeling, S.L., Gad, J.M. & Cooper, H.M., 1997. Mouse Neogenin, a DCC-like molecule, has four splice variants and is expressed widely in the adult mouse and during embryogenesis. *Oncogene*, 15(6), pp.691–700.

Keller, R., Shih, J. & Sater, a, 1992. The cellular basis of the convergence and extension of the Xenopus neural plate. *Developmental dynamics : an official publication of the American Association of Anatomists*, 193(3), pp.199–217.

Keynes, R. & Lumsden, Andrew, 1989. Segmental pattens of neuronal development in the chick hindbrain. *Nature*, 337, pp.424–429.

Korematsu, K. & Redies, C., 1997. Restricted expression of cadherin-8 in segmental and functional subdivisions of the embryonic mouse brain. *Developmental dynamics*, 208(2), pp.178–189.

Kraus, F., Haenig, B. & Kispert, A., 2001. Cloning and expression analysis of the mouse T-box gene tbx20. *Mechanisms of development*, 100(1), pp.87–91.

Köntges, G. & Lumsden, A., 1996. Rhombencephalic neural crest segmentation is preserved throughout craniofacial ontogeny. *Development*, 122(10), pp.3229–3242.

Lawrence, Peter A., Struhl, G. & Casal, J., 2008. Do the protocadherins Fat and Dachsous link up to determine both planar cell polarity and the dimensions of organs? *Nature cell biology*, 10(12), pp.1379–1382.

Lei, Y.-P. et al., 2010. VANGL2 mutations in human cranial neural-tube defects. *The New England journal of medicine*, 362(23), pp.2232–2235.

Lucas, E.P. et al., 2013. The Hippo pathway polarizes the actin cytoskeleton during collective migration of Drosophila border cells. *The Journal of cell biology*, 201(6), pp.875–885.

Lumsden, A., Sprawson, N. & Graham, A., 1991. Segmental origin and migration of neural crest cells in the hindbrain region of the chick embryo. *Development*, 113(4), pp.1281–1291.

Ma, D. et al., 2003. Fidelity in planar cell polarity signalling. *Nature*, 421(6922), pp.543–547.

Macatee, T.L. et al., 2003. Ablation of specific expression domains reveals discrete functions of ectoderm- and endoderm-derived FGF8 during cardiovascular and pharyngeal development. *Development*, 130(25), pp.6361–6374.

Mahoney, P. a et al., 1991. The fat tumor suppressor gene in Drosophila encodes a novel member of the cadherin gene superfamily. *Cell*, 67(5), pp.853–868.

Mao, Y. et al., 2011. Characterization of a Dchs1 mutant mouse reveals requirements for Dchs1-Fat4 signaling during mammalian development. *Development*, 138(5), pp.947–957.

Mao, Y. et al., 2006. Dachs: an unconventional myosin that functions downstream of Fat to regulate growth, affinity and gene expression in Drosophila. *Development*, 133(13), pp.2539–2551.

Mapp, O.M. et al., 2010. Prickle1b mediates interpretation of migratory cues during zebrafish facial branchiomotor neuron migration. *Developmental dynamics*, 239(6), pp.1596–1608.

Mapp, O.M. et al., 2011. Zebrafish Prickle1b mediates facial branchiomotor neuron migration via a farnesylation-dependent nuclear activity. *Development*, 138(10), pp.2121–2132.

Mardia, K. V. & Jupp, P.E., 2000. *Directional Statistics*,Wiley Series in Probability and Statistics.

Marshall, H. et al., 1992. Retinoic acid alters hindbrain Hox code and induces transformation of rhombomeres 2/3 into a 4/5 identity. *Nature*, 360(6406), pp.737-741.

Matakatsu, H. & Blair, S.S., 2004. Interactions between Fat and Dachsous and the regulation of planar cell polarity in the Drosophila wing. *Development*, 131(15), pp.3785–3794.

Matakatsu, H. & Blair, S.S., 2012. Separating planar cell polarity and Hippo pathway activities of the protocadherins Fat and Dachsous. *Development*, 139(8), pp.1498–1508.

Matakatsu, H. & Blair, S.S., 2006. Separating the adhesive and signaling functions of the Fat and Dachsous protocadherins. *Development*, 133(12), pp.2315–2324.

McNeill, H. & Woodgett, J.R., 2010. When pathways collide: collaboration and connivance among signalling proteins in development. *Nature reviews. Molecular cell biology*, 11(6), pp.404–413.

Meléndez-Herrera, E. & Varela-Echavarría, A., 2006. Expression of secreted semaphorins and their receptors in specific neuromeres, boundaries, and neuronal groups in the developing mouse and chick brain. *Brain research*, 1067(1), pp.126–137.

Merte, J. et al., 2010. Sec24b selectively sorts Vangl2 to regulate planar cell polarity during neural tube closure. *Nature cell biology*, 12(1), pp.41–46.

Mitsui, K. et al., 2002. Mammalian fat3: a large protein that contains multiple cadherin and EGF-like motifs. *Biochemical and biophysical research communications*, 290(4), pp.1260–1266.

Moeller, Marcus J et al., 2004. Protocadherin FAT1 binds Ena/VASP proteins and is necessary for actin dynamics and cell polarization. *The EMBO journal*, 23(19), pp.3769–3779.

Montcouquiol, M. et al., 2006. Asymmetric localization of Vangl2 and Fz3 indicate novel mechanisms for planar cell polarity in mammals. *The Journal of neuroscience : the official journal of the Society for Neuroscience*, 26(19), pp.5265–5275.

Montcouquiol, M. et al., 2003. Identification of Vangl2 and Scrb1 as planar polarity genes in mammals. *Nature*, 423(6936), pp.173–177.

Moon, R.T. et al., 1993. Xwnt-5A: a maternal Wnt that affects morphogenetic movements after overexpression in embryos of Xenopus laevis. *Development*, 119(1), pp.97–111.

Muzumdar, M.D. et al., 2007. A Global Double-Fluorescent Cre Reporter Mouse. *Genesis*, 45, pp.593–605.

Müller, M. et al., 2003. Nkx6.1 controls migration and axon pathfinding of cranial branchio-motoneurons. *Development*, 130(23), pp.5815–5826.

Nagae, S., Tanoue, T. & Takeichi, Masatoshi, 2007. Temporal and spatial expression profiles of the Fat3 protein, a giant cadherin molecule, during mouse development. *Developmental dynamics : an official publication of the American Association of Anatomists*, 236(2), pp.534–543.

Nagafuchi, A. et al., 1987. Transformation of cell adhesion properties by exogenously introduced E-cadherin cDNA. *Nature*, 329(6137), pp.341–343.

Nakajima, D et al., 2001. Identification of three novel non-classical cadherin genes through comprehensive analysis of large cDNAs. *Brain research. Molecular brain research*, 94(1-2), pp.85–95.

Nakayama, M et al., 2002. MEGF1/fat2 Proteins Containing Extraordinarily Large Extracellular Domains Are Localized to Thin Parallel Fibers of Cerebellar Granule Cells. *Molecular and Cellular Neuroscience*, 20(4), pp.563–578.

Nakayama, Manabu et al., 1998. Identification of High-Molecular-Weight Proteins with Multiple EGF-like Motifs by Motif-Trap Screening. *Genomics*, 51(1), pp.27–34.

Niederreither, K. et al., 2000. Retinoic acid synthesis and hindbrain patterning in the mouse embryo. *Development*, 127(1), pp.75–85.

Nikolaev, S.I. et al., 2012. Exome sequencing identifies recurrent somatic MAP2K1 and MAP2K2 mutations in melanoma. *Nature genetics*, 44(2), pp.133–139.

Ohshima, T. et al., 2002. Cyclin-dependent kinase 5/p35 contributes synergistically with Reelin/Dab1 to the positioning of facial branchiomotor and inferior olive neurons in the developing mouse hindbrain. *The Journal of neuroscience : the official journal of the Society for Neuroscience*, 22(10), pp.4036–4044.

Pachnis, V., Mankoo, B. & Costantini, F., 1993. Expression of the c-ret proto-oncogene during mouse embryogenesis. *Development*, 119(4), pp.1005–1017.

Pan, G. et al., 2013. Signal transduction by the Fat cytoplasmic domain. *Development*, 140(4), pp.831–842.

Pattyn, A. et al., 2000. Control of hindbrain motor neuron differentiation by the homeobox gene Phox2b. *Development*, 127(7), pp.1349–1358.

Pettitt, J., 2005. The cadherin superfamily. *WormBook : the online review of C. elegans biology*, pp.1–9.

Ponassi, M. et al., 1999. Expression of the rat homologue of the Drosophila fat tumour suppressor gene. *Mechanisms of development*, 80(2), pp.207–212.

Pringle, J.R. et al., 1995. Establishment of cell polarity in yeast. *Cold Spring Harbor symposia on quantitative biology*, 60, pp.729–744.

Probst, B. et al., 2007. The rodent Four-jointed ortholog Fjx1 regulates dendrite extension. *Developmental biology*, 312(1), pp.461–470.

Qi, C. et al., 2009. Identification of Fat4 as a candidate tumor suppressor gene in breast cancers. *International journal of cancer,* 124(4), pp.793–798.

Qu, Y. et al., 2010. Atypical cadherins Celsr1-3 differentially regulate migration of facial branchiomotor neurons in mice. *The Journal of neuroscience : the official journal of the Society for Neuroscience*, 30(28), pp.9392–9401.

Reddy, B.V.V.G. & Irvine, K.D., 2008. The Fat and Warts signaling pathways: new insights into their regulation, mechanism and conservation. *Development*, 135(17), pp.2827–2838.

Rida, C, G, P. & Chen, P., 2009. Line up and listen: planar cell polarity regulation in the mammalian inner ear. *Seminars in cell & developmental biology*, 20(8), pp.978–985.

Rock, R., Heinrich, A.C., et al., 2005b. Fjx1: a notch-inducible secreted ligand with specific binding sites in developing mouse embryos and adult brain. *Developmental dynamics : an official publication of the American Association of Anatomists*, 234(3), pp.602–612.

Rock, R., Schrauth, S. & Gessler, M., 2005. Expression of mouse dchs1, fjx1, and fat-j suggests conservation of the planar cell polarity pathway identified in Drosophila. *Developmental dynamics : an official publication of the American Association of Anatomists*, 234(3), pp.747–755.

Rogulja, D., Rauskolb, C. & Irvine, K.D., 2008. Morphogen control of wing growth through the Fat signaling pathway. *Developmental cell*, 15(2), pp.309–321.

Rossel, M. et al., 2005. Reelin signaling is necessary for a specific step in the migration of hindbrain efferent neurons. *Development*, 132(6), pp.1175–1185.

Saburi, S. et al., 2012. Functional interactions between Fat family cadherins in tissue morphogenesis and planar polarity. *Development*, 139(10), pp.1806–1820.

Saburi, S. et al., 2008. Loss of Fat4 disrupts PCP signaling and oriented cell division and leads to cystic kidney disease. *Nature genetics*, 40(8), pp.1010–1015.

Schwarz, Q. et al., 2004. Vascular endothelial growth factor controls neuronal migration and cooperates with Sema3A to pattern distinct compartments of the facial nerve. *Genes and Development*, 18(22), pp.2822–2834.

Sharma, P. & McNeill, H., 2013. Regulation of long-range planar cell polarity by Fat-Dachsous signaling. *Development,* 140, pp.3869–3881.

Silva, E. et al., 2006. The tumor-suppressor gene fat controls tissue growth upstream of expanded in the hippo signaling pathway. *Current biology : CB*, 16(21), pp.2081–2089.

Simon, M. A. et al., 2010. Modulation of fat:dachsous binding by the cadherin domain kinase four-jointed. *Current biology : CB*, 20(9), pp.811–817.

Simon, M. A., 2004. Planar cell polarity in the Drosophila eye is directed by graded Four-jointed and Dachsous expression. *Development*, 131(24), pp.6175–6184.

Sittaramane, V. et al., 2009. The cell adhesion molecule Tag1, transmembrane protein Stbm/Vangl2, and Lamininalpha1 exhibit genetic interactions during migration of facial branchiomotor neurons in zebrafish. *Developmental biology*, 325(2), pp.363–373.

Skouloudaki, K. et al., 2009. Scribble participates in Hippo signaling and is required for normal zebrafish pronephros development. *Proceedings of the National Academy of Sciences of the United States of America*, 106(21), pp.8579–8584.

Smith, T.G. et al., 2007. The expression of Fat-1 cadherin during chick limb development. *International Journal of Developmental Biology*, 51, pp.173–176.

Song, M. R., 2007. Moving cell bodies: understanding the migratory mechanism of facial motor neurons. *Archives of pharmacal research*, 30(10), pp.1273–1282.

Song, M. R. et al., 2006. T-Box transcription factor Tbx20 regulates a genetic program for cranial motor neuron cell body migration. *Development*, 133(24), pp.4945–4955.

Sopko, R. & McNeill, H., 2009. The skinny on Fat: an enormous cadherin that regulates cell adhesion, tissue growth, and planar cell polarity. *Current opinion in cell biology*, 21(5), pp.717–723.

Soriano, P., 1999. Generalized lacZ expression with the ROSA26 Cre reporter strain. *Nature genetics*, 21, pp.70-71.

Strutt, D., 2005. Organ shape: controlling oriented cell division. *Current biology : CB*, 15(18), pp.758–759.

Strutt, D.I., 2001. Asymmetric localization of frizzled and the establishment of cell polarity in the Drosophila wing. *Molecular cell*, 7(2), pp.367–375.

Strutt, H. et al., 2004. Cleavage and secretion is not required for Four-jointed function in Drosophila patterning. *Development* , 131(4), pp.881–890.

Strutt, H. & Strutt, D., 2002. Nonautonomous planar polarity patterning in Drosophila: dishevelled-independent functions of frizzled. *Developmental cell*, 3(6), pp.851–863.

Studer, M et al., 1996. Altered segmental identity and abnormal migration of motor neurons in mice lacking Hoxb-1. *Nature*, 384(6610), pp.630–634.

Studer, M, 2001. Initiation of facial motoneurone migration is dependent on rhombomeres 5 and 6. *Development (Cambridge, England)*, 128(19), pp.3707–3716.

Swartz, M. et al., 2001. Sparking new frontiers: using in vivo electroporation for genetic manipulations. *Developmental biology*, 233(1), pp.13–21.

Tanoue, T. & Takeichi, Masatoshi, 2004. Mammalian Fat1 cadherin regulates actin dynamics and cell-cell contact. *The Journal of cell biology*, 165(4), pp.517–528.

Thomas, C. & Strutt, D., 2012. The roles of the cadherins Fat and Dachsous in planar polarity specification in Drosophila. *Developmental dynamics : an official publication of the American Association of Anatomists*, 241(1), pp.27–39.

Tissir, F. & Goffinet, A.M., 2010. Planar cell polarity signaling in neural development. *Current opinion in neurobiology*, 20(5), pp.572–577.

Topczewski, J. et al., 2001. The zebrafish glypican kypnek controls cell polarity during gastrulation movements of convergent extension. *Developmental Cell*, 1(2), pp.251–264.

Ulloa, F. & Marti, E., 2010. Wnt won the war: Antagonistic role of Wnt over Shh controls dorso-ventral patterning of the vertebrate neural tube. *Developmental Dynamics*, 239(1), pp.69-76.

Valiente, M. & Marín, O., 2010. Neuronal migration mechanisms in development and disease. *Current opinion in neurobiology*, 20(1), pp.68–78.

Ventura, A. et al., 2007. Restoration of p53 function leads to tumour regression in vivo. *Nature*, 445(7128), pp.661–665.

Viktorinová, I. et al., 2009. The cadherin Fat2 is required for planar cell polarity in the Drosophila ovary. *Development (Cambridge, England)*, 136(24), pp.4123–4132.

Villano, J.L. & Katz, F N, 1995. four-jointed is required for intermediate growth in the proximal-distal axis in Drosophila. *Development*, 121(9), pp.2767–2777.

Vinson, C.R. & Adler, P.N., 1987. Directional non-cell autonomy and the transmission of polarity information by the frizzled gene of Drosophila. *Nature*, 329, pp.549–551.

Vivancos, V. et al., 2009. Wnt activity guides facial branchiomotor neuron migration, and involves the PCP pathway and JNK and ROCK kinases. *Neural development*, 4(7), doi: 10.1186/1749-8104-4-7.

Wada, H. et al., 2006. Frizzled3a and Celsr2 function in the neuroepithelium to regulate migration of facial motor neurons in the developing zebrafish hindbrain. *Development*, 133(23), pp.4749–4759.

Wallingford, J. B., 2002. Neural tube closure requires Dishevelled-dependent convergent extension of the midline. *Development*, 129(24), pp.5815–5825.

Wallingford, John B, 2012. Planar cell polarity and the developmental control of cell behavior in vertebrate embryos. *Annual review of cell and developmental biology*, 28, pp.627–653.

Walsh, G.S. et al., 2011. Planar polarity pathway and Nance-Horan syndrome-like 1b have essential cell-autonomous functions in neuronal migration. *Development*, 138(14), pp.3033–3042.

Wang, B. et al., 2011. Disruption of PCP signaling causes limb morphogenesis and skeletal defects and may underlie Robinow syndrome and brachydactyly type B. *Human molecular genetics*, 20(2), pp.271–285.

Wang, J. et al., 2006. Dishevelled genes mediate a conserved mammalian PCP pathway to regulate convergent extension during neurulation. *Development*, 133(9), pp.1767–1778.

Wanner, S.J. & Prince, V.E., 2013. Axon tracts guide zebrafish facial branchiomotor neuron migration through the hindbrain. *Development*, 140(4), pp.906–915.

Warchol, M.E. & Montcouquiol, M., 2010. Maintained expression of the planar cell polarity molecule Vangl2 and reformation of hair cell orientation in the regenerating inner ear. *Journal of the Association for Research in Otolaryngology : JARO*, 11(3), pp.395–406.

Wilkinson, D.G. et al., 1989. Segmental expression of Hox-2 homoeobox-containing genes in the developing mouse hindbrain. *Nature*, 341(6241), pp.405–409.

Willecke, M. et al., 2008. Boundaries of Dachsous Cadherin activity modulate the Hippo signaling pathway to induce cell proliferation. *Proceedings of the National Academy of Sciences of the United States of America*, 105(39), pp.14897–14902.

Wingate, R.J.T. & Hatten, Mary E., 1999. The role of the rhombic lip in avian cerebellum development. *Development*, 126(20), pp.4395–4404.

Yang, C., Axelrod, J.D. & Simon, M. a, 2002. Regulation of Frizzled by fat-like cadherins during planar polarity signaling in the Drosophila compound eye. *Cell*, 108(5), pp.675–688.

Yang, Lei et al., 2006. Isl1Cre reveals a common Bmp pathway in heart and limb development. *Development*, 133(8), pp.1575–1585.

Yaoita, E. et al., 2005. Role of Fat1 in cell-cell contact formation of podocytes in puromycin aminonucleoside nephrosis and neonatal kidney. *Kidney International*, 68(2), pp.542–551.

Yee, K. et al., 1999. Extension of Long Leading Processes and Neuronal Migration in the Mammalian Brain Directed by the Chemoattractant Netrin-1. *Neuron*, 24(3), pp.607–622.

Zaidi, S.K. et al., 2004. Tyrosine phosphorylation controls Runx2-mediated subnuclear targeting of YAP to repress transcription. *The EMBO journal*, 23(4), pp.790–799.

Zeidler, M.P., Perrimon, N. & Strutt, D.I., 2000. Multiple roles for four-jointed in planar polarity and limb patterning. *Developmental biology*, 228(2), pp.181–196.

Zoltewicz, J.S. et al., 2004. Atrophin 2 recruits histone deacetylase and is required for the function of multiple signaling centers during mouse embryogenesis. *Development*, 131(1), pp.3–14.